SKB

TECHNICAL REPORT 93-19

Mechanical properties of fracture zones

Bengt Leijon

Conterra AB

May 1993

SVENSK KÄRNBRÄNSLEHANTERING AB
SWEDISH NUCLEAR FUEL AND WASTE MANAGEMENT CO
BOX 5864 S-102 48 STOCKHOLM
TEL 08-665 28 00 TELEX 13108 SKB S
TELEFAX 08-661 57 19

MECHANICAL PROPERTIES OF FRACTURE ZONES

Bengt Leijon

Conterra AB

May 1993

MECHANICAL PROPERTIES OF FRACTURE ZONES

Bengt Leijon

Conterra AB

May 1993

Keywords: Fracture zone, mechanical properties, rock mechanics, stress, strength, stiffness, deformability.

ABSTRACT

Available data on mechanical characteristics of fracture zones are compiled and discussed. The aim is to improve the basis for adequate representation of fracture zones in geomechanical models. The sources of data researched are primarily borehole investigations and case studies in rock engineering, involving observations of fracture zones subjected to artificial load changes. Boreholes only yield local information about the components of fracture zones, i.e. intact rock, fractures and various low-strength materials. Difficulties are therefore encountered in evaluating morphological and mechanical properties of fracture zones from borehole data. Although often thought of as macroscopically planar features, available field data consistently show that fracture zones are characterized by geometrical irregularities such as thickness variations, surface undulation and jogs. These irregularities prevail on all scales. As a result, fracture zones are on all scales characterized by large, in-plane variations of strength- and deformational properties. This has important mechanical consequences in terms of non-uniform stress transfer and complex mechanisms of shear deformation. Field evidence for these findings, in particular results from the Underground Research Laboratory in Canada and from studies of induced fault slip in deep mines, is summarized and discussed.

ABSTRACT (IN SWEDISH)

Sprickzoners mekaniska egenskaper är dåligt kända, vilket återspeglar sig i stora osäkerheter vid analys av bergmekaiska problem där effekterna av sprickzoner måste beaktas. Föreliggande arbete är en sammanställning och granskning av data som finns tillgängliga avseende sprickzoners mekaniska egenskaper. Merparten av informationen har hämtats från borrhålsundersökningar och från gruvsektorn. Förhoppningen är att arbetet skall bidra till en bättre kvalitativ och kvantitativ förståelse för sprickzoners egenskaper och därmed deras respons på olika typer av belastningar. Sprickzoner av alla storlekar och inom ett vitt spektrum av geologiska miljöer kännetecknas av undulerande geometri, variationer i vidd och inhomogen sammansättning. En viktig konsekvens av dessa generella egenskaper är att deformations- och hållfasthetsegenskaperna varierar på motsvarande sätt i alla skalor. Det påverkar i sin tur den spänningsfördelning som råder i och kring sprickzoner, och komplicerar rörelsemönstret vid eventuell skjuvning. Detta styrks av data från omfattande in-situ mätningar i AECL's underjordslaboratorium (URL) i Kanada och av observationer av inducerade förkastningsrörelser i gruvor. Konsekvenser av resultaten med avseende på möjligheter och metoder att simulera sprickzoner i bergmekaniska modeller diskuteras i allmänna termer.

CONTENTS

(continued)

SUMMARY

Not only are data on the mechanical characteristics of fracture zones sparse, but they occur over a wide range of geoscience, including structural geology, seismotectonics, mining and civil engineering. The aim of the present work is to bring together information from some of these sources, and to compile it in such a way that it facilitates proper consideration of fracture zones in analysis of geomechanical problems related to construction and performance of nuclear waste repositories in hard rock. Problems posed in this field include assessment of the risk for future shear displacements along fracture zones, which can directly or indirectly affect repository integrity. Such movements may be induced by future load changes attributable to natural processes such as glaciation, possibly assisted by disturbances caused by the repository itself. Furthermore, since repository excavations shall likely penetrate fracture zones, their mechanical properties are of concern also with regard to local stability during repository construction.

Information was gathered primarily from the rock engineering field, and the data compilation focussed parameters describing deformational properties and shear strength. Available data fall into two categories:

- Indirect estimates of fracture zone parameters on the basis of small-scale observations, primarily by means of boreholes, of the properties of the components of the zones, i.e. intact rock, fractures and various low-strength materials like fault gouge and alteration products.

- Direct observations of fracture zone behavior, either by means of specifically designed experiments or in connection with rock engineering efforts involving large-scale load changes.

Case studies reviewed consistently underline the difficulties encountered in estimating the properties of fracture zones on the basis of borehole-scale sampling and testing. One reason is that conventional core drilling technology does not provide adequate sampling of poor-quality material commonly encountered in fracture zones. Another is that scaling procedures commonly applied to estimate the mechanical properties of individual fractures on the basis of borehole-scale data cannot be readily extended and applied to evaluate the characteristics of fracture zones.

The results from tentative application of empirical systems, commonly used in rock engineering to estimate rock mass deformability from borehole information, to three fracture zones representing different degrees of shear disturbance illustrate these problems. Using data from boreholes penetrating these zones, it was found that the empirical methods provided meaningful upper bound estimates of the deformability of fracture zones with a morphology comparable to moderately fractured rock masses. They failed, however, to predict the deformability of more intensely deformed fracture zones.

Seismology has provided a large amount of data that may be referred to as full-scale observations of fracture zone behavior. There are, however, uncertainties as to stress conditions, and interpretation in terms of mechanical properties is hampered by the fact that parameters measured refer to the dynamic range only. Examples of direct observation of fracture zone behavior in connection with man-made, large-scale alteration of loading conditions are uncommon. The phenomena of induced fault slip in deep mines is an important exception that has been extensively studied due to its major impact on mining safety and operation. Research and practical experiences from this field have produced important results with respect to both fundamental understanding of shear deformation of fault zones and the degree to which current modelling technology can resemble such events.

Field observations consistently show that fracture zones are characterized by geometrical irregularities such as variations in thickness, surface undulations and jogs that prevail on all scales. This implies that strength- and deformational properties can show large local variations over the plane of the discontinuity. This, in turn, induces non-uniform stress transfer. Observations of stability conditions in Swedish mines also provide indirect evidence for significant alteration of the stress field, extending at least tens of meters from major fracture zones. Comprehensive investigations at the Underground Research Laboratory (URL) in Canada have demonstrated an extremely non-uniform transfer of normal stress across a major fracture zone. These results have been explained in terms of local variations of the stiffness of the zone. A survey of results from stress measurements within Sweden, however, did not reveal any case where measured stress anomalies can be distinctly correlated with the presence of a fracture zone. This does not imply that stress perturbations induced by fracture zones are insignificant, but merely shows that current data are insufficient to allow conclusions in this respect.

Studies of induced fault slip in deep mines show that the deformation of destabilized faults is composed of both aseismic creep and seismic stick-slip behavior. This complex mode of shear deformation is a consequence of the presence of the indicated types of macroscopic surface irregularities, affecting the distribution of stress and strength over the fault plane. Determination of fault zone geometry has therefore been found critical in order to qualitatively understand the deformation process, whilst attempts to accurately determine strength properties like friction angle have been found less rewarding. Modelling, in combination with experience-based strength criteria is useful for indicating areas liable to slip deformation, but is essentially incapable of predicting the different modes of shear deformation observed.

The cohesive contribution to the shear strength of fracture zones is generally insignificant. Frictional properties were extracted from observations in mining and from stress measurements in seismically active areas. Values of friction angles were found to vary within the range 20-40°, but clustered at some 30-35°. Data are insufficient to discuss possible relationships between friction angle and level

of normal stress. Furthermore, no correlation could be established between size (taken as in-plane dimensions) of fracture zones and frictional strength. This is as would be expected, considering the fact that surface irregularities, decisively influencing shear resistance, occur on all scales.

With respect to representation of fracture zones in geomechanical models, conclusions from the present study are as follows:

- The internal structure of fracture zones can conceptually be represented in several ways by geomechanical models (distinct discontinuity, equivalent rock mass, fractured medium etc). The choice depends on, among other things, the relation between the scale of the problem to be analyzed and the size (in-plane dimensions and thickness) of the fracture zone. Although this is well recognized, mistakes are not uncommon.

- In geomechanical models, fracture zones are macroscopically almost invariably simulated as planar features, to which properties describing strength and deformability can be assigned. The inherent assumption is that surface irregularities controlling, for example, frictional resistance, occur on a scale that is much smaller than the scale of the fracture zone or problem under study. However, this assumption may be invalid since undulations and surface irregularities are found on all scales. The substitution of the fracture zone with a planar frictional feature may thus be principally incorrect.

- It follows that the current focus on more accurate determination of "standard" mechanical properties, as requested by the models, and on parametric studies to investigate the effects of these properties, needs to be complemented by investigations to clarify the actual geometry and morphology of fracture zones, such that they can be more realistically represented. Borehole investigations are not sufficient for this purpose. Existing knowledge in structural geology can contribute, but there is also a need for direct field investigations, including observations from underground facilities.

- Current modelling technology is essentially incapable to resemble the complex combination of stable shear deformation and stick-slip behavior that characterize fault slip, as induced by natural or artificial forces.

1 INTRODUCTION

In recent years, major research efforts have been devoted to the mechanical behavior of discontinuities in rock. This growing research interest is partly a result of the development of geomechanical modelling tools capable of simulating discontinuous rock masses, provided that realistic material properties are available. Another contributing factor is the evolvement of geoscientific issues requiring understanding of the mechanics of individual discontinuities as well as their contributions to overall rock mass behavior. This applies in particular to the problem of hazardous waste disposal in hard rock formations.

The bulk of investigations on the mechanical properties of discontinuities refer to the laboratory scale, i.e. up to about 1 m. A lesser number of field investigations producing results in the meter - or at most 10 m - scale have also been conducted. Thus, the scale interval considered roughly corresponds to the in-plane extensions of typical joints and fractures.

Despite their importance in many geomechanical applications, much less attention has been paid to characterization of large scale discontinuities like fracture zones. In a nuclear waste context, for example, the mechanical behavior of fracture zones is of concern in several respects. Problems posed include assessment of the risk for large-scale shear displacements along fracture zones, induced by future changes of the stress field and the potential effects of such phenomena on repository integrity. It also appears unavoidable that fracture zones will be encountered within the volume of rock hosting the repository, and their characteristics will therefore have practical consequences for repository construction.

The shortage of mechanical data for fracture zones is not difficult to explain. Firstly, there are major difficulties associated with predicting the character of large structural features on the basis of small-scale observations. Furthermore, the number of "full-scale" experiments involving controlled alteration of loading conditions on fracture zones and monitoring of rock mass response are, for obvious reasons, extremely few. Underground mining is about the only form of rock engineering activity that causes stress perturbations on a scale that is large enough for this purpose and that also allows close monitoring of fracture zone response to the load changes imposed.

It also appears that the information available on the topic is diversified and occurs over a wide range of geoscience. As indicated above, underground mining is one such branch. It is more or less unique in that it hosts many examples of actual large scale observation of fracture zone behavior under well defined loading conditions. Other applications in rock engineering, such as dam construction and reservoir engineering, have contributed data on a more occasional basis. The most substantial body of knowledge on fracture zone characteristics is undoubtly to be found in the field of structural geology. Besides the purely descriptive part, this includes a developing framework of mechanical theories and concepts to explain

many of the complex mechanisms responsible for initiation and development of fracture zones in brittle rock. Seismotectonics, in turn, can provide data on slip events of faults involving seismic energy release. Although the amount of data available from this source is substantial, there are limitations associated with the fact that parameters measured refer to the dynamic range only. Finally, research related to disposal of nuclear waste has included comprehensive investigations of fracture zones, essentially by means of surface- and borehole methods.

Unfortunately, each of these geoscientific disciplines providing such information are concerned with their own specific set of problems, use different terminologies and often represent different conditions as regards depths, stress levels and scale. Work seems to progress with far to little interaction between the various fields. As a result the available knowledge on the mechanical characteristics of fracture zones is diversified and difficult to overview.

The present study is an effort to bring together and condense information from some of these sources, and to present it in such a way that it can be viewed in context. It is hoped that this will facilitate proper consideration of fracture zones in addressing the geomechanical issues related to siting, construction and performance a repository for nuclear waste in crystalline rocks. The data compiled have primarily been gathered from borehole investigations and observations in connection with rock engineering activities, including mining, in relevant geological environments. The fracture zones considered represent a scale interval that can loosely be described as large enough to be out-of-reach by conventional methods of laboratory and in-situ testing, but small enough to be of concern in problems on the scale of a nuclear waste repository.

2 DEFINITIONS AND CONCEPTS

2.1 Definitions

The basic definition of the term "zone" in geoscience has been formulated as follows (AGI, 1960):

> "A belt, band, or strip of earth material, however disposed, characterized as distinct from surrounding parts by some particular property or content."

Following this general definition, the definition of the term "fracture zone" has been formulated as a zone exhibiting an intensity of natural fracturing that is at least two times higher than in the surrounding rock (Bäckblom, 1989).

The term fracture zone is thus by definition non-genetic and has a relative meaning only. The present study, however, is confined to fracture zones that are results of localized shear deformation. Such fracture zones are commonly termed shear zones, and are sub-planar features with extensions in their own planes that are at least two orders of magnitudes larger than their widths. The mode of deformation responsible for shear localization may be either brittle or ductile, and in most shear zones both modes are represented. This is especially so in rock with a long and complicated tectonic history, like the Swedish bedrock. Faults and fault zones can be defined as shear zones that exhibit appreciable brittle shear deformation (fault displacement) localized to one or a few through-going shear planes. The mechanical parameters discussed here refer to brittle deformation. Many of the fracture zones from which information has been gathered are either faults or fault zones.

2.2 The scale problem

Figure 1 illustrates a fracture zone as it may be conceived when observed in different scales. It is important to note that even if the feature, as observed at some scale, appears as a single distinct discontinuity, closer examination will always reveal that it comprises smaller structural elements. Inversely, if the scale were expanded, the fracture zone would be found to be genetically related to some larger, lower order structure.

Similarly to "ordinary" fractures, fracture zones may be considered in conceptually different ways in geomechanical analysis. The choice of conceptual representation is essentially governed by two factors:

- The scale of the problem to be considered in relation to the scale of the fracture zone

- The possibilities to determine the desired properties of the fracture zone

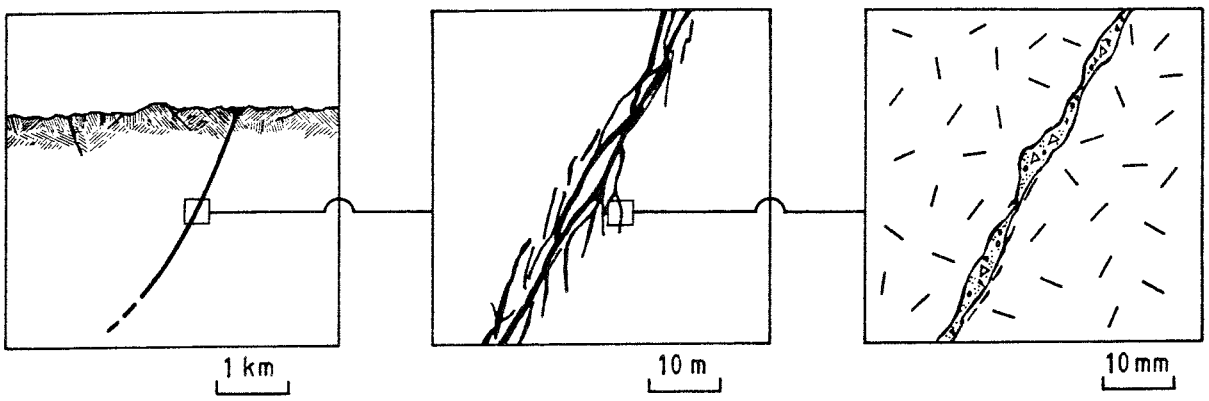

Figure 1. A fracture zone and its elements as viewed in different scales.

The importance of scale relations become obvious when considering the two examples in Figure 2. In general terms, the problem to be analyzed may concern either alterations of the system imposed by human activity, or natural processes. The figure shows one example of each category, both of direct relevance in a nuclear waste disposal context. The stability of the hypothetical fracture zone during periods of future glaciation is of concern because of the risk for large shear displacements affecting repository integrity. In analyzing this problem, it is clear that the fracture zone can be viewed as a single feature, and that its global strength properties are of concern. In contrast, the excavation of an access tunnel through the same fracture zone holds potential problems in terms of tunnel stability. Here, the features of concern are the local fractures and their properties, degree of rock alteration etc, while the global characteristics of the fracture zone are not important.

In the case of "man-made" perturbations, it is important to recognize that scale relations also govern the extent of mechanical interference between the fracture zone and the created structure. This is illustrated in Figure 3 for some examples of artificial loading on different scales. As indicated in the upper part of the figure, the conditions within the comparably small rock volume disturbed by, for example, tunnels of conventional dimensions, may be affected by neighboring fracture zones of much larger dimensions (e.g. in terms of stress conditions forming boundary conditions to the tunnel problem). The large zone is, however, not mechanically affected by the creation of the tunnel, other than perhaps locally if the tunnel intersects the zone (see the case in Figure 2).

Proceeding to cases where the dimensions of the fracture zone are comparable with the dimensions of the engineered structure, here exemplified by mines and nuclear waste repositories, there may be mechanical interaction between the zone and the engineered facility, which must of course be considered in analyzing the situation. Thus, mining at depth is often seen to cause changes of stresses acting across fault zones, sometimes resulting in fault slip and associated deformations that can seriously affect mining. Similarly, the thermomechanical loading of the rock mass accompanying heat dissipation from a nuclear waste repository will affect large volumes and eventually interact with neighboring fracture zones. Due

to the small magnitudes of the thermomechanical stresses involved, it is unlikely, though possible in principal, that this interaction will alter global stability.

Finally, applications where fracture zones represent a smaller or much smaller scale than the engineering effort as such are uncommon. As indicated in Figure 3 loadings from large water reservoirs is an example. The loadings on fracture zones in the bedrock beneath the reservoir will undoubtly change when the reservoir is filled. Whether or not the response of the zones has any effect on the reservoir depends on the more exact scale relations as well as other factors.

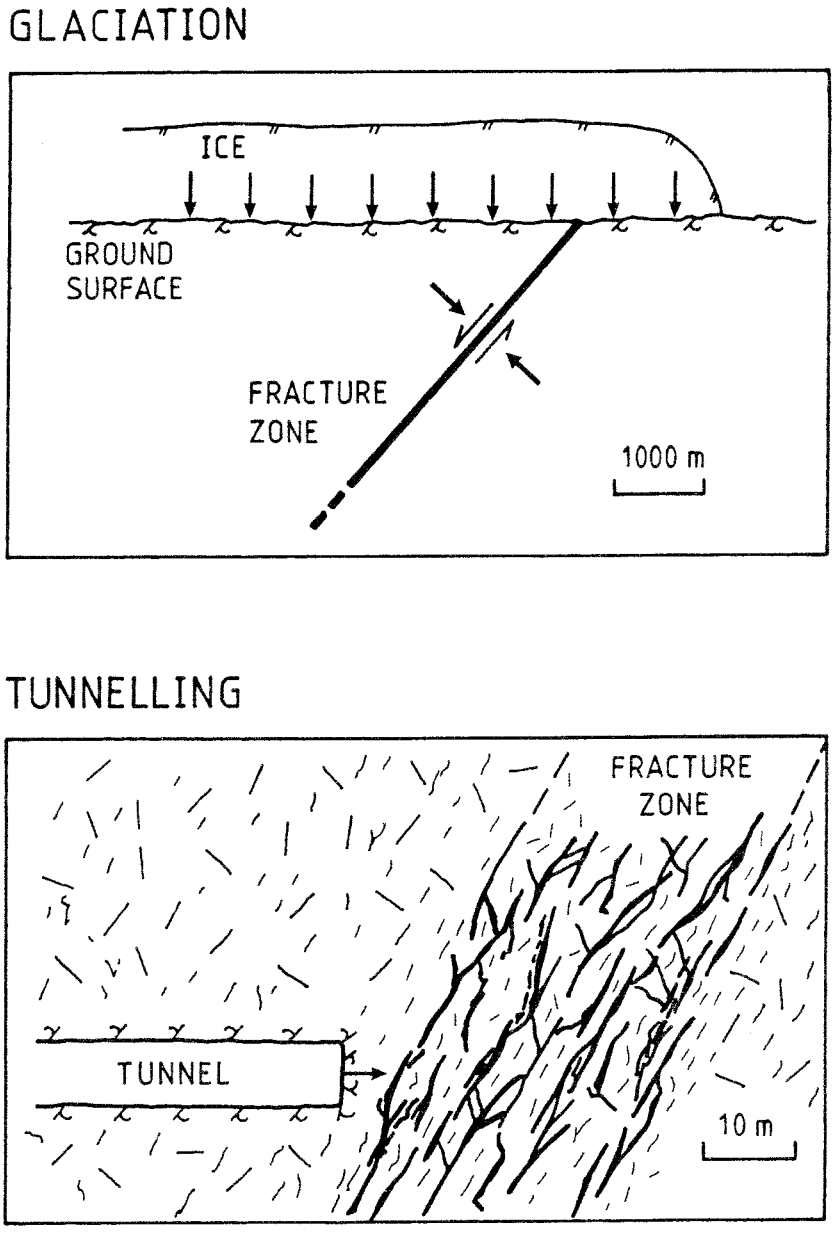

Figure 2. Two different geomechanical problems requiring different representations of a fracture zone; Global stability of the fracture zone during periods of glaciation, and stability of a tunnel being excavated through the zone.

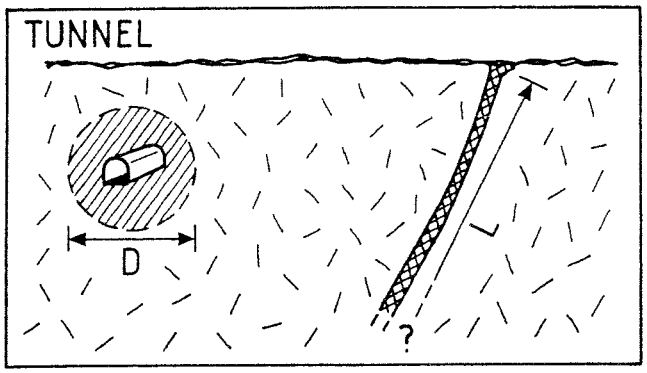

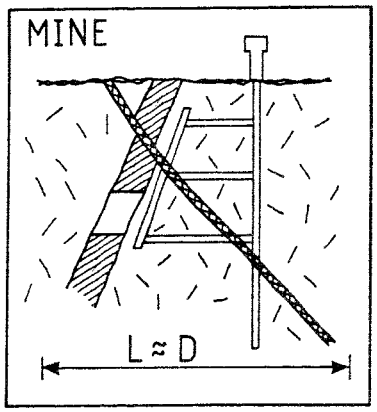

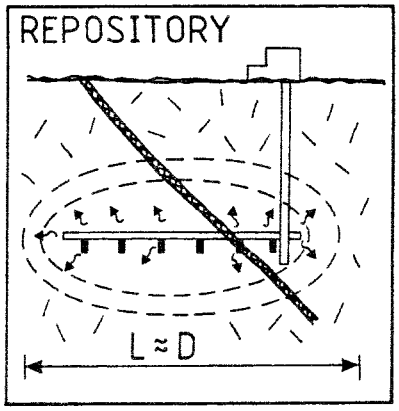

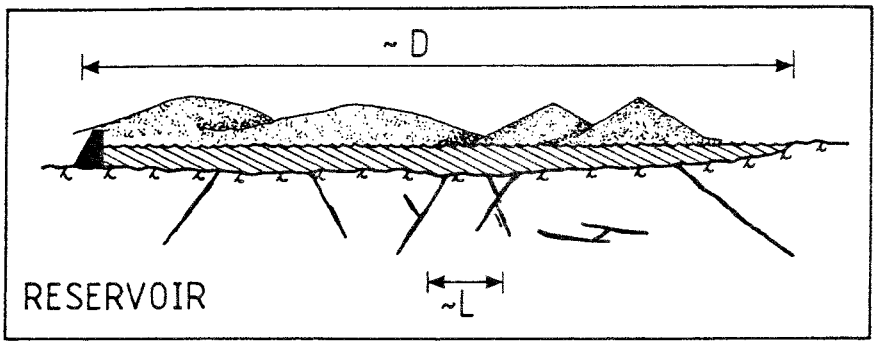

Example	Scale relation	Zone affects problem	Problem affects zone
Tunnel	L >> D	Yes	No
Mine	L ≈ D	Yes	Yes
Repository	L ≈ D	Yes	Yes
Reservoir	L<D, L<<D	?	Yes

Figure 3. Four examples of scale relations between fracture zones and engineered structures in rock. L denotes extension of fracture zones, and D is the dimension of the engineered structure/problem to be analyzed.

2.3 Available models

2.3.1 Simple stress models

Major achievements in the study of the mechanics of fracture zones have been made by applying simple, analytical models, of which some are limited to stress analysis only. This includes, for example, the problem of shear strength and potential for reactivation of existing fault zones and its relation to in-situ stress conditions. The Mohr-diagram shown in Figure 4 illustrates the fundamental concept of frictional strength and effective static stress that is commonly applied in such analysis. Basically, the discontinuity is seen as a plane subjected to normal -and shear stress components that are readily obtained from the Mohr circle of stress, defined by the maximum and minimum effective principal stresses, σ_1 and σ_3. Figure 4 refers to a two-dimensional analysis, but the concept is easily extended to the three-dimensional case. The discontinuity is assigned a Coulomb-type failure criteria, which states that the shear strength is fully determined by a stress-independent friction angle, possibly with the support from a cohesive component that is:

$$\tau_s = c + \sigma_n \tan\phi \qquad (1)$$

where

τ_s = shear strength
c = cohesion
σ_n = effective normal stress
ϕ = friction angle

Alternatively, the friction is expressed by the coefficient of friction, μ, given by:

$$\mu = \tan\phi \qquad (2)$$

Note that the analysis does not consider deformations, and hence the parameters involved are those describing stress and strength only.

In Figure 4, the concept is applied to investigate the problem of reactivation of existing structures versus formation of new ruptures by shear failure of the "intact" rock. It is assumed that the intact material has a cohesive strength component, while the strength of the pre-existing structures is due to frictional resistance only. In the example, the given stress state is just sufficient to cause shear failure of intact rock in the direction given by the angle $\pm\alpha$. However, prior to that, any preexisting structure oriented within the interval $\pm\beta_1$-β_2 will have been reactivated. The illustration is schematic only, but the concept can be extended, and has been extensively applied to study the relations between fault stability, in-situ stress regimes, pore water pressure and strength parameters (Ivins et al., 1990; Ranalli and Yin, 1990; Sibson, 1985).

a)

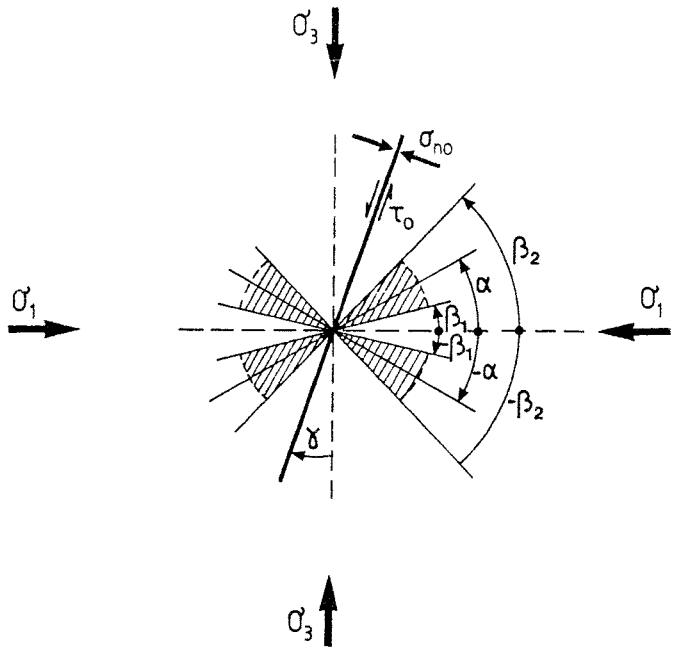

b)

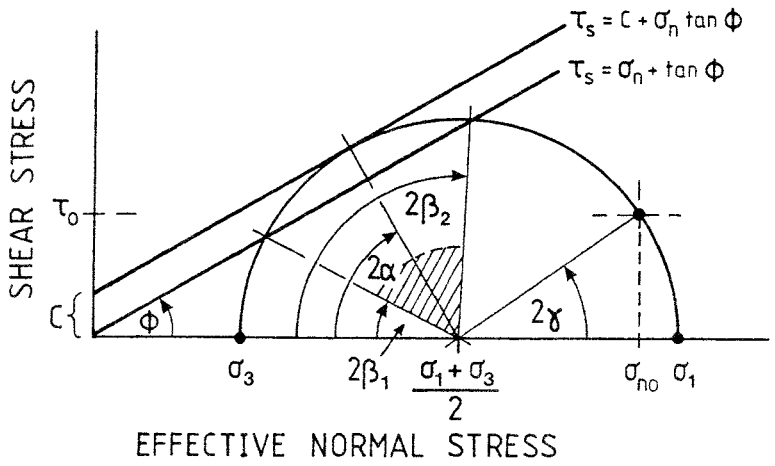

Figure 4. Example of application of simple stress analysis to study the potential for fault reactivation.

a) Physical situation in the plane containing the maximum and minimum principal stresses.

b) Representation of stress conditions (half-circle) and failure criteria for intact rock (upper straight line) and fault (lower straight line) in a Mohr-diagram.

σ_1, σ_3 = maximum and minimum effective principal stresses

$\pm\alpha$ = angles in which shear failure through intact rock is possible

$\pm\beta_1$, β_2 = for the given stresses, preexisting faults oriented within the angular section defined by β_1 and β_2 will be reactivated

σ_{n0}, τ_0 = normal- and shear stresses acting on indicated fault plane. The fault will remain stable under the given stress field.

ϕ = friction angle

c = cohesion of intact rock.

Simple stress analysis and Mohr-diagrams are also very useful for qualitatively understanding stress changes, and potential consequences thereof, related to man-made disturbances. The case of a water reservoir as was illustrated in Figure 3 is one example. Figure 5 shows the principal nature of stress changes associated with reservoir filling, fluid injection of faults and quarrying. These are all activities that have been proven to trigger fault movements, sometimes in the form of earthquakes.

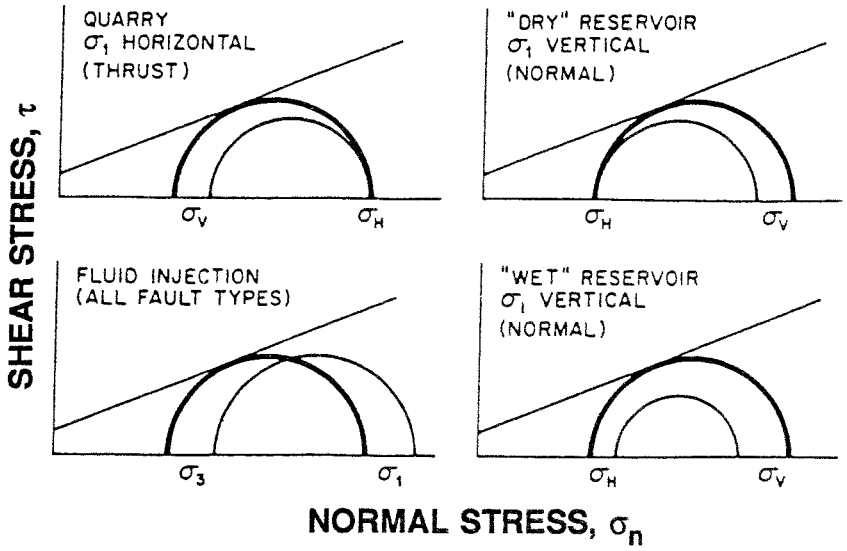

Figure 5. Mohr-diagram representation of stress changes associated with induced fault movements. Thin circle is before - and heavy circle after - load change. σ_H and σ_V are horizontal and vertical stresses, also assumed to be principal stresses. σ_1 and σ_3 are arbitrarily oriented principal stresses.
Upper left: Removal of overburden by quarrying reduces vertical stress.
Lower left: Hydraulic pressurization of a fault plane reduce effective normal stresses, cf. section 8.2.
Right: Reservoir filling that increases vertical stress (upper) and reduces effective stress by increasing pore water pressure (lower) underneath the reservoir (from Scholz, 1990).

2.3.2 Models in rock engineering

In rock engineering applications the general purpose is to quantify rock mass deformational response to imposed loadings. This often includes analysis of rock behavior both before -and after failure. This requires quantification of both loading conditions and deformational properties of the rock mass, and simple stress models are obviously no longer sufficient. As indicated in section 2.2, fracture zones may have to be considered in conceptually different ways depending on the relations between the scale of the structure and the problem of concern. Figure 6 attempts to summarize commonly used modelling concepts and associated mechanical key properties. Various combinations of these concepts may also be applied.

On a global scale, the effects of fracture zones may be accounted for in an indirect manner, by weighting the contribution of the fracture zones into averages of bedrock properties taken over larger volumes This "equivalent rock mass" approach is often relevant in problems related to crustal mechanics, but rarely in engineering applications. It is therefore not indicated in Figure 6.

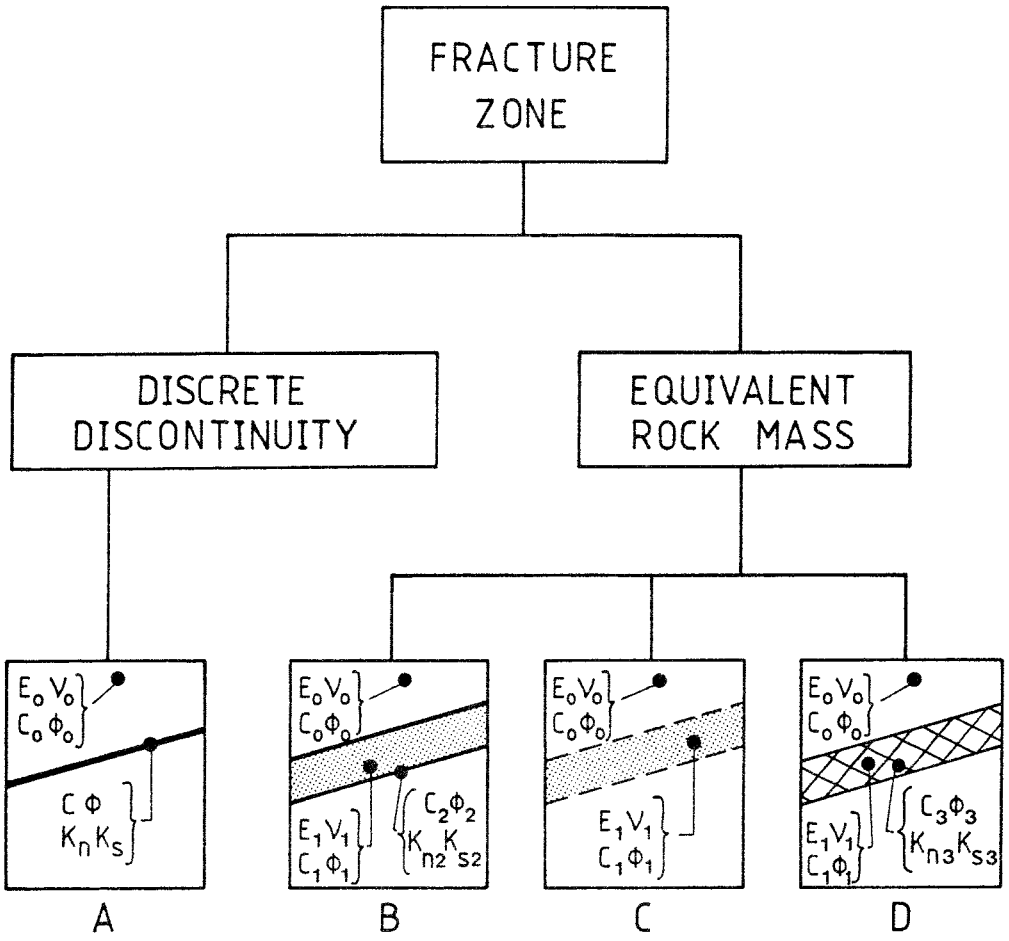

Key properties	Unit				
	Zone	Host rock	Material within zone	Bounding discont.	Discont. within zone
Deformation modulus		E_0	E_1		
Poisson's ratio		υ_0	υ_1		
Cohesion	c	c_0	c_1	c_2	c_3
Friction angle	ϕ	ϕ_0	ϕ_1	ϕ_2	ϕ_3
Normal stiffness	K_n			K_{n2}	K_{n3}
Shear stiffness	K_s			K_{s2}	K_{s3}

Figure 6. Representation of fracture zones in geomechanical models, and associated key properties.
A: Discrete discontinuity.
B: Equivalent rock mass, discontinuities at boundaries
C: Equivalent rock mass, all-continum
D: Discrete representation of internal fracturing within zone.

When a fracture zone is modelled as a discrete discontinuity, or an array of discrete discontinuities, the model concepts available are identical to those used to simulate individual joints and fractures. The discontinuity is generally not assigned any specific width. This, however, does not preclude normal deformation across the discontinuity to be adequately simulated. Initial deformational behavior is given by the normal stiffness, K_n, and the shear stiffness, K_s of the discontinuity. Strength characteristics and post-failure behavior attributed to the discontinuity can be more or less complicated functions of stress or deformation. This topic is discussed in more detail in chapter 5. Key properties with respect to shear failure are friction angle and cohesion. Shear displacement can alter discontinuity surfaces in several ways, e.g. by breakage of cohesive bridges or frictional wear of asperities accompanied by formation of granular material. These processes affect shear strength, and different strength values may have to be specified to represent conditions at onset of loading, at mobilization of maximum shear resistance and at residual conditions. Figure 7 shows a simplified shear strength - shear deformation representation that is commonly used in geomechanical modelling. Another important parameter, that is not discussed here, is the dilation, which expresses the separation or contraction that the discontinuity surfaces will undergo during shear displacement. Dilation is strongly dependent on the level of normal stress across the discontinuity.

The deformation- and strength properties are intended to indirectly account for the effects of surface irregularities on a scale much smaller the extension of the discontinuity in its own plane. Macroscopically, discontinuities are generally simulated as planar features with deformation- and strength properties that do not vary over the plane. However, important exceptions exist. One is the assessment of the potential for induced, seismic fault slip in connection with deep underground mining, where it has been found crucial to adequately represent true fault zone geometry, including undulations on a scale similar to -and smaller than the scale of the problem studied.

If the fracture zone has a significant width in comparison to the problem studied, it must be represented as a section of the rock mass, characterized by properties that contrast to those of its' surroundings. Boundaries to the host rock mass may be assumed to be continuous or defined by discontinuities. To define the internal characteristics of the zone, the effects of the constituents - intact rock, fractures, granular material etc - must be considered. This may be done either by superimposing the contributions of these components and defining bulk parameters of the resulting equivalent rock mass, or by discrete representation of the internal fracturing. In the former case, important mechanical properties are deformation modulus, E, Poisson's ratio, υ and strength properties like c and ϕ (or others depending on strength criteria used). Alternatively, deformability can be expressed in terms of K_n and K_s, which are functions of E, υ and fracture zone dimensions.

All these parameters may be stress-dependent. Anisotropic behavior, i.e. different properties in different directions, may be simulated. In the case of discrete representation of internal fracture network within the zone itself, one set of parameters is required to define fracture geometry and mechanical properties and another set to specify the intact rock material.

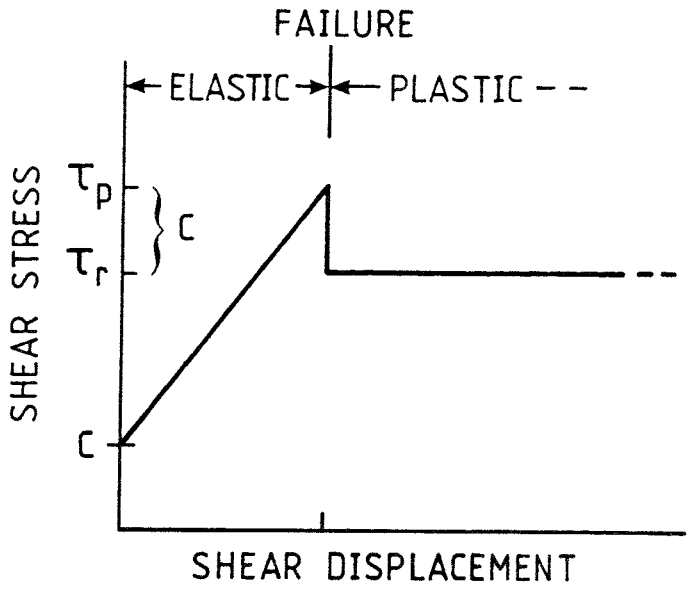

Figure 7 Shear deformation behavior of a discrete discontinuity, commonly assumed in rock engineering analysis. Shear deformation is elastic up to failure, at which cohesive strength is lost. Post failure behavior is ideally-plastic. τ_p and τ_r denote peak- and residual shear strength respectively.

2.3.3 Models in structural geology and earthquake analysis

While simple stress models of the kind described in a previous section are often applied in fundamental studies of fracture zones from a structural geological viewpoint, analysis of many of the problems posed in this field requires much more complex models. These include phenomena such as brittle formation and growth of individual discontinuities, and linking of preexisting fractures, i.e. localized shear deformation in brittle rock. Presently, fracturing through intact rock can not be well simulated by means of the modelling techniques that are well established in engineering practice. The more recently evolved concepts and theories of fracture mechanics and damage mechanics have, however, found extensive application in this field. The present status of development in this area may to some extent be characterized as experimental. Some examples of fracture patterns that are results of localized shear, and often observed in fracture zones, are given in chapter 4. The framework available for mechanical analysis of these phenomena will however not be further discussed.

Earthquake mechanics is another area where complex models have evolved. An important issue is the understanding of mechanisms and parameters that govern transition from fault slip by stable creep, to the development of stick-slip behavior accompanied by seismic energy release. Stick-slip shear deformation may be described as the process of accumulation of elastic strain energy due to locally enhanced shear resistance of a discontinuity, followed by dynamic, partial or complete, release of this energy. Important properties in this process are friction and its dependence on magnitude and rate of shear displacement, and stiffness parameters of the system.

3 SOURCES OF DATA

3.1 Geological observations

The long geological history of Swedish bedrock reflects fracture zones characterized by a complicated deformational history, including the formation at large depths and later brittle deformation resulting from multiple phases of reactivation under different stress regimes. Assessment of the these modes and sequences of deformation is largely based on interpretation of data from geological observations. Furthermore, laboratory tests and mathematical models can be used as aids to resolve the fundamental mechanisms responsible for the deformation modes observed in the field.

However, besides known deformations, quantitative determination of material properties defining strength and deformability requires knowledge about the generating stress field. Unfortunately, the stress field and its variation over geological time can not be inferred from observations of today's conditions, to the same level of accuracy as deformation. There remains, for example, considerable uncertainty as regards stress conditions accompanying even recent loading epochs such as the latest sequence of glaciation (Leijon and Ljunggren, 1992). As a consequence, data on mechanical characteristics of fracture zones, as inferred from geological evidence of past deformation phases, tend to be qualitative or at best semi-quantitative.

An obvious alternative to indirect interpretation of past sequences of events is the observation of ongoing deformation resulting from currently acting stress fields. Thus, seismology has provided insight into fault slip behavior in the dynamic range. Parameters that can be determined from seismic data include stress drop, radius of the slip surface and slip magnitude (see e.g. Scholz, 1990 for an overview). There are, however, important limitations associated with the seismic results. Firstly, there are uncertainties in the interpretation procedures as such. Secondly, the majority of seismic events recorded in Swedish bedrock occur at depths below some 3000 m. This implies stress levels that are poorly known, but definitely much higher than those within the uppermost 1000 m, which is approximately the horizon presently covered by stress measurements. Thirdly, out of the total energy released in the process of shear deformation, only the seismic component is observable. This component can be related to dynamic stress drop, but not to total stress which is one of the key parameters required. In relative terms, the stress drop associated with most seismic events in Sweden is at most a few percent of the absolute stress level.

3.2 Sampling, testing and case studies

The alternative to geological interpretation is direct sampling and/or testing at some scale. Determination of strength- and deformational properties should preferably refer to a scale that comply with that of the fracture zone and the load case considered (cf. Figure 3). This requirement is obviously very difficult to meet

in practice, which is the reason for the current shortage of "hard data" on mechanical properties of fracture zones. As for rock mass characterization in general, two approaches are available:

1) Small-scale sampling and testing to determine geometrical distribution and properties of the components of fracture zones, i.e. intact rock, fractures, fracture filling material etc. Superposition of these component characteristics, possibly in combination with scaling procedures, then yields characteristics at the desired scale.

2) Large-scale field observations, either by means of specifically designed experiments, in connection with rock engineering efforts involving load changes.

Most data refer to the small-scale approach, i.e. category 1) above. Available information include a wealth of laboratory-scale data and a lesser amount of field testing data in a scale interval ranging up to at most a few meters. Borehole testing is another source of small-scale data. Considerable efforts have been devoted to the development of procedures allowing mechanical properties of intact rock and fractures to be combined/scaled up such that rock mass characteristics can be predicted. Much of this work is empirical and utilizes large-scale observations to calibrate the procedures. Cunha (ed., 1990) provides a good coverage of the current status in this field.

There are some important drawbacks attached to the "small-scale approach". One is that the fundamental mechanisms of deformation as occurring at some larger scale may be difficult or impossible to predict, simply because they are not observed in the small scale. Another is potential sampling bias. Besides the general problem of collecting enough and appropriately distributed samples to describe the desired properties and their spatial variation, there are practical limitations. Sampling by core drilling is an illustrative example. Cores provide good sampling in sections with good rock quality, whereas sections containing low-strength material such as clay or fault gouge are typically represented as core loss. With respect to fracture zones, the difficulties encountered in sampling and testing of poor-quality rock material have serious implications because these materials constitute weak links that can have a major impact on overall behavior of a zone.

Case studies involving large-scale observation of fracture zone behavior (i.e. producing data of category 2 above) are rare. The main reason is that underground facilities, which are otherwise the main sources for collection of information on "full-scale" rock behavior, represent a scale that is still too small in the present context. Fracture zones are thus not disturbed other than at most locally (cf. Figure 3) and resulting deformations are confined to correspondingly small volumes. As indicated earlier, important exceptions are found in the field of mining. In some deep mines where high rock stresses prevail, strength properties of fault zones are of particular concern because of the potential risk for mining-induced seismic fault slip - a phenomena that can have serious implications on mining safety (e.g. van Aswegen, 1990). In such environments, even rather local excavation-related disturbances of the stress field can trigger movements on much

larger scales along critically loaded faults. Another rock engineering application that requires accurately determined large-scale rock mass properties is design of dam foundations. Experience from this field, however, relates primarily to low-stress (shallow) environments and mostly concern rock mass properties in general, rather than focusing on large-scale structures. Water reservoirs, finally, have already been mentioned as an engineering activity resulting in very large-scale loadings. Observations of fracture zone behavior in that context are however confined to seismic data.

Fracture zones have been extensively investigated within nuclear waste isolation programs in a number of countries. Swedish contributions include field investigations at several study sites (Ahlbom et al., 1991a; 1991b; 1992), detailed characterization of fracture zones at the Finnsjön site and work done within the international Stripa Project (Martel, 1992; Olsson, 1992). These investigations have embraced a wide spectrum of geological, hydrogeological and geochemical issues, and involved characterization of fracture zones by means of surface and borehole techniques as well as observations from excavations. No large-scale mechanical experiments involving fracture zones have however been conducted in Sweden to date. As far as known, the only experiments, aimed specifically at investigating mechanical properties of fracture zones by means of observing response to controlled stress changes, are those conducted at the URL facility in Canada (Martin et al., 1990).

4 LOCALIZED SHEAR DEFORMATION IN BRITTLE ROCK

4.1 Introduction

From a macroscopic perspective, shear deformation of discontinuities is commonly seen simply as sliding along the contact plane between two more or less planar surfaces. As indicated earlier, this idealization may be appropriate in many applications. However, the formation and development of fracture zones involves complex modes of fracturing that characterizes shear localization. These fracturing processes and resulting fracture patterns display remarkable similarities at scales ranging from millimeters to several kilometers.

It is self-evident that the geometrical properties of the fracture pattern resulting from brittle shear localization will have a large influence on the mechanical properties of the fracture zone formed. The existing knowledge in this field has largely evolved within the realm of structural geology, and it is felt that it is not always fully recognized within the rock mechanics community. Therefore, a few but commonly observed modes of primary and secondary fracturing are illustrated below, and some useful references are given.

4.2 Homogeneous material

Figure 8 shows, in idealized form, structures typically developing in homogeneous, brittle material. The material is subjected to shear deformation, concentrated over the section A-B. Incipient fracturing occurs as extension cracking in the direction of the maximum principal stress. Rotational movement in later stages of the shearing process may cause propagation of the extension cracks such that they form characteristic "integral-shape" fracture surfaces (formation of tension gashes in more ductile material is an analogue mechanism). Following the extensional cracking is the formation of often prominent shear fractures in én-echelon arrangements with respect to the direction of overall shear deformation. These fractures are commonly termed "Riedel-shears", as a result of observations reported by Riedel (1929), who conducted shear experiments in clay. Two conjugate sets of Riedel shears may be distinguished, termed R_1 and R_2 respectively. R_1 fractures are generated first, and associated alterations of the local kinematics and stress field initiate R_2 fracturing. R_2-fractures are less prominent and typically terminate at intersections with R_1-fractures. A third category of shear fractures (termed P-shears or thrust shears) can under certain conditions develop in a direction as indicated in Figure 8.

Progression of shearing often forms curved fractures that interconnect the already existing én-echelon oriented (Riedel and thrust) shear cracks, Figure 9. The result is a zone with an anastomosed pattern of undulating structures, inter-layered by elongated lenses of relatively undisturbed material. With increasing total shear deformation, the amount of rock destruction by abrasive wear increases. Displacements become gradually more concentrated to a reducing number of through-going shear planes that grow in length and width. Eventually, these shear planes develop into one distinct "fault zone".

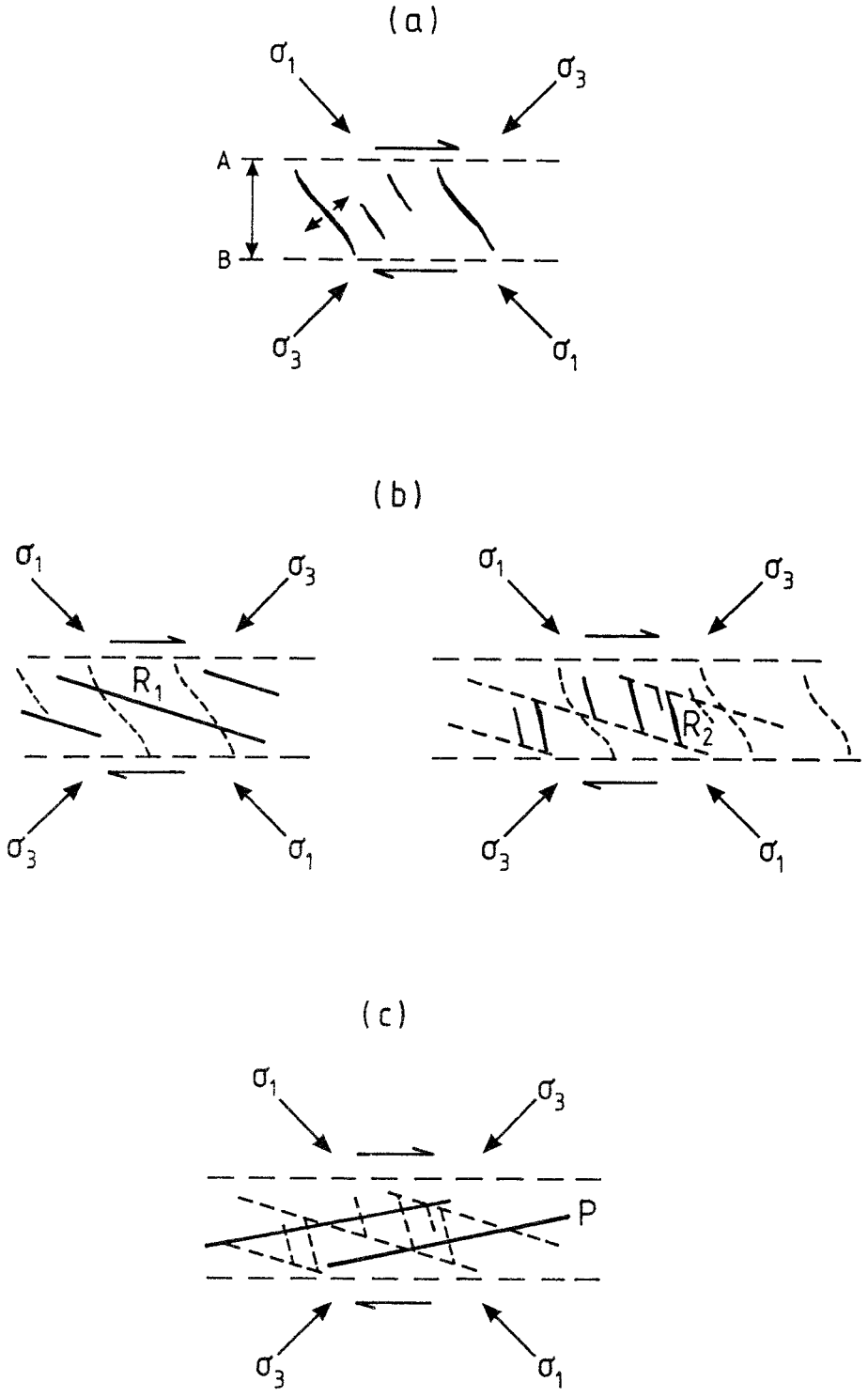

Figure 8. Schematic illustration of basic fracture types generated in homogeneous, brittle material subjected to localized shear deformation.

a) Extension cracks, parallel to the maximum principal stress, form within the section subjected to shear (A-B).

b) Development of Riedel shears (R_1) and conjugate Riedel shears (R_2).

c) Development of P-shears.

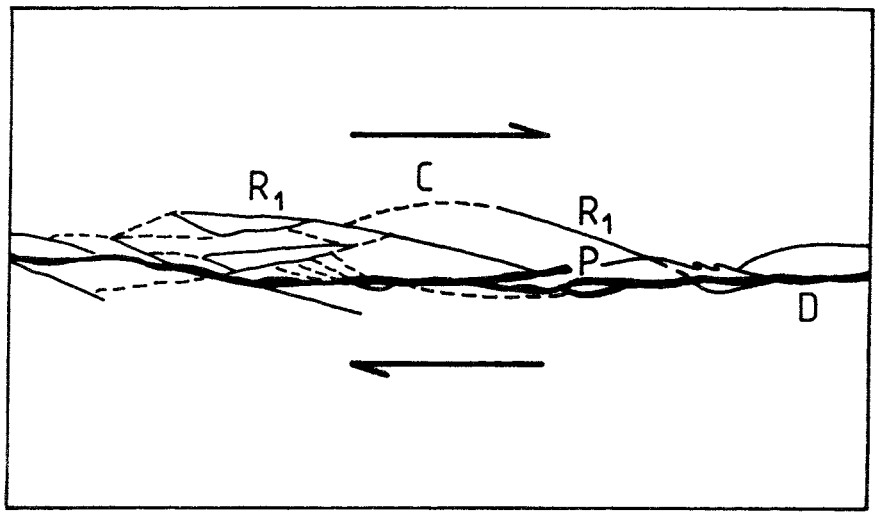

Figure 9. Interconnection of R -and P shears by curved "crack-to-crack" fractures (C) to form anastomosing fractures, through-going shear planes (D) and shear lenses (after Price and Cosgrove, 1990).

Figure 10 has been reproduced from Tchalenko (1970) and is a good illustration of the fracture patterns typically observed during formation of a shear zone according to the mechanism described above, i.e. from the onset of Riedel shears to formation of the first, major shear planes.

Riedel-type fracturing and resulting fracture zone development as indicated above is primarily observed in cases where the location and orientation of localized shear deformation is pre-determined by overall loading conditions, and when the material within the section subjected to shear is initially homogeneous. It has been extensively studied under laboratory conditions (Riedel, 1929; Tchalenko, 1970), in particular with reference to shear deformation in fault gouge (e.g. Chester and Logan, 1986; Marone et al., 1990). Field observations have been reported by several authors (e.g. Skempton, 1966). Passive development of fracture zones in cover rocks as a consequence of strike-slip faulting of underlying basement is often referred to as situation that well fits the requirement for Riedel fracturing, i.e. initially homogeneous material and externally controlled location of shear displacement (Price and Cosgrove, 1990). In old basement rocks, fracture zones exhibiting the described fracture patterns appear to be less abundant. This may be attributed to i) that these fractures are primary structures that are often obscured by different forms of brittle fracturing from subsequent phases of deformation, and ii) the often ductile origin of fracture zones in these rocks. However, two recent studies, both involving observations of fracture zones from intersecting drifts, have revealed primary Riedel shear structures (as well as fracturing attributable to other mechanisms) in granitic environments; One is the "Room 209 fracture zone" at the URL-facility in Canada (Tannant, 1990) and the other is "Zone H" at Stripa (Olsson, 1992).

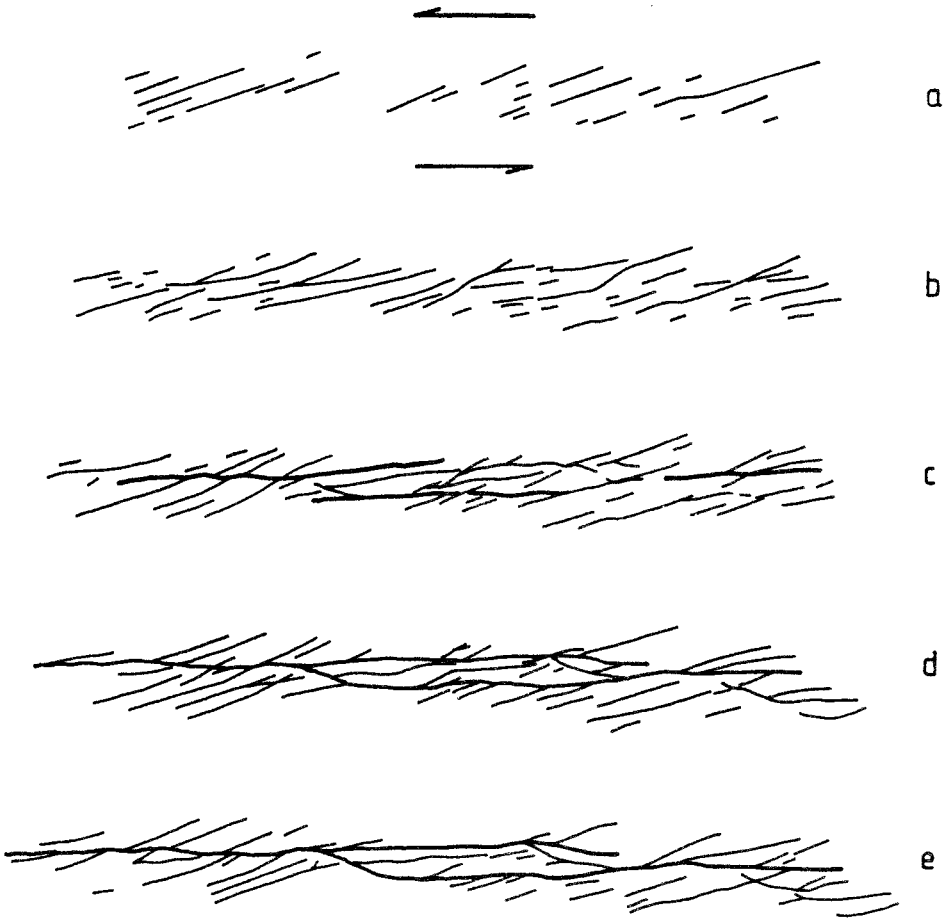

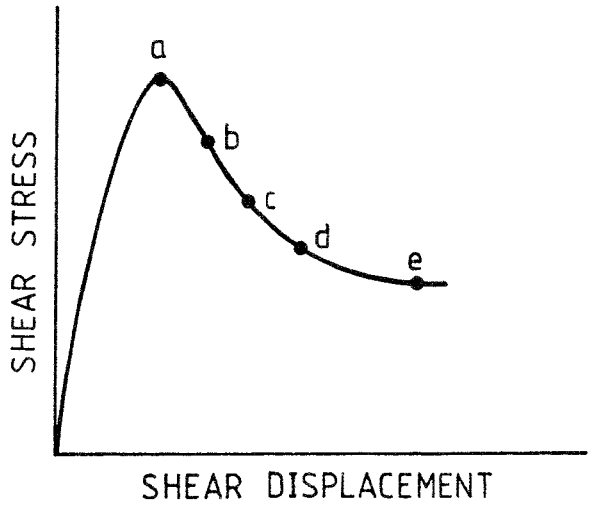

Figure 10. Illustrative example of the development of a shear zone in homogeneous material, from the occurrence of the first Riedel-shears (a) to development of the first through-going shear planes subparallel to the zone (e). The diagram shows qualitatively the corresponding stress-displacement curve (after Tchalenko, 1970).

4.3 Material with preexisting fractures

It is well recognized that development of localized shear deformation, especially faulting, takes advantage of pre-existing fractures that may have been formed by completely different mechanisms. This causes fracture patterns that are different from those discussed above for the case of homogeneous material. The range of combinations of pre-existing fracture geometries, external boundary conditions and resulting fracture patterns formed by localized shear is obviously almost infinite. The following figures attempt to illustrate, without further explanations in mechanical terms, examples of secondary fracturing observed for two simple cases of pre-existing fractures. Thus Figure 11 shows fracturing near the edge of a single crack parallel to the direction of an applied, simple shear loading. This case is of particular importance since it applies to the conditions at the ends of strike-slip faults. Figure 12 exemplifies fracturing linking together two right-stepping fractures subjected to right-lateral shear loading.

The above examples of fracturing related to localized shear deformation are given without further explanation in terms of stress conditions or mechanisms of fracturing, which are topics outside the scope of the present report. The figures illustrate, however, that formation of fracture zones are highly path-dependent processes, associated with complex local stress perturbations. In principal, the mechanisms are governed by three factors:

- The material characteristics (cohesion, friction, brittleness, state of pre-existing fracturing etc)

- The far-field stress conditions

- The kinematics of the system

The introduction of continuum fracture mechanics theory and advanced numerical modelling techniques have significantly improved the understanding of these processes (Atkinson, 1987; Segall and Pollard, 1980; Pollard et al., 1990) and the field is under rapid development.

Existing field studies clearly support the conclusion that whenever fracture zones are exposed well enough to allow detailed examination, a certain regularity in their internal structure is revealed. The extent to which early-stage fracture patterns prevail is of course highly dependent on the age and tectonic history of the structure. For example, visual observations of fracture zones intersected by drifts at Stripa (Martel, 1992) and URL (Tannant, 1990) have demonstrated a number of typical secondary fracturing features, including some of the patterns shown in Figures 11 and 12. A more large-scale example is shown in Figure 13; Wallace and Morris (1986) investigated in detail a large number of fault zones in deep mines in North America. They underlined as general conclusions the importance of dense observations from excavations to be able to resolve the morphology of fault zones, and that borehole information was insufficient for this purpose. The figure shows fault zones and typical secondary structures observed in the Coeur d'Alene mine, Idaho.

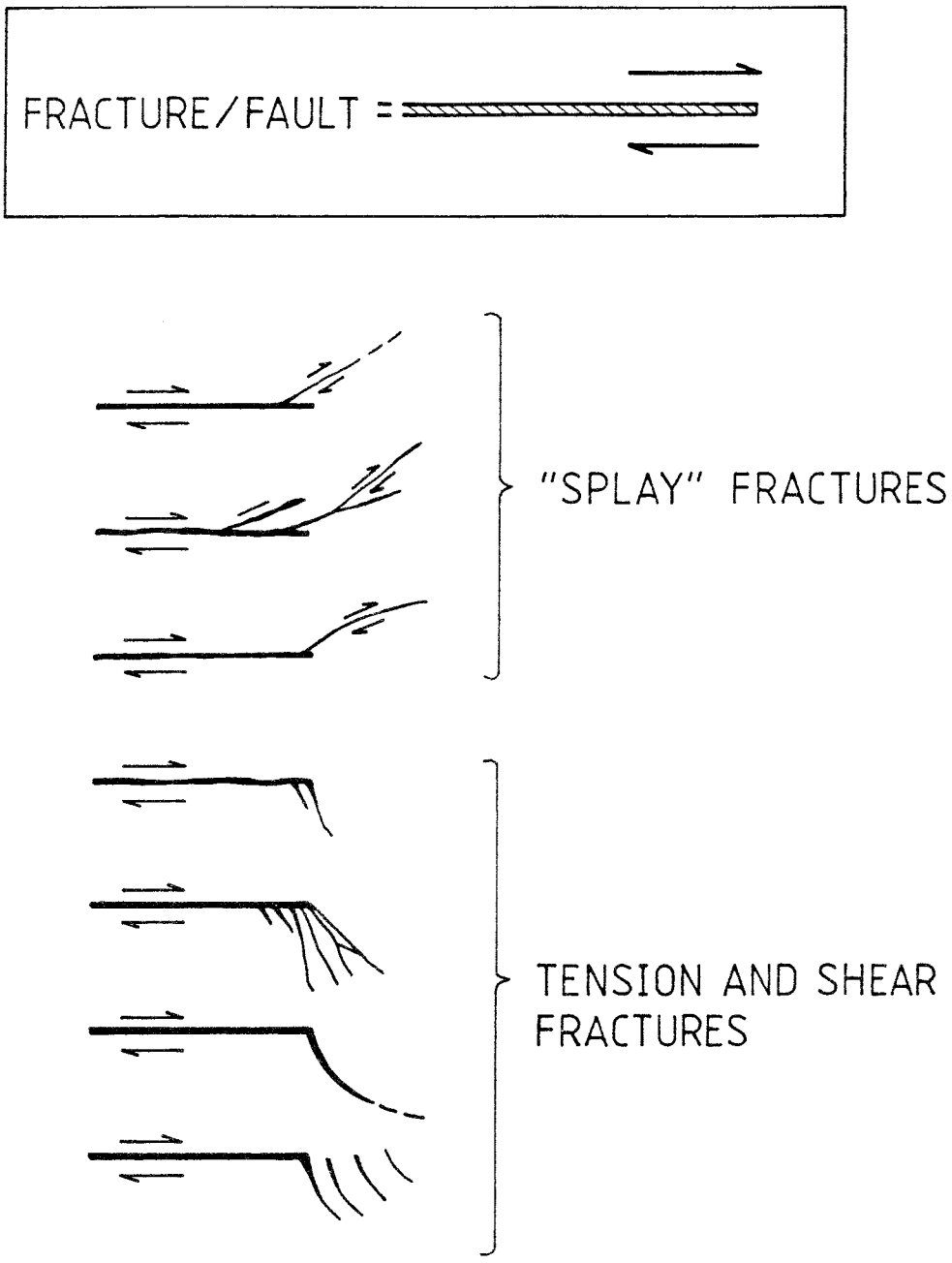

Figure 11. Examples of secondary fracturing due to stress concentrations at the edge of a fracture or fault subjected to right-lateral shear loading. Nomenclature according to Price and Cosgrove (1990).

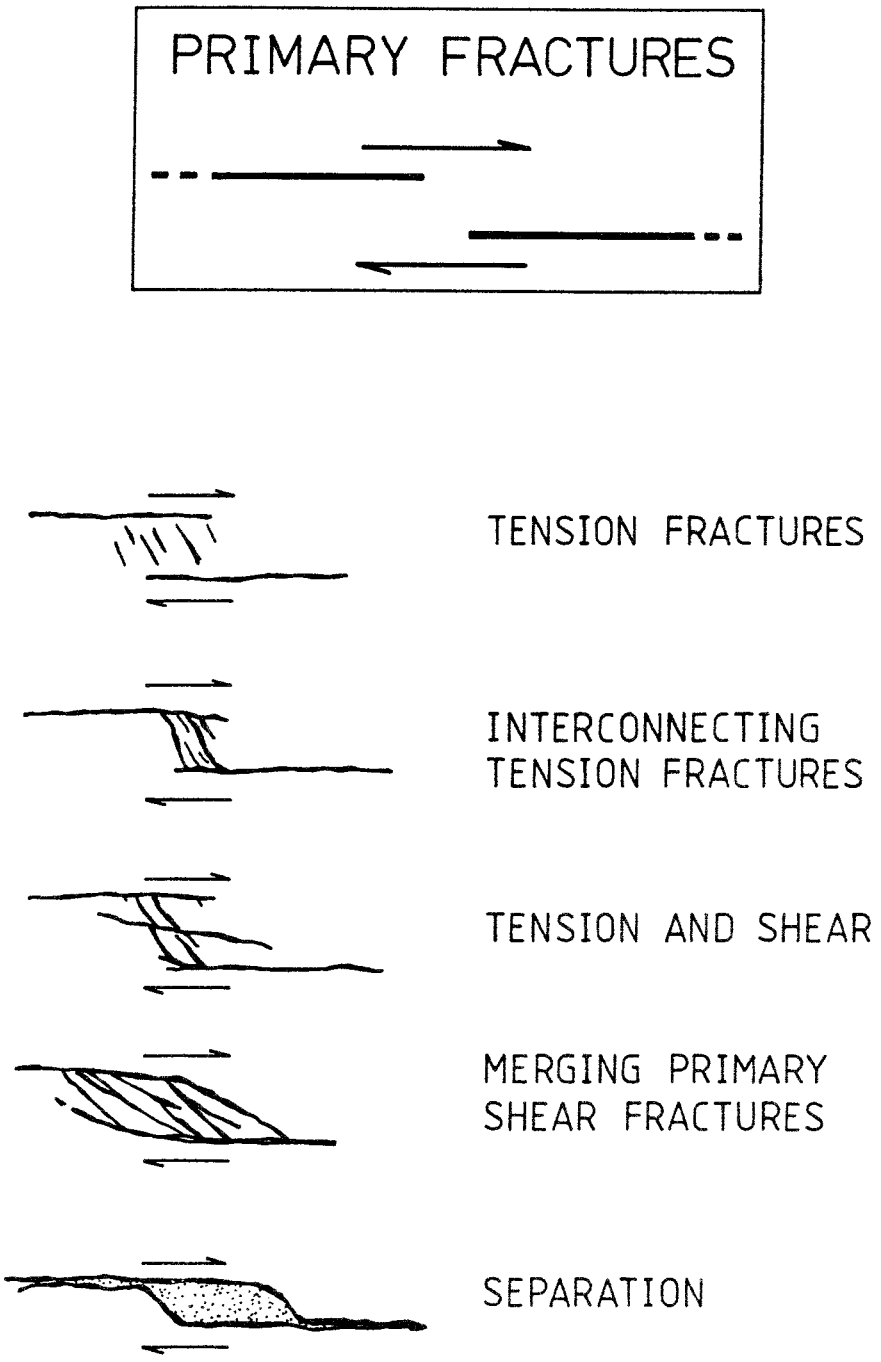

Figure 12. Examples of secondary fracturing, interlinking two right-stepping fractures subjected to right-lateral shear loading.

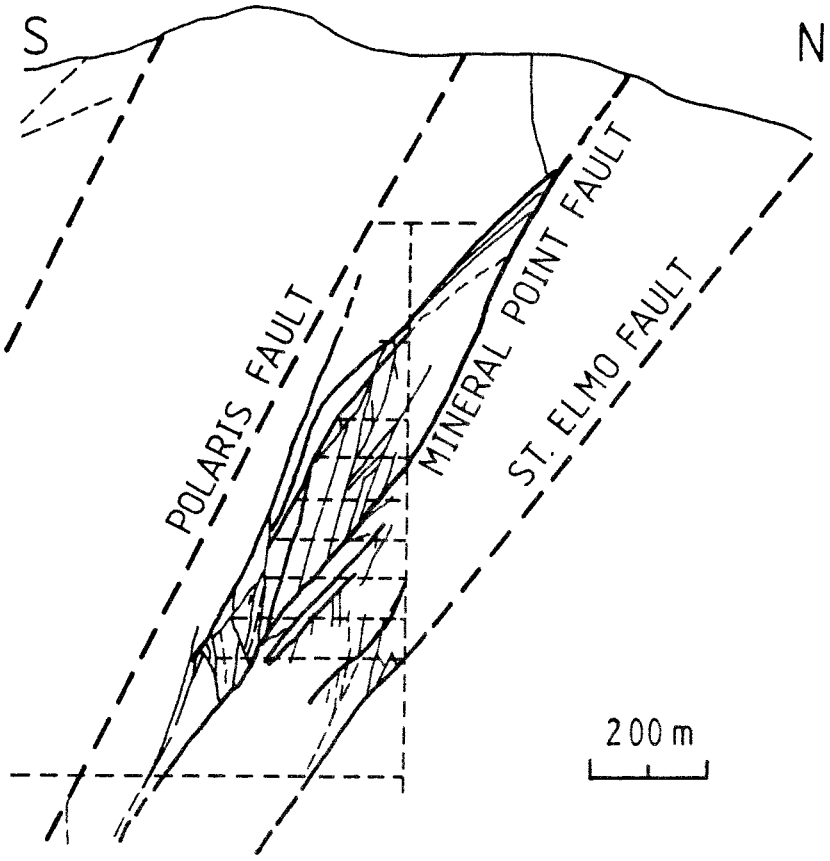

Figure 13. Vertical section showing fault zones at the Coeur d'Alene Mine, Idaho. Because of the dense network of mine workings (thin dashes) allowing observation, it was possible to determine the secondary structures within the Mineral Point fault zone. By contrast, note the crude interpretation of the adjacent Polaris- and St. Elmo faults at locations from which only borehole data were available (from Wallace and Morris, 1986).

The limitations associated with borehole data can also be illustrated with the subhorizontal fracture zone, termed Zone 2, at the Finnsjön Site, Figure 14. As summarized by Ahlbom and Tirén (1991), this fracture zone has been thoroughly investigated by means of a large number of boreholes. Results show that it originated from ductile shear deformation at depth, and that it has been repeatedly reactivated in the brittle regime, although resulting fracturing has probably not been accompanied by any major shear movements. Figure 14 shows a vertical profile, indicating the conceptual status of the fracture network composing Zone 2. As interpreted, it is a compound fault zone, comprising major, subparallel shear planes (faults) arranged in a stepwise pattern and interconnected by secondary

fractures of largely extensional origin (cf. Figure 12). It is interesting to note that, despite the dense borehole information, the geometrical model of the zone still relies partly on general knowledge about secondary fracturing and formation of compound fracture zones (notably work by Martel, 1990).

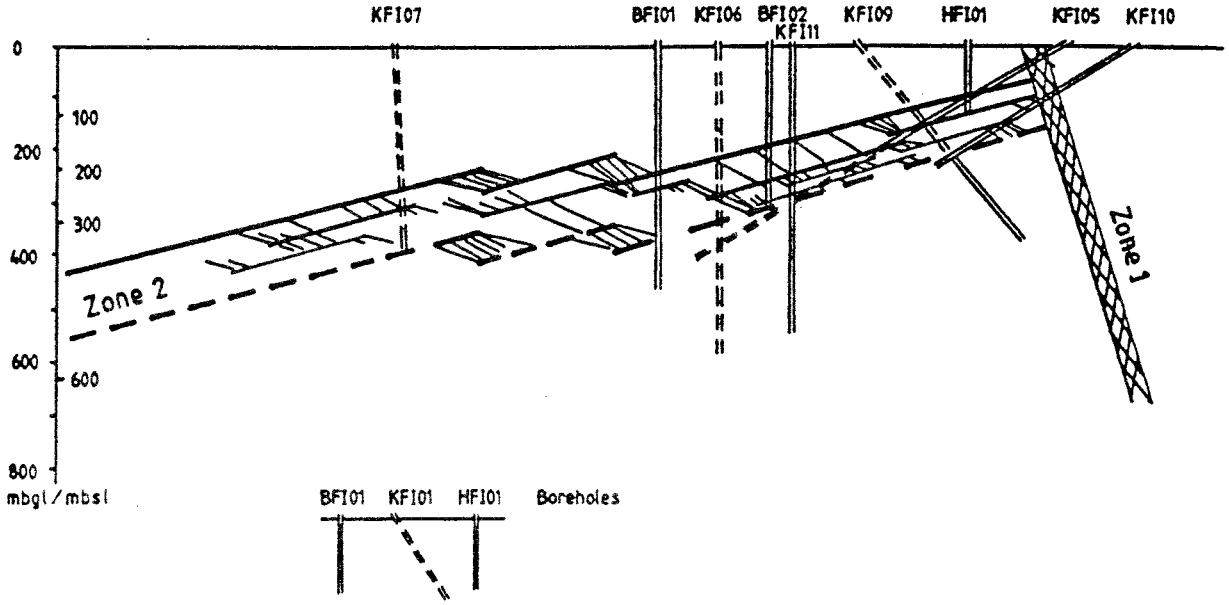

Figure 14. Vertical section showing the conceptual model of Fracture Zone 2 at Finnsjön. Interpretation is based on comprehensive borehole information and shows that major shear planes are interconnected by secondary extension -and splay fractures (from Ahlbom and Tirén, 1991).

In summary, it may be concluded that exploring the fundamentals of localized shear deformation in brittle material may not contribute much in terms of quantitative data on mechanical properties of fracture zones. It is, however, important in order to develop mechanically realistic conceptual models of fracture zones. It is felt that rock mechanic models, as applied for various purposes and involving fracture zones, are often developed without sufficient awareness of the fact that i) the internal structure of fracture zones may not be "hopelessly" nonsystematic, and ii) fracture zones of different orders are often genetically correlated such that certain patterns are formed.

5 PROPERTIES OF FRACTURE ZONE COMPONENTS

5.1 Introduction

As discussed in section 2.2, the "small-scale sampling and testing approach" to fracture zone mechanical characterization involves determination of the properties of the system components, i.e:

- Intact rock
- Fractures
- Filling material or, more generally defined, components that can neither be classified as intact rock, nor as fractures. Examples are soil-like material like clay and fault gouge

Having determined the properties of these components, the next step is to use indirect superposition procedure to estimate overall fracture zone mechanical characteristics.

Unfortunately, the degree of knowledge about the mechanical characteristics of the three components listed do not comply with their relative influence on fracture zone behavior. Thus, the material properties of intact rock are comparably well understood. A wealth of literature is available on the topic and it will not be discussed here.

The mechanics of fractures and joints has been subject to intense research over the last few decades. An overview of the current status in the field may be obtained from Barton and Stephansson (1990). The amount of information available on rock joint mechanical behavior is extensive, and the degree of understanding of the problem may perhaps be characterized as fair.

However, increasing problems are encountered when dealing with fractures containing thick infillings of material that differs drastically from that of the host rock. This is schematically illustrated in Figure 15; most of the data available refer to discontinuities characterized by mechanical interaction between the discontinuity surfaces. In practice, this means discontinuities that are either unfilled, contain only thin fillings of poor-quality material, or are filled with competent material such as quartz and calcite. For these conditions, the effects of filling material can be indirectly accounted for through properties describing friction, joint surface roughness and dilation effects. The fundamental model is still that of two contacting surfaces.

Increased thickness of the filling material, Figure 15b, leads to mixed-mode cases where discontinuity behavior is difficult to understand and predict because it is governed by both the surface contact mechanism and by the filling material as such. If the width of the filling material is further increased in relation to the magnitude of the surface asperities, the influence of the rock surfaces will

gradually disappear. The behavior of the discontinuity becomes completely controlled by the properties of the filling material, Figure 15c, and must be assessed on the basis of concepts and principles borrowed from soil mechanics.

Below, properties of unfilled joints (or, more correctly, joints characterized by rock surface interaction) and methods available for scaling these properties to similar discontinuities of larger dimensions are discussed in general terms. Properties of common filling materials are briefly considered in section 5.3.

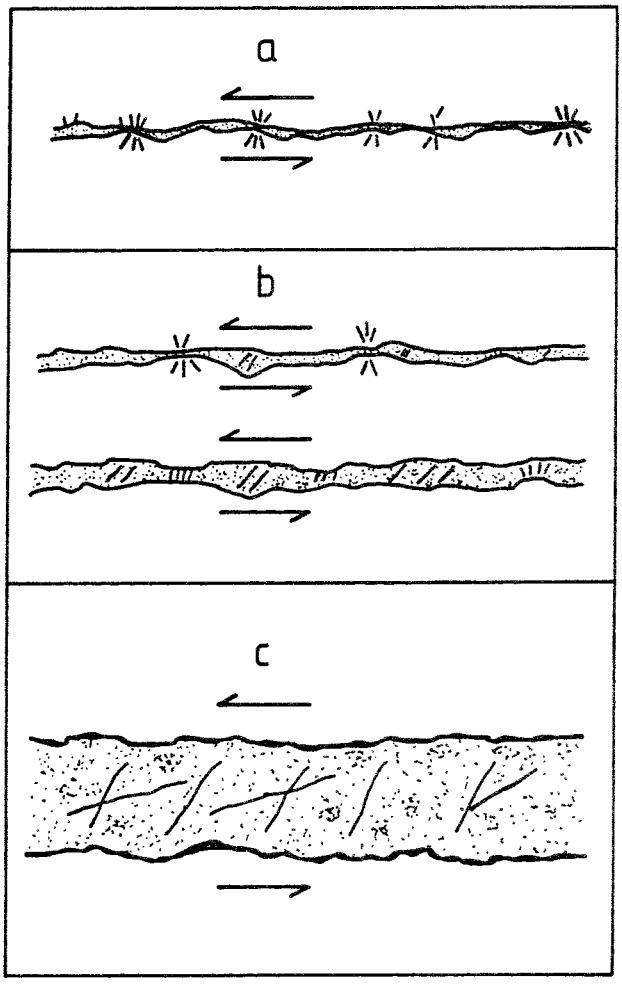

Figure 15. Categories of discontinuity behavior with respect to thickness of filling material.

a) Little or no filling. Mechanical behavior governed by contact between rock surfaces.

b) Thickness of filling is comparable to surface asperity magnitudes. Mechanical behavior governed by complex interaction of rock surface contacts and filling material.

c) Thickness of filling is much larger than surface asperity magnitudes. Mechanical behavior governed entirely by properties of the filling substance.

5.2 Properties of rock joints

5.2.1 Shear deformation

The shear deformational behavior of rock joints is complex and depends on the frictional- and topographic characteristics (extent and geometry of asperities) of the joint surfaces, the strength of the rock material forming the surface asperities, and on the effective normal stress acting across the joint plane. Figure 16 shows shear displacement versus shear stress for a typical rock joint subjected to a constant normal stress. The curve can be separated into a pre-peak part and a post-peak part. Important parameters are:

τ_p = peak shear strength
τ_r = residual shear strength
δ_p = peak shear displacement (or more correctly, displacement at mobilization of peak shear strength)
K_s = shear stiffness. This parameter refers to the pre-peak stage and is defined as the slope of the stress-displacement curve. It is commonly approximated by the slope of the straight line as given in Figure 16.

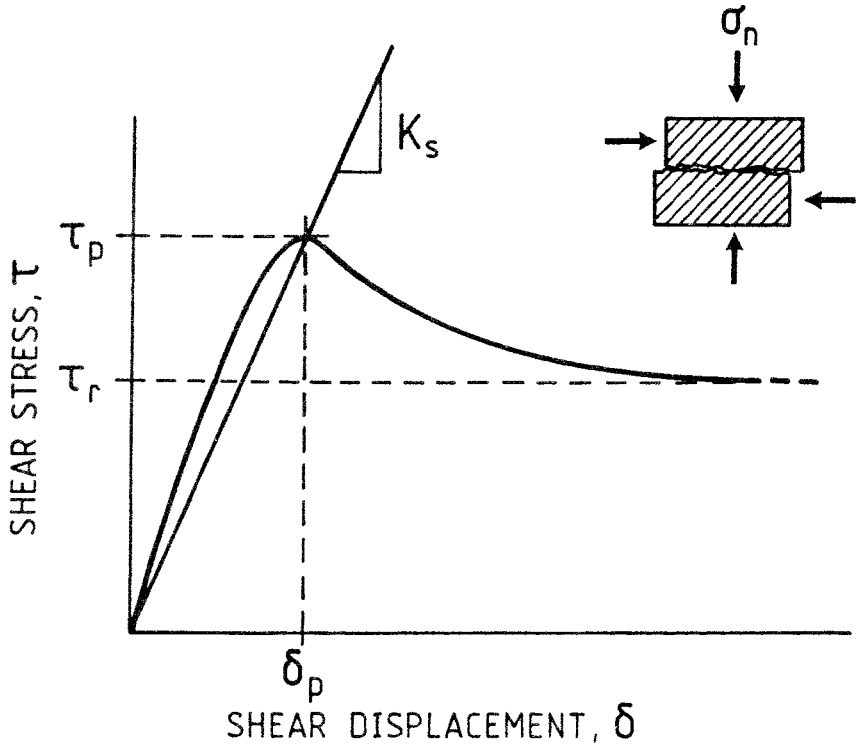

Figure 16. Shear stress versus shear displacement for a rock joint subjected to shear under constant normal stress.

The shear strength of joints can be described with the previously introduced Coulomb type relationship:

$$\tau_s = c + \sigma_n \tan\phi$$

where τ_s = shear strength
c = cohesion or "inherent strength" of the joint
σ_n = effective normal stress
ϕ = apparent friction angle

The cohesive component is zero for open joints. The apparent friction angle describes the total, normal stress dependent shear resistance and may thus involve contributions from both "true" surface friction and effects related to surface roughness. Figure 17 shows typical envelopes for peak shear strength and residual shear strength as a function of applied normal stress, for the case of zero cohesion. The residual strength is usually a near-linear function of the normal stress, which allows the definition of a stress independent residual friction angle, ϕ_r. The peak strength envelope is typically curved for low and intermediate stress levels. The curvature reflects stress dependency in mode in which surface roughness influence on the shearing process. At low normal stress, asperities tend to override each other, causing separation (dilation) of the joint surfaces. Higher normal stress increases the amount of asperity damage during shearing. Very high normal stress precludes dilation and the asperities are completely sheared off.

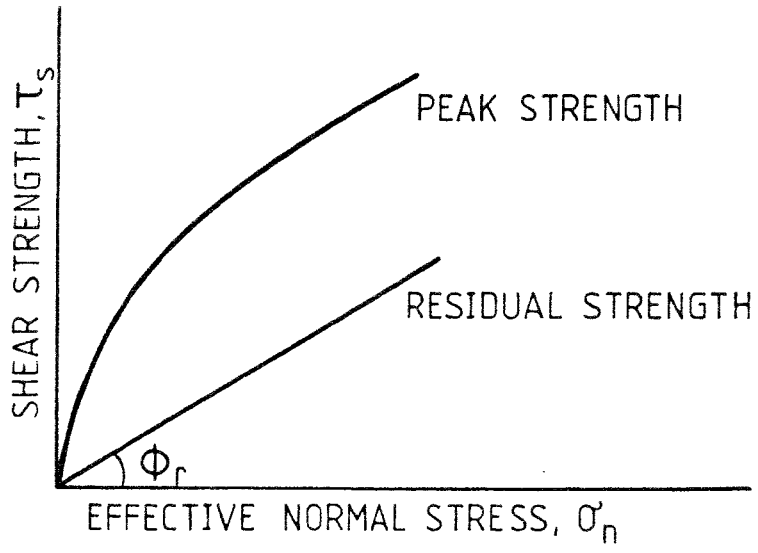

Figure 17. Typical envelopes for peak shear strength and residual shear strength of a rock joint as a function of effective normal stress.

Joint shear behavior is of major concern in rock engineering and a large amount of theoretical and experimental research has been devoted to the topic. Most of the work deals with strength characteristics and post-peak behavior. Among the many contributions published, those by Patton (1966) and Ladanyi and Archambault (1969) can be noted since they have found considerable practical application. Patton presented a bi-linear relationship that accounts for asperity effects at low normal stresses. Ladanyi and Archambault developed a non-linear empirical relationship for shear strength that also considered shearing through asperities.

The most widely adopted procedure to determine joint shear behavior is the set of relationships developed by Dr Nick Barton and co-workers. This system is empirical, and from originally focussing on estimation of joint shear characteristics (Barton and Choubey, 1977), it has been gradually expanded and refined to now include schemes for assessment of complete joint mechanical behavior and joint water conductivity (Barton and Bandis 1982; Bandis et al., 1983; Barton et al., 1985; Barton, 1990). Factors contributing to the popularity of this system in engineering practice include its capability to provide realistic estimates of a suite of important joint parameters on the basis of simple index tests, and the fact that it is comparably well supported by experimental results. An additional feature that is important in the present context is that it explicitly suggests means to, at least approximately, handle the problem of scale dependency of joint mechanical behavior. Below, the most important components in describing joint shear behavior and its scale dependency, according to Barton, will be summarized. It should be noted that the summary does not contain enough detailed information to actually apply the system - this requires the indicated references to be consulted.

The fundamental "input" parameters of Bartons system are:

ϕ_r = The residual friction angle of smoothed joint surface (dry conditions)
JCS = Joint wall compressive strength
JRC = Joint roughness coefficient

For clean, unweathered joints, the residual friction angle is equal to the basic friction angle, ϕ_b. The latter parameter can be determined from simple tilt tests on core specimens. Reasonably accurate estimates can also be made on the basis of data from shear tests available from the literature. Estimation is facilitated by the fact that the parameter shows moderate variation, and generally falls within the interval 25-35^o. For weathered or altered joints, empirical correction factors can be applied to derive ϕ_r from values of ϕ_b.

JCS, the compressive strength of the material constituting the joint walls, can be determined by means of Schmidt hammer rebound tests. For perfectly clean joint surfaces, JCS is equal to the compressive strength of the surrounding rock material. Weathering or alteration of the joint surfaces will however drastically

decrease the value of JCS. For calcite- or mica coated joint surfaces typical in crystalline rocks, JCS is typically a factor of 2-4 less than the compressive strength of the intact rock.

JRC, finally, is a dimensionless parameter to account for the degree of roughness of the joint surfaces. Values of JRC ranges between 0-20. This parameter can also be estimated from tilt tests of core specimens or blocks containing samples of the joints under investigation. Graphical guides, relating joint surface appearance to JRC-value, are also available and can serve to verify estimates.

Having determined these three basic parameters, the peak shear strength of the joint is given by the relationship:

$$\tau_p = \sigma_n \tan[JRC \log\left(\frac{JCS}{\sigma_n}\right) + \phi_r] \qquad (3)$$

Equation (3) suggests that there are two components of shear strength - a basic frictional component given by ϕ_r and a roughness component, i, given by:

$$i = JRC \log\left(\frac{JCS}{\sigma_n}\right) \qquad (4)$$

The roughness component, in turn, decomposes into a geometrical component represented by JRC and an asperity failure component controlled by the ratio JCS/σ_n. The equation also suggests a stress dependency such that the contribution of the roughness component to the shear resistance decreases with increasing confining stress ($i = 0$ for $\sigma_n = JCS$). Since the stress level increases with depth, this implies that roughness effects contribute significantly to the shear resistance of joints at shallow depth. This applies, for example, to conditions in slopes and shallow tunnels. At great depth, shear resistance is controlled by the friction of the material itself.

Equation (3) refers to the peak shear strength. Considering the contributions to the shear resistance provided by the different components as a function of shear displacement, it is found that initial pre-peak deformation is controlled by material friction. The geometrical roughness component is then gradually mobilized to reach its maximum at peak strength. This process is accompanied by dilation, and as indicated its significance is highly normal stress dependent. In the post-peak phase, asperities are gradually destroyed and residual conditions dominated friction are reached. It follows that the material parameter JRC is only partly mobilized in the pre-peak range, and actually changes its value (decreases) in the post-peak range because the joint surface is smoothed.

5.2.2 Scale considerations

Shear strength

Laboratory testing of samples containing natural or artificial joints forms the experimental basis on which Barton and his co-workers developed their system. The experimental results thus refer to a scale interval up to a few tens of centimeters, in terms of length of joints investigated. By investigating scale dependency within this laboratory scale interval, however, they obtained some fundamentally important results. By combining these results with data available from field tests and back-calculations, referring to much larger scales, a set of empirical relations were devised that are commonly used to predict scale effects of joint mechanical behavior.

It is important to observe that small-scale sampling of a (larger scale) joint introduces apparent scale effects, even if the scale of sampling is large enough to provide representation of all features controlling joint behavior. This means that increasing the scale does not introduce any larger scale joint features, but may still alter joint behavior. This form of sampling bias should be distinguished from scale effects that are attributable to features such as large scale joint undulations, which remain undetected unless observations are made on a correspondingly large scale. The effects of sampling scale are qualitatively illustrated in Figure 18. The four curves show shear displacement - shear stress diagrams representing testing of samples taken from the same joint, but with successively increased base length of the surfaces being sheared.

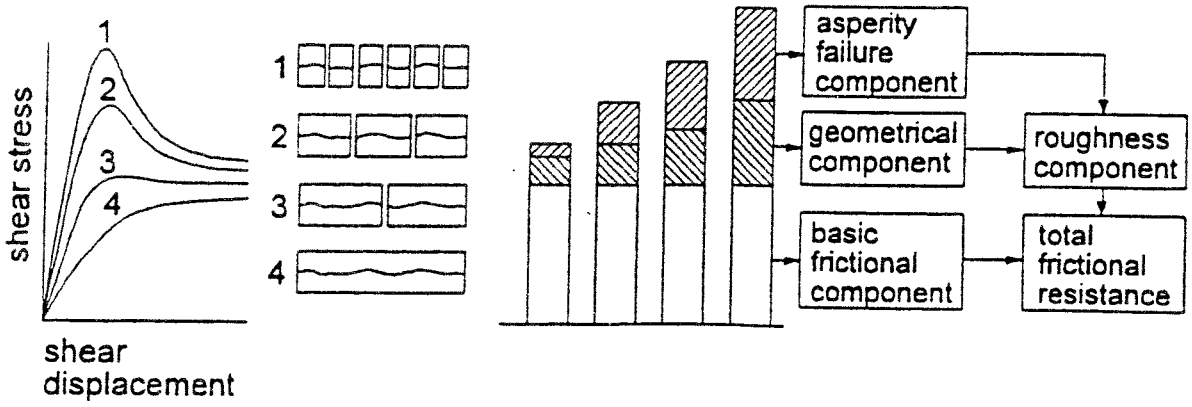

Figure 18. Influence of sampling scale on shear strength. The four curves represent testing of samples of different size, all taken from the same joint. Contributions to the shear strength by different components (geometrical, asperity failure and basic friction) are also indicated (after Barton and Bandis, 1981).

It is obvious from the figure that the difference between peak strength (curve peak) and residual strength (curve asymptote) decreases with increased base length. This means that the roughness component of eq. (3) decreases which implies that the properties JRC and/or JCS must reduce with increased scale. A reduction of the geometrical component (JRC) can be envisaged, since dilation in the small-scale case will be governed by small but steep asperities, while shear displacement of larger surfaces will follow larger, low-angle asperities. The asperity failure component (JCS) also decreases with increasing scale, which is an effect analogous to the decrease in uniaxial compressive strength with scale observed for intact rock specimens. Approximate empirical relations describing the scale dependency of JRC and JCS are given by:

$$JRC_n \approx JRC_0 \left[\frac{L_n}{L_0}\right]^{-0.02\,JRC_0} \tag{5}$$

and

$$JCS_n \approx JCS_0 \left[\frac{L_n}{L_0}\right]^{-0.03\,JRC_0} \tag{6}$$

where JRC_n and JCS_n are the parameter values in "full scale", and JRC_0 and JCS_0 the corresponding values obtained from laboratory size specimens. L_n denotes the length of the joint at "full scale". L_n is generally synonymous to the natural block size of the rock mass considered. L_0, finally, is the joint length of the laboratory size specimen (nominal 0.1 m).

These relationships are visualized in normalized form in Figures 19 and 20. It is seen that both JRC and JCS drop initially, but that values stabilize reasonably well for ratios of L_n/L_0 less than about 10, at least for smooth and moderately rough joints (JRC_0 less than about 10). In absolute numbers, this suggests that most of the scale effects in these parameters occur in the scale interval of less than about 1 m.

It should be emphasized again that the scaling procedures discussed above do not account for contributions to the shear resistance resulting from possible undulation on a scale larger than the natural block size. Denoting this contribution i′, the net apparent friction angle at "full scale" becomes:

$$\phi = JRC \log\left(\frac{JCS}{\sigma_n}\right) + \phi_r + i' \tag{7}$$

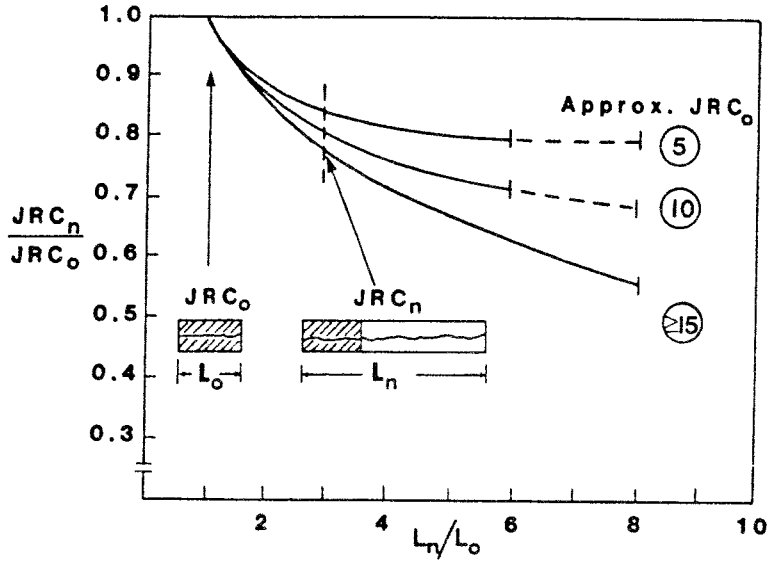

Figure 19. Empirical relationship for scaling JRC-values on the basis of block size (from Barton, 1990).

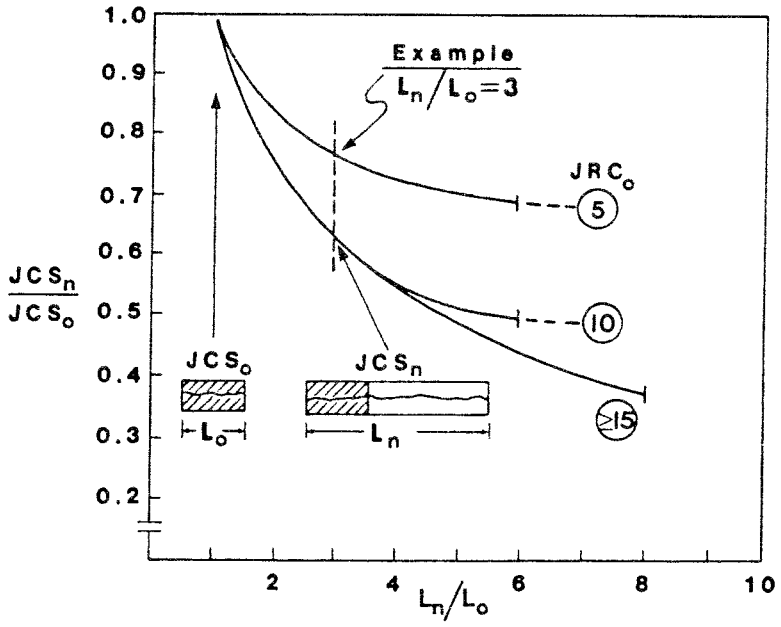

Figure 20. Empirical relationship for scaling JCS-values on the basis of block size (from Barton, 1990).

Another important result drawn from Figure 18 is that scale dependency essentially affects the roughness component of the shear strength, i.e. the component governed by JRC and JCS, cf. eq. (4). The residual friction angle, manifested by the residual shear strength, shows little or no variation. In fact, this result appears to hold within wide ranges of geometric scale and stress level. Furthermore, as indicated earlier, the roughness component decreases rapidly with increasing normal stress. The conclusion is, therefore, that scale dependency in discontinuity shear strength is much less pronounced at high stress levels (large depths) than low stress levels (small depths).

A third observation that can be made from Figure 18 is that the shear displacement required to mobilize peak shear strength increases with the size of the block sheared. Analysis of data available produces the approximate relationship:

$$\delta_p = \frac{L}{500}\left[\frac{JRC}{L}\right]^{0.33} \tag{8}$$

where δ_p is the shear displacement at peak shear strength and L is the length, in meters, of the discontinuity (block size). Figure 21 shows the data used to derive this relationship in relative form, i.e. the ratio δ_p/L plotted as a function of L.

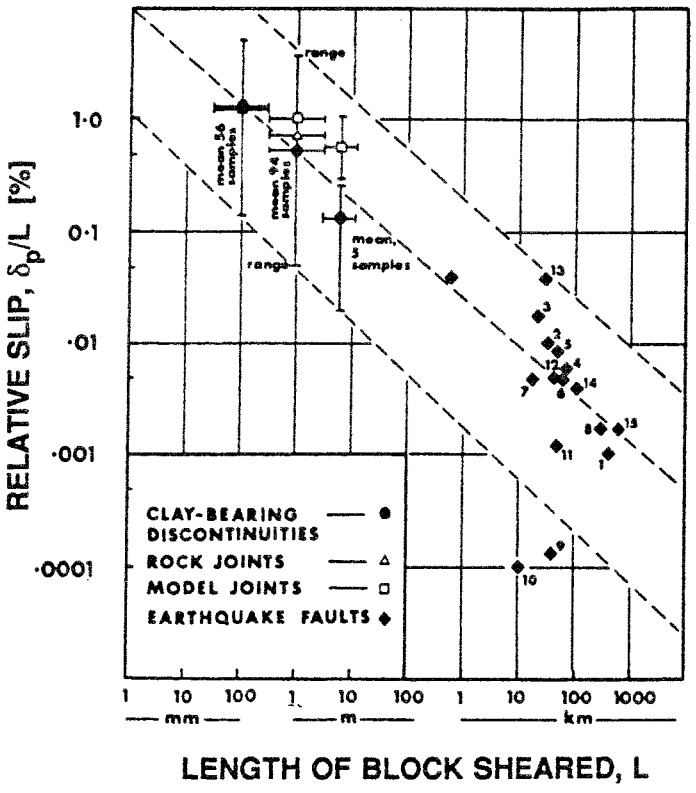

Figure 21. Relative shear displacement versus length of block sheared. Experimental data (upper left) refers to peak shear displacement during loading. Earthquake fault displacements refer to unloading (from Barton, 1990; earthquake data originally from Nur, 1974).

The data fall into two mutually rather different groups. One contains results from experiments in meter-scale or less and at low normal stress (generally less than 5 MPa). The features tested are model- and rock joints and clay-bearing discontinuities. The other is data from surface observations of fault displacements in connection with major earth quakes, thus representing high normal stress levels. The figure clearly demonstrates the almost complete absence of data referring to the scale interval in between these two groups, i.e. roughly the interval 10 m <L< 10 km.

The introduction of data from earthquake displacements together with data from controlled experiments may be questioned. The experiments represent complete loading sequences up to failure. Earthquake slip, however, is the result of rapid release of a probable small fraction of the unknown, total shear stress accumulated across the fault. This partial unloading is heavily influenced by parameters such as system stiffness and dynamic friction. Thus, the experimental loading does not seem to be comparable to the earthquake mechanism.

Shear stiffness

The pre-peak portion of the shear stress - shear displacement curve can be more or less nonlinear, implying corresponding variation of shear stiffness. Both linear approximations (constant shear stiffness) and hyperbolic functions have been proposed. The assumption of constant shear stiffness is justified in most applications. A more important effect, which follows from the scale effects discussed above, is that K_s decreases considerably with scale. The presented relationships describing peak shear strength and peak shear displacement can be used to estimate peak shear stiffness. Approximating K_s with the slope of the straight line according to Figure 16, the following relationship is obtained:

$$K_s = \frac{\sigma_n \tan\phi}{\delta_p} \tag{9}$$

Combining equations (3), (8) and (9), yields:

$$K_s = \frac{\sigma_n \tan\left[JRC \log\left(\frac{JCS}{\sigma_n}\right) + \phi_r\right]}{\frac{L}{500}\left[\frac{JRC}{L}\right]^{0.33}} \tag{10}$$

Measured values of joint shear stiffness, as reported in the literature, are shown as a function of block size in Figure 22. Without going into detail, the large variation in this parameter may be noted.

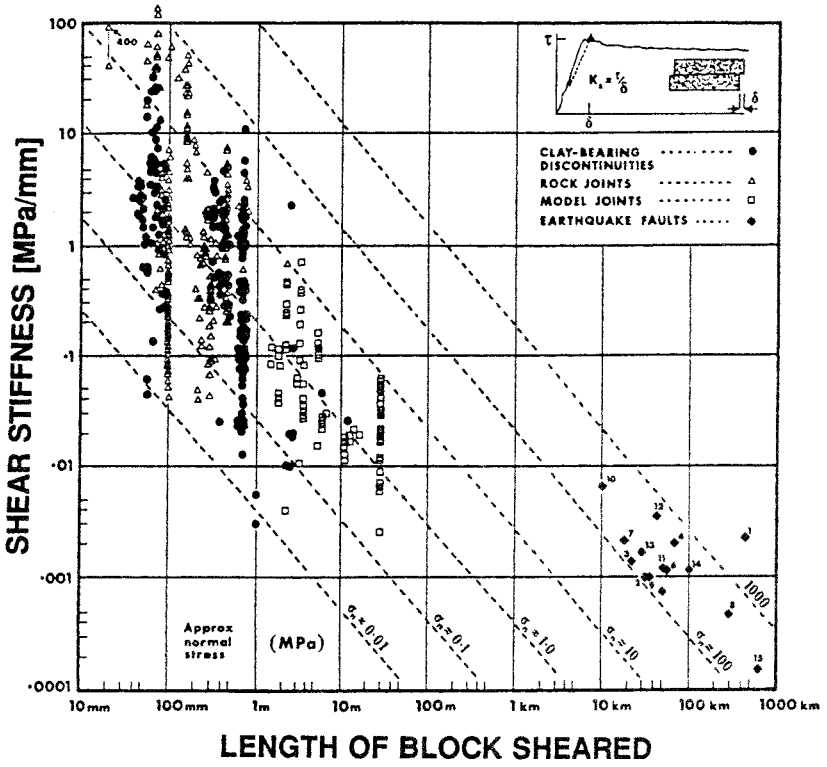

Figure 22. Measured values of shear stiffness of discontinuities as reported in the literature. Lines indicating different normal stress levels have been established on the basis of laboratory values and extrapolated to larger scales (from Barton, 1990).

It should be recalled, finally, that the system for joint shear characterization developed by Barton applies only to discrete discontinuities with surfaces in mechanical interaction with each other. It is not applicable to structures containing weaker filling material of thickness enough to completely isolate the discontinuity surfaces from the shearing process. Furthermore, several aspects of the system may be (and have been) criticized, and a number of alternative approaches have been suggested. Careful assessment of the validity of the equations and procedures must thus be exercised in each particular case. The system is, however, unique in that i) it is well supported by experimental data, including engineering applications; ii) it allows the necessary characteristics to be predicted on the basis of simple, small-scale properties that can actually be determined in practice, and iii) it suggests explicit and realistic means for scaling of joint shear properties. The relevance of these scaling procedures in predicting properties of fracture zone will be discussed in a subsequent chapter.

5.2.3 Normal deformation

Normal deformation of rock joints generally contribute a major part of the bulk deformability of jointed rock masses. Joint deformation is also responsible for most of the stress dependency in rock mass deformability that is often observed. The effect of the joints decreases with increasing stress, and at high confinement the rock mass deformability approaches that of the intact rock.

Figure 23 shows a typical normal stress - normal closure behavior recorded when testing rock joints under laboratory conditions. It is seen that normal closure response is strongly non-linear, at least for low normal stresses. Closure rate is initially very high, but decreases gradually to approach zero if and when the joint becomes completely closed. The normal stiffness, K_n, is defined as the slope of the stress-closure curve and is thus stress-dependent. It becomes undefined (goes to infinity) when complete joint closure, V_m, is approached. Despite the overall non-linearity, stress-independent normal stiffness values are often assumed in calculations. Unloading reveals hysteresis effects, that decrease at repeated loading but rarely disappear completely. Both the total closure upon loading and the degree of permanent deformation is strongly dependent on the degree of interlocking between the joint surfaces. Not unexpectedly, joints with mismatched surfaces show significantly larger total closure.

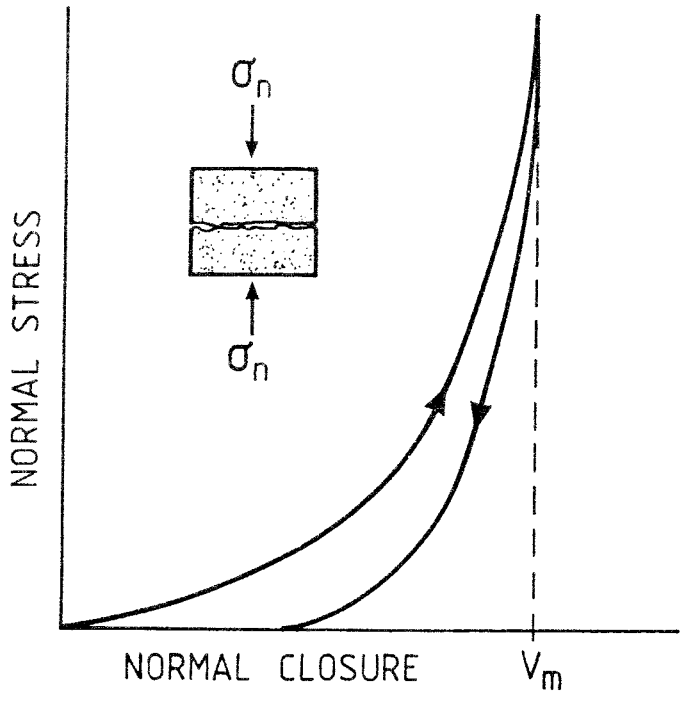

Figure 23. Typical normal stress - normal closure curve obtained from laboratory testing of rock joints.

A number of procedures have been suggested to predict joint normal closure behavior. These include methods for geometrical characterization of joint surface topography, followed by predictions based on explicit mechanical models (e.g. Swan, 1983; Tsang and Witherspoon, 1983; Gerrard, 1985). Much of the work has been done in order to establish fluid flow behavior of fractures, which is strongly dependent on normal deformation characteristics.

Empirical approaches have also been adopted. These have so far produced the results found most applicable in practice, taking factors like input data requirements and resemblance of experimental data into account. The most commonly applied normal closure functions are hyperbolic relationships developed by Goodman (1974; 1976) and Bandis et al. (1983). Here the presentation is restricted to a number of empirical relations suggested by Bandis et al. (1983) that allow prediction of the complete stress-closure curve for an interlocked joint. Similarly to the shear strength relations discussed above, these equations are based on the JCS and JRC parameters. Thus, according to Bandis et al., the initial aperture, a_j, is approximately given by:

$$a_j = \frac{JRC}{5}\left(0.2\,\frac{\sigma_c}{JCS} - 0.1\right) \tag{11}$$

where σ_c denotes the uniaxial compressive strength of the rock. Furthermore, the initial normal stiffness, K_{ni} can be obtained from:

$$K_{ni} = -7.15 + 1.75\,JRC + 0.02\left(\frac{JCS}{a_j}\right) \tag{12}$$

The maximum closure, V_m, depends on JRC, JCS and the initial aperture; the empirical function expressing the effects of all three variables is:

$$V_m = A + B \cdot JRC + C\left(\frac{JCS}{a_j}\right)^D \tag{13}$$

where A, B, C and D are constants determined to:

A = -0.1032
B = -0.0074
C = 1.135
D = -0.251

Finally, the joint normal stiffness, K_n, at any given normal stress level, σ_n is given by the equation:

$$K_n = K_{ni}\left(1 - \frac{\sigma_n}{V_m K_{ni} + \sigma_n}\right)^{-2} \qquad (14)$$

The above equations are given (without further discussion of their background) because they will prove applicable in the prediction of the rock mass modulus, as discussed in chapter 6.

As opposed to shear deformation, joint normal deformation does not show any significant scale dependency, provided that observations are made on a scale large enough to allow adequate representation of surface roughness. This conclusion becomes obvious, if one considers that "scale" in this case refers to the in-plane dimensions of the joint (i.e. joint trace length or joint radius) only, and not to discontinuity width. Increased width of a discontinuity will certainly affect normal stiffness.

5.3 Properties of filling material

Filling materials found in rock discontinuities are substances representing a variety of genetic histories, mineralogic compositions, grain size distributions etc. Mechanically this wide variety of materials may have little in common, except that they are "weaker" and "softer" than the surrounding rock. Cataclastic material, ranging in grain size from breccia to clay-rich fault gouge, constitute one broad group of filling material. Products of various forms of alteration may be defined as another and even more diverse category.

Data on the mechanical characteristics of filling materials that are too poorly consolidated to be termed rocks can be drawn from essentially two fields. From soil mechanics, comprehensive knowledge is available on the behavior of granular and low-cohesion materials in the low-stress range, up to at most a few MPa. The other area is earthquake-related research where various filling materials, in particular clay-rich fault gouges, have been extensively studied. Here, the stress regime of interest is in the very high range, typically 100 MPa or more.

To some extent, the gap between soil mechanics data (low stress) and data from earthquake related work (very high stress) can be supplemented with observations from mines. Some results of interest from Swedish mines are summarized in section 5.4.

Given the diversity and complicated behavior of soil-like filling materials, a comprehensive treatment of their mechanical characteristics falls far outside the scope of the present study. A brief description of shear strength characteristics under low and high confining stress conditions will however be given.

5.3.1 Low confining stress

The shear resistance soil-like filling materials is contributed by complicated interaction of several factors including:

- mineralogy
- particle size distribution
- loading history
- water situation (pore water pressure, water content and sometimes water composition)
- loading rate

The influence of mineralogy is evidenced by data on residual friction angles for pure minerals, as given in Table 1.

Figure 24 shows ranges of residual friction angles as a function of clay fraction for a variety of soil materials. In the absence of a clay fraction, i.e. in sands and silts, friction angles are similar to those of quartz, feldspar and calcite. Friction angles for more coarse-grained aggregates like gravel are similar or higher. At very high clay fraction percentages, friction angles approach those of minerals such as chlorite, talc and biotite.

Table 1. Ranges of residual friction angles for groups of minerals at effective stresses less than 1 MPa (after Barton, 1980).

Minerals	Res. friction angle (deg)
Quartz, feldspar, calcite	30-35
Mica, hydrous-mica, illite	17-25
Montmorillonitic minerals	4-10

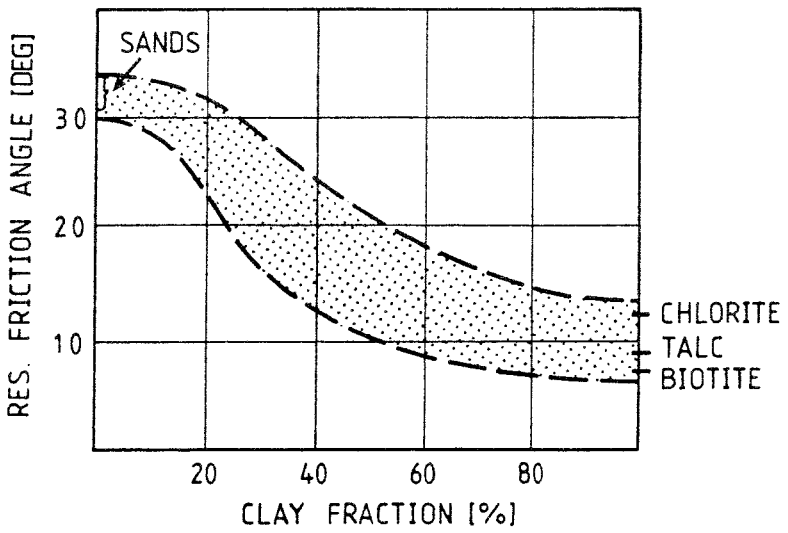

Figure 24. Residual friction angle as a function of clay fraction (after Barton 1980).

More coarse grained filling materials show small differences between peak- and residual friction angles, but in overconsolidated clay fillings this difference can amount to 10^{0} or more. The majority of cataclastic filling materials can be assumed to be deformed to residual conditions. Materials in discontinuities that have been healed by secondary alteration processes are however obviously undisturbed.

Filling materials that have been deformed to residual states exhibit insignificant cohesion. For soil-like materials, cohesive strength can generally be ignored even under undisturbed conditions since the cohesion does not exceed 1 MPa. More competent filling substances like chlorite, biotite and calcite can exhibit undisturbed cohesion values of a few MPa.

Table 2 shows data from the civil engineering literature on shear strength properties of filled discontinuities, as obtained from in-situ shear tests. Most of the data are reproduced from a summary given by Barton (1980); results presented by Infanti and Kanji (1978) have been included. In-situ shear tests involve block sizes up to a few meters and low normal stress levels. For the cases tabulated, it may be assumed that the discontinuity shear strength is governed by the properties of the filling material, with little or no contribution from rock surface asperities (cf. Figure 15c). The results verify low cohesion and large scatter in friction angles, though with a clear tendency to low friction for cases with high clay content of the filling material.

Table 2. Shear strength characteristics as obtained from in-situ shear tests of filled discontinuities.

Rock	**Filling**	**Eff. normal stress (MPa)**	**Cohesion (MPa)**	**Friction angle (deg)**	
				peak	**residual**
Chalk	bentonite clay, 8 cm		0.02	8	
	(mostly montmorillonite)	0.14-0.33	0.02	12	
Greywacke	1-2 mm clay in bedding plane	0-2.5			21
Granite	clay filled faults	0.1-1	0.1	24-45	
Limestone	6 cm clay layer	0.8-2.5			13
Basalt	clayey breccia, wide variation from clay to basalt content	0-2.5	0.2	42	
Granite	tectonic shear zone, schistose and broken granite, disintegrated rock and gouge	0.4-0.7	0.3	45	
Schistose quartzite	rock completely separated by clay	0.2-0.4	0.4	31	
Schists	10-15 cm clay filling	0.3-1.2	0.1	32	
Quartzites and siliceous schists	10-25 cm clay and altered rock filling	0-0.7	0	32	
Basalt	weathered basalt, clay-silt-sand in variable proportions	0-2.0	0	20-35	

5.3.2 High confining stress

The mechanical behavior of fault gouge at high confining stresses has been investigated in considerable detail by laboratory experiments (e.g. Marone et al., 1990; Rutter and Maddock, 1992). The background to this research is the major influence that gouge properties exert on overall fault shear behavior, especially the transitions from stable creep deformation to the stick-slip behavior resulting in earthquakes. In order to comply with in-situ conditions in active fault zones, laboratory investigations of fault gouge mechanics primarily refer to the very-high stress range, typically confining stresses of 50 MPa or more.

Figure 25 shows typical shear stress - shear displacement curves obtained at different levels of effective normal stress. Note that the plastic component of shear deformation is associated with strain hardening that increases with normal stress. This behavior is not observed in tests at low normal stress. The strain hardening effect has fundamentally important implications in that it promotes accumulation of strain energy in the surrounding rock, which is one prerequisite for transition from stable shear (creep) to unstable, dynamic shear (stick-slip deformation).

Friction angles determined from tests of fault gouges at high stresses vary within the approximate range 15-35°. Dependency on mineral composition and grain size distribution is less pronounced, and much less consistent, than at low stresses. Other parameters, however, add further complications to the frictional behavior. The strain-hardening effect, as illustrated in Figure 25, will obviously result in increase of the apparent friction angle with shear displacement. Figure 26 shows an example of friction angle/coefficient of friction of clay fault gouge as a function of shear strain and confining pressure. The figure also illustrates the very large influence that the degree of saturation has in the case of clay-rich fault gouges. The frictional characteristics have also been found to be dependent in a complex manner on shear velocity, which has important implications as to the nature of shear movement. Velocity weakening of fault zone material can explain repeated stick-slip type fault movements that are often observed (Scholz, 1990).

In summary, it appears that laboratory testing of soil-like filling materials have produced scattered data, as would be expected given the diversity of the materials. Crude relationships may be established between strength properties and parameters like grain size distribution and mineralogical compositions. However, the degree of saturation and the rate of displacement also have a large influence, especially when clay fractions are present. Friction angles are higher at high stresses, but scatter is still considerable. Strain hardening effects and displacement rate dependency observed under high stresses (conditions resembling faults) have important consequences with respect to the mode of shear deformation. Materials like clay-rich fault gouge that intuitively are ascribed very plastic behavior can, under these conditions, exhibit brittle characteristics promoting stick-slip shear movement.

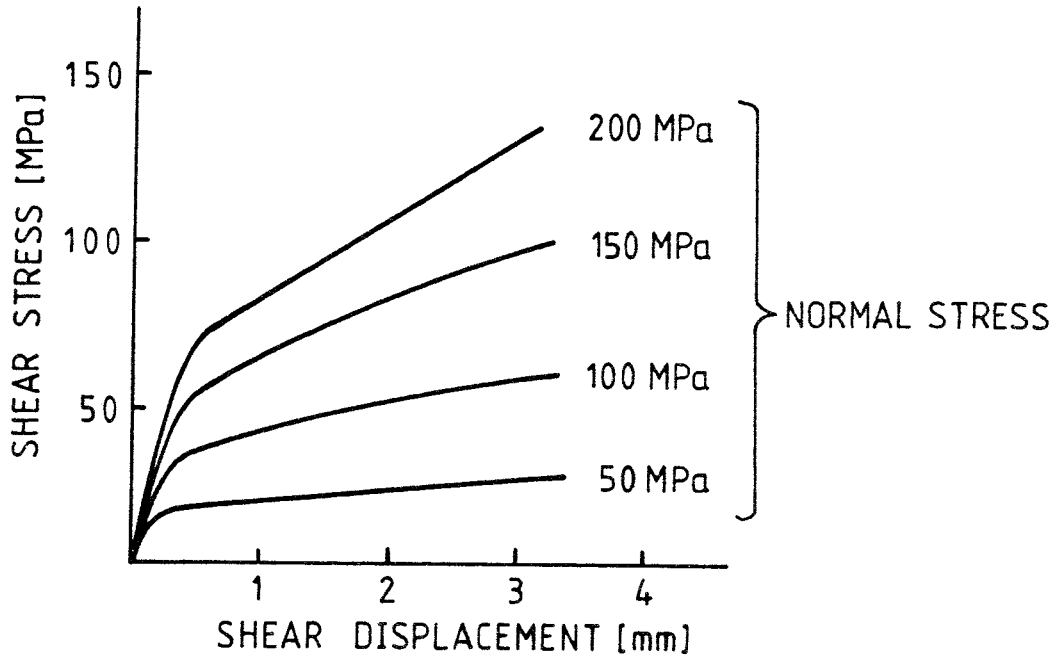

Figure 25. Example of result from shear tests at different normal stresses involving a layer of fault gouge. Note the strain-hardening effect that increases with normal stress.

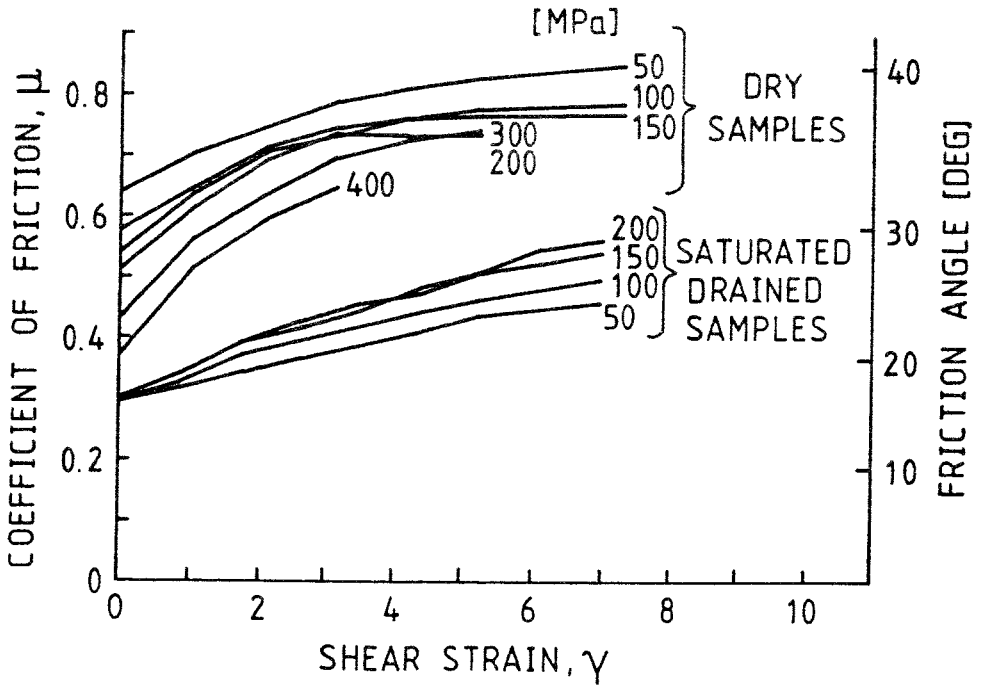

Figure 26. Friction angle versus shear strain as obtained from laboratory tests of clay-rich fault gouge (Tejon Pass, San Andreas Fault) under dry and saturated condition and for different confining pressures (after Morrow et al., 1982).

5.4 Properties of weak contact zones in mines

Alteration at the boundaries between ore bodies and their host rocks commonly forms contact zones with poor-quality rock. The dimensions and characteristics of these zones can vary widely, but they invariably have major implications on local mine stability. As a consequence, assessment of their deformational- and strength properties is often required as input to rock mechanics analysis related to mine planning.

Altered contact zones are found in several of the Swedish sulphide ore mines. This includes, among others, the mines within the Skellefte district in northern Sweden and the Zinkgruvan Mine in the central part of the country. Rock types typically encountered in the contact zones include chlorite- and biotite schists, skarn and sericite quartzites. Highly variable degrees of alteration yield strength properties ranging down to values comparable to those of overconsolidated clay. These mines have been subject to a long sequence of rock mechanics research effort, focussing development of the means to predict and solve potential stability problems. Among other things, this work has produced a reasonably well verified set of data on the geomechanical properties of rock units present in the mines, including the altered contact zone.

The data from the mines are of interest in the present context because they refer to in-situ conditions, and because the rocks found in the contact zones bear similarities with alteration products often encountered in fracture zones. Furthermore, the depths (down to about 800 m) and in-situ stress levels (roughly 10-40 MPa) represented by the mines are similar to those discussed in connection with waste disposal.

Kristineberg Mine

Tables 3 and 4 shows data from a recent investigation at the Kristineberg Mine, within the Skellefte ore district (Board et al., 1992; Rosengren et al., 1992). Figure 27 indicates the mine geology. The ore deposit is situated in a sericitic quartzite which ranges is competence from sound to highly altered. Immediately bounding the orebody are highly altered, talcy chlorite schists. As indicated by the Q-index values given in Table 3, these materials are very weak and friable. Diamond drilling through the schists yields little or no core recovery.

The values of compressive strength and Young's modulus reported in Table 3 are approximate ranges obtained from testing rock samples using conventional methods. Hence, they refer to the sample-scale and not to the rock mass scale. Furthermore, a bias may be suspected, such that the lower tail of the true distribution is not represented because the rock is too poor to allow sampling of the most low-strength sections. A reasonable interpretation would be to consider the lower bounds of the intervals given in the table as upper bound estimates of the corresponding properties on the rock mass scale. This indicate a rock mass deformation modulus of 10 GPa or less.

The values presented for friction angle and cohesion are estimates of "excavation-scale" properties at stress levels of the order of 10 MPa. They were obtained using rock mass classification combined with empirical procedures that, though approximate, are well established in engineering practices. The large intervals given for the friction angle illustrates well the difficulties encountered in this prediction process, despite good access to direct field observations. This is due both to the inherent uncertainty in procedures used when applied to poor-quality rock masses, and to the observed large variability in appearance of the rock units. Applying the same procedures to rock masses of better quality yields much more accurate estimates.

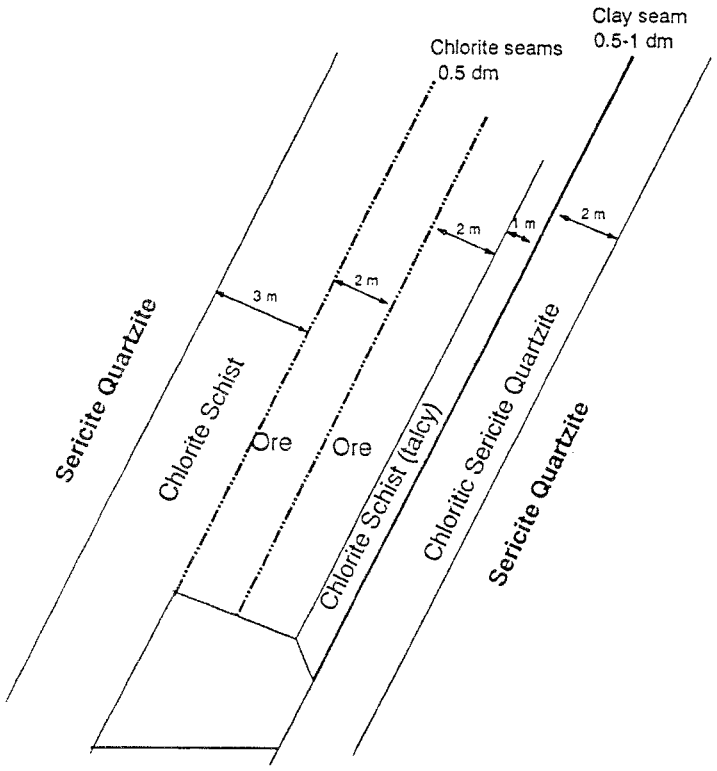

Figure 27. Schematic, vertical cross section showing the local geology at the Kristineberg Mine (from Nyström and Board, 1991).

Table 3. Estimates of mechanical properties of weak rocks at the Kristineberg Mine (after Nyström and Board, 1991).

Unit	Rating, Q-value	Compressive strength, σ_c (MPa)	Young's Modulus, E (GPa)	Friction angle ϕ_p = peak ϕ_r = residual	Cohesion (MPa) c_p = peak c_r = residual
Chlorite schist	very poor to poor 0.5<Q<5	20-60	10-20	ϕ_p = 19-25 ϕ_r = 5-7	c_p = 2.5-3.0 c_r = 0.5-1.4
Sericite quartz-ite	very poor 0.1<Q<1	10-80	10-25	ϕ_p = 20-34 ϕ_r = 5-17	c_p = 3.5-5.0 c_r = 1.0-3.0
Clay-bearing interface				zero (?)	low

Table 4 shows best-fit strength values that emerged from a comprehensive sequence of modelling of stope behavior, calibrated against visual observations and field measurements. They are, in other words, the best averages that can be deduced from back-calculation of actual excavation behavior. A Mohr-Coulomb strength criterion (constant friction angle) was assumed. It is seen that to reproduce observed behavior, rather low values had to be assigned to the friction angles of the contact zones.

Table 4. Best fit, Mohr-Coulomb strength property estimates obtained by back-calculation of actual excavation behavior, Kristineberg Mine (from Board et al., 1992).

Unit	Friction angle (deg)	Cohesion (MPa)
Footwall schist	9	1.5
Hangingwall schist	19	2.5
Interfaces	9	0

Näsliden Mine

The Näsliden Mine, also located within the Skellefte district, has been subject to several rock mechanics investigations of which the contribution by Borg (1983) is the most comprehensive. In comparison to the Kristineberg mine rock conditions at Näsliden are much better. However, within parts of the mine a relatively homogeneous chlorite schist occurs that is probably mechanically comparable to chlorites typically found as fracture fillings in granitic rocks.

Core data revealed the following specimen-scale properties for the chlorite schist:

Compressive strength: Average 70 MPa, large variation
Young's modulus: Average 40 GPa
RQD: Average 30 (poor rock)

Full-scale values were obtained by back-calculation of mine behavior in combination with field measurements. Properties determined included:

Young's modulus: 10 GPa
Residual friction angle: 20^{o}

The full-scale estimate of Young's modulus is fairly well supported by measurement data, and refers to approximate stress levels of 20-50 MPa. The value of the friction angle probably represents an upper limit. Later failure observations indicate friction angles of at most 20^{o}.

Zinkgruvan Mine

Most rock units encountered in this mine are very competent and are thus of little interest here. The exceptions are occurrences of biotite layers sometimes forming a weak contact zone of variable thickness on the footwall side of the orebody. Specimen-scale properties of the biotite have not been determined. Stress conditions are however well known, and from numerical simulations of observed failures Sjöberg (1992) concluded the following full-scale strength parameters for the biotite:

Friction angle:	15°
Cohesion:	2 MPa

Viewed together, the investigations at the Kristineberg, Näsliden and Zinkgruvan mines have produced surprisingly consistent mechanical data for low-strength, low-friction rocks that are common components in faults and fracture zones. The data refer to the "excavation-scale" i.e. meters and tens of meters.

6 ESTIMATING DEFORMABILITY FROM BOREHOLE DATA

6.1 Introduction

Due to the importance of scale effects in many rock engineering situations, empirical scaling procedures have been developed that aim at converting properties observed on core samples to corresponding properties on some larger scale. Procedures for scaling some of the properties controlling shear deformation were indicated in section 5.2.2. In addition, a number of empirical methods for the prediction of rock mass deformation modulus on the basis of small-scale data have been developed. These methods are oriented towards practical application and based on input parameters that can be obtained from core logging and relatively simple laboratory tests. As would be expected, the accuracy of the predictions that can be made improves with the quality of the rock mass investigated. The full scale data required to verify the various empirical relationships have been obtained from observations of deformation induced around excavations, or by specifically designed field tests such as tunnel jacking- or plate bearing tests. This means that the data refer approximately to the 10 m scale.

The in-situ deformability can be expressed by the rock mass deformation modulus. In cases when a fracture zone is considered as an "equivalent rock mass", cf. Figure 6, this parameter defines (although not completely) the deformability of the zone. The applicability of empirical methods for estimating rock mass deformation modulus is well verified for rock masses of "ordinary" quality, but indeed not for rock masses of the kind typically found in fracture zones. Below, some commonly used procedures will therefore be reviewed, and their potential in the present context is tested by tentative application to three well documented fracture zones:

- "Fracture zone 2" at the Finnsjön site
- "Eastern regional zone" at the Fjällveden site
- "Fracture zone 3" at the Kamlunge site

These sites have all been subject to investigation within SKB's Study site investigation program, and cores from boreholes penetrating the fracture zones are available. Fracture zone 2 at Finnsjön is gently fractured and, when viewed by rock engineering standards, would rank as a fair or good quality rock mass. The Eastern regional zone at Fjällveden and Zone 3 at Kamlunge are both more intensely fractured and contrast more distinctly to their surroundings.

6.2 Methods

Because of the presence of discontinuities, the rock mass deformation modulus, E_m, is always lower than the deformation modulus of intact core specimens, E_i. The simplest method available for estimating E_m using borehole data requires two input parameters only - the modulus of intact core samples, determined by conventional laboratory testing, and the RQD-index (Rock Quality Designation) as

determined from standard core logging. This method was suggested by Coon and Merrit (1970). They used data from several dam construction projects, some of which include granitic rocks, and inferred a linear relationship between the ratio E_m/E_i and RQD-value. Later studies have provided similar relationships, and the method has been found to yield reasonable predictions of E_m, provided however that RQD values are not less than about 60. The applicability is thus restricted to rock masses classified as being of "fair" quality or better. Figure 28 shows data compiled by Bieniawski (1978).

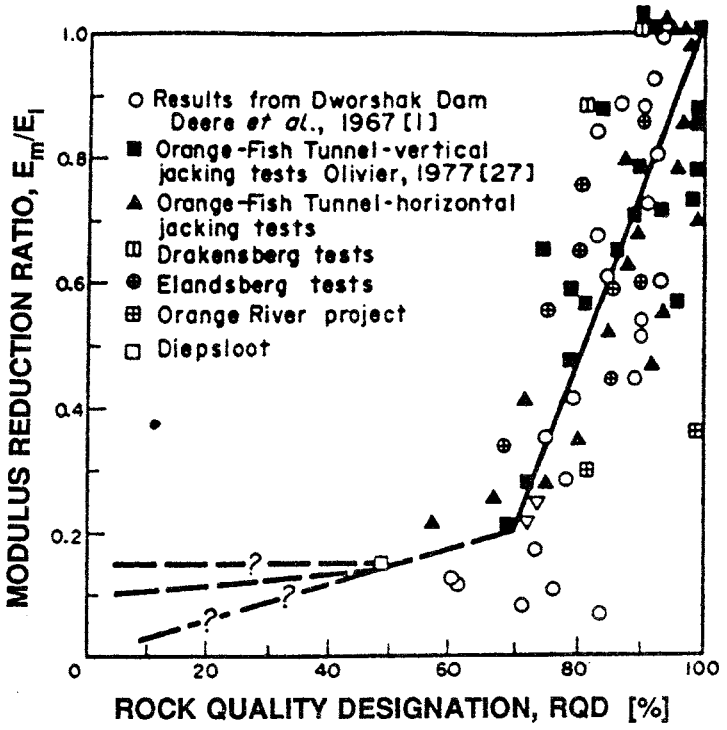

Figure 28. Ratio of rock mass- to intact rock deformation modulus versus RQD-value (after Bieniawski, 1978).

Besides the RQD-index, there are two systems in frequent use for engineering classification of rock masses. These are the Geomechanics Rock Mass Rating (RMR system; Bieniawski, 1979) and the NGI Tunnelling Quality Index (Q-system; Barton et al., 1974). Both are based on RQD and a number of additional parameters, specific for each system, accounting primarily for the nature of jointing but also relating to stress- and groundwater conditions. Classification procedures originally assume in-situ observations, but applications based on core information have only been attempted with varying success (Cameron-Clarke and Budavari, 1981).

Among the many extensions of the RMR and Q systems, simple empirical relationships for estimating rock mass deformation modulus on the basis of classification ratings have evolved. Thus, for the Q-system, Barton (1983) suggested the following relationship:

$$E_m = 25 \log Q \tag{15}$$

Correspondingly, Bieniawski (1978) presented the equation:

$$E_m = 2\,RMR - 100 \tag{16}$$

These equations are shown in Figure 29, together with data from case studies.

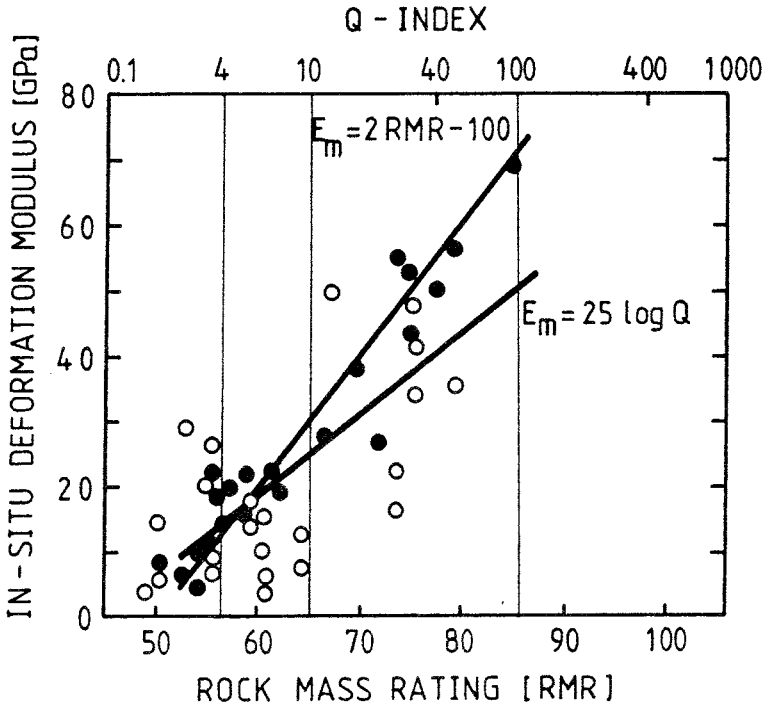

Figure 29. Empirical relations for estimating rock mass deformation modulus on the basis of classification indexes. Open and filled symbols represent Q-system and RMR-system cases studies respectively (after Bieniawski, 1989).

Besides the empirical procedures, analytical methods have been suggested by which the deformation characteristics of intact rock and joints are superimposed to yield an effective rock mass deformation modulus. The simplest method was proposed by Barton (1983) and assumes the rock mass model illustrated in Figure 30. Layers of intact rock with deformation modulus E_i are separated by parallel joints occurring with spacing S and having normal stiffness K_n. Loading is assumed to be perpendicular to the plane of jointing. By superposition of the contributions from intact rock and from the joints, the total deformability is obtained by:

$$\frac{E_m}{E_i} = \frac{K_n S}{K_n S + E_i} \tag{17}$$

The normal stiffness can be determined from equations (11) - (14).

The method is obviously best suited for bedded rock, Figure 30, but may be realistic for the case of fracture zones characterized by pronounced, subparallel fracturing. As compared to the wholly empirical methods described above, it has the important advantage of allowing joint deformational characteristics and stress dependency to be directly incorporated.

The uniaxial model in Figure 30 may be extended to include jointing and/or loading in more than one direction (Kulhawy, 1978). Furthermore, Fossum (1985) derived equations for determination of the elastic properties of a randomly jointed rock mass on the basis of intact rock modulus, average joint spacing and joint normal- and shear stiffness.

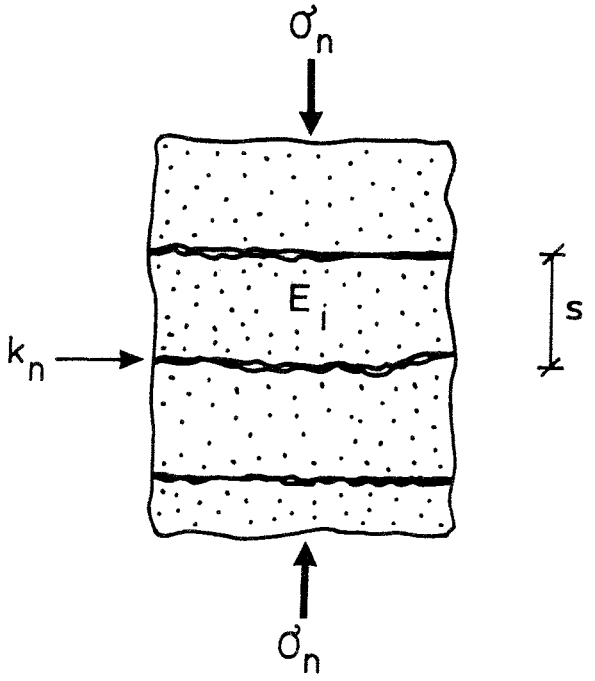

Figure 30. Rock mass model assumed for calculation of rock mass deformation modulus according to equation (17) (from Leijon and Ljunggren, 1992).

6.3 Fracture Zone 2, Finnsjön

In a recent study of Fracture Zone 2 at the Finnsjön site, Leijon and Ljunggren (1992) applied the procedures presented above to estimate the deformation modulus of both the fracture zone and of the rock mass hosting it. As the zone does not outcrop the study was based exclusively on core data; the results are summarized in Figure 31. The fracture zone was conceptually illustrated in Figure 14. Closer examination of core information revealed a width of about 100 m and a quite moderate fracture density averaging 5 fractures/m, though with considerable local variations (Ahlbom and Tirén, 1991). Calculated RQD-values generally

did not fall below 60, excluding local drops over sections of a few meters width. For the purpose of estimating deformability, it was felt realistic to consider Zone 2 as a fractured rock mass, rather than as one discontinuity.

Figure 31 indicates that the three methods applied produced reasonably consistent results. The values are well in line with data available from other case studies in similar environments (Lama and Vutukuri, 1978). Thus, the empirical approach taken would appear valid in this particular case.

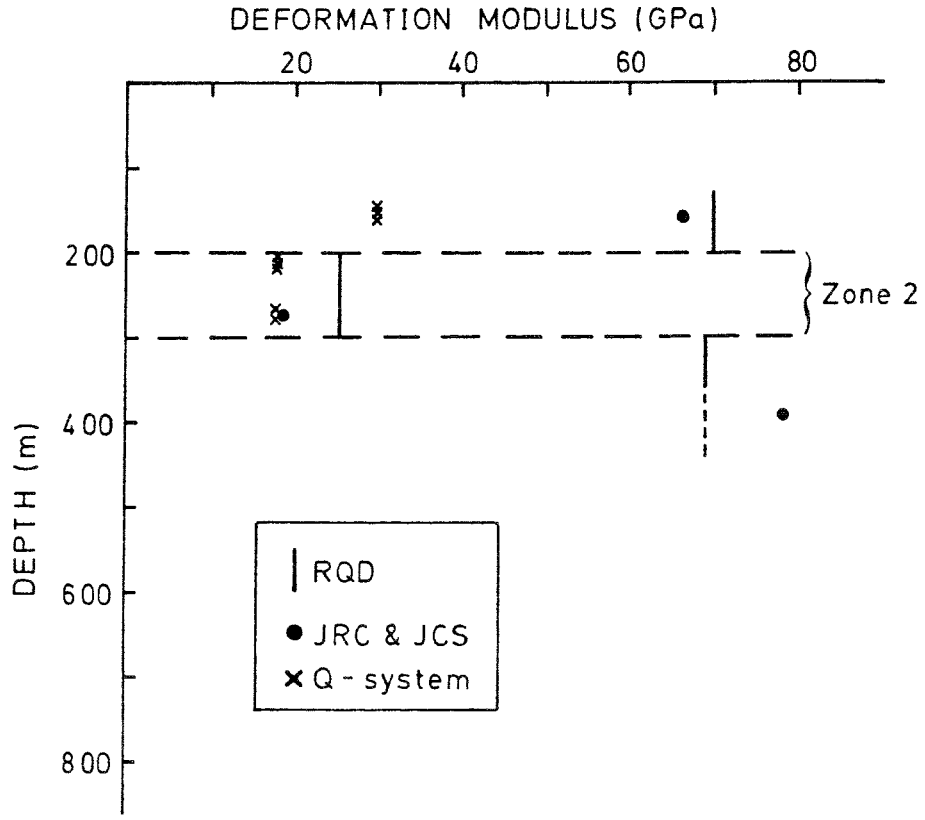

Figure 31. Estimated rock mass deformation modulus at the Finnsjön site as a function of depth. Data obtained by applying three different empirical methods to drillcore data from borehole KFI06. Data points denoted "JRC & JCS" have been obtained from eq. (17). Fracture Zone 2 is located approximately within the interval 200 -300 m (from Leijon and Ljunggren, 1992).

There is, however, some uncertainty associated with sections showing low rock quality. Core drilling provides poor representation of such sections, and neither the RQD method nor the classification systems can be reliably applied. In the Zone-2 case, poor rock sections (apparent RQD less than about 30) totalled less than 10 m out of the 100 m section constituting the zone, and core losses were less than 0.5 m. Thus, even if these sections are characterized by deformation modulus values that are much lower than for the remainder of the zone, this will not seriously affect the overall deformability of the entire zone.

6.4 Eastern regional zone, Fjällveden

The so called Eastern regional zone at Fjällveden is a well expressed regional shear zone that extends laterally for several tens of kilometers (Ahlbom et al., 1991). It is about 90 m wide and extensive shear deformation is evidenced by crushed sections, mylonites and breccias. Clay altered fractures and slickensides are abundant. A diamond-drilled borehole intersects the zone at a steep angle to a depth of about 100 m. Logging data and a brief visual inspection of the core for the present purpose reveals the following:

- The main rock type is migmatitic gneiss

- Average fracture frequency over the 90 m long borehole interval constituting the zone is about 20 fractures/m. This excludes sections with crushed rock or core losses.

- Crushed rock and core losses comprise a total of 10 m (11%) of the 90 m borehole section.

- Shear disturbances are unevenly distributed over the section. Heavily disturbed sections are separated by thicknesses showing little or no signs of shear movements, despite sometimes high fracture frequency. This indicates a morphology with major "shear bands" delineating better preserved shear lenses.

- Clay altered fracture surfaces are common. Roughness is very variable but relatively high for the majority of fractures outside the heavily tectonised zones.

By applying the methods presented above to estimate the modulus of deformation for the zone, the following becomes apparent:

- Considering first the RQD-method, the average fracture frequency (20 per meter) immediately indicates that at most a small portion of the borehole interval can have RQD-values exceeding say 50, and average values must be much lower (this is easily verified by consulting core logs which are not shown here). This means that the RQD-method is not applicable, Figure 28. The only conclusion that can be made is that the ratio E_m/E_i will probably not exceed 0.15. This value can therefore be used to calculate an upper bound estimate for the rock mass deformation modulus. Assuming an intact-sample modulus of E_i = 65 GPa, which is realistic, the value obtained for the rock mass is 10 GPa. The real value may be much lower than this upper bound estimate.

- For similar reasons, rock mass classification schemes will not prove useful as a basis for estimating deformability. While heavily fractured rock can be reasonably well classified by observations from accessible excavations, this

is not so for the case of core observations only. Estimates that can be given are confined to upper bound estimates, no better than the one given above using the RQD-method.

- Superimposing the contributions from the intact rock and the joints, Figure 30, is an improvement over the other methods in accounting for the heavy fracturing, although straight application of the concept to the present zone involves gross simplifications of the actual conditions. According to equation (17) parameters such as intact rock modulus, mean joint spacing and joint normal stiffness, K_n, need to be determined. No data exist for these parameters and determination would require a testing program to be carried out. Using, for example, the procedure outlined in chapter 5 to determine joint normal stiffness, one would first investigate the core in detail in order to delineate joint sets with similar characteristics. Then, the parameters JRC and JCS would be determined by tests conducted on a large number of jointed samples, and parameter distributions would be established for the joint sets identified. These would provide input to calculation of similar distributions for joint stiffness and finally for rock mass modulus. Performing such a sequence of testing is however outside the scope of the present study. For the purpose of illustrating the nature of the relationship only, calculations for four combinations of assumed parameter values were performed according to Table 5.

Table 5. Assumed parameter values for calculation of modulus of deformation for the Eastern regional zone, Fjällveden.

Combination	JRC	JCS (MPa)	S (m^{-1})	σ_c (MPa)	E_i (GPa)
1	4	30	0.025	150	60
2	4	30	0.075	150	60
3	8	60	0.025	150	60
4	8	60	0.075	150	60

Joint normal stiffness for combinations of parameters is then estimated from equations (11) - (14). Substituting the values obtained into equation (17) then yields the rock mass modulus as plotted in Figure 32, where the calculated values are plotted as a function of the normal stress. Given the lack of adequately determined input data as described above, the modulus values must be seen as indicators rather than as bounding estimates. The curves also serve to illustrate the effects of joint spacing and joint surface characteristics. It should be remembered also that even if thorough joint characterization was attempted, the method would fail to incorporate the contribution to the deformability by the 11% section characterized by crushing or an absence of core. An important observation that can be made

from Figure 32 is that the deformation modulus of a jointed rock mass is highly stress dependent, at least at low stress levels. This follows from the strong stress dependency of the joint normal stiffness, cf. Figure 23. When using the RQD- and rock classification methods to estimate deformation modulus, as described earlier, this stress dependency is not taken into account. Considering the origin of the "full-scale" data used to calibrate these methods (shallow tunnels, plate bearing tests etc) it is fair to assume a normal stress level of the order of 5 MPa. The modulus values indicated in Figure 32 at this stress level fall roughly in the interval 5-15 GPa. This is comparable to the upper bound estimate - about 10 GPa - obtained with the RQD-method.

The overall conclusion would be that the indicated method can at best provide upper bound estimates for the deformation modulus of the Eastern regional zone.

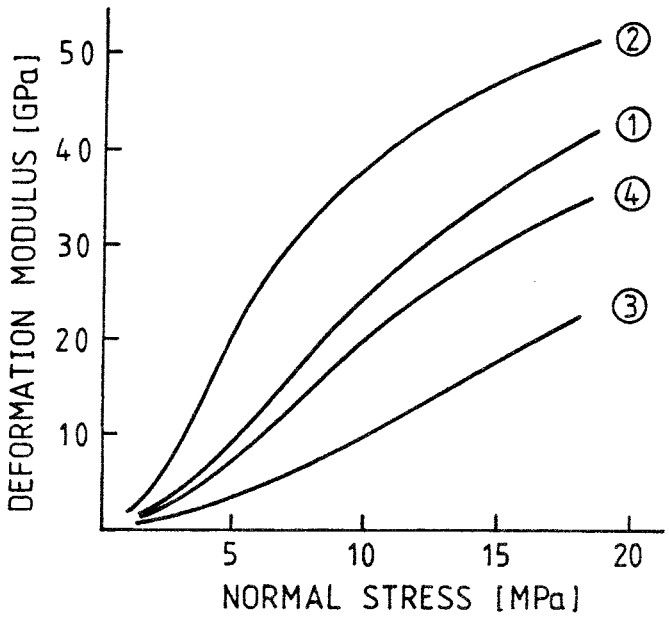

Figure 32. Estimated rock mass deformation modulus of the Eastern regional zone at Fjällveden as a function of normal stress. Numbers 1-4 refer to combinations of input parameters according to Table 5.

6.5 Zone 3, Kamlunge

Fracture Zone 3 at the Kamlunge site is situated mainly in granitic rocks (Ahlbom et al., 1992). It is steeply dipping, 1-10 m in width, and has been traced over a distance of about 3 km at the surface. It is thus a much smaller feature than the zones described from Finnsjön and Fjällveden.

During field investigations at the Kamlunge site four cored boreholes were drilled to intersect the zone at various depths. The core data are summarized in Table 6; it was found that up to 27 % of the zone remained unsampled by the drilling due

to poor core recovery (losses and crushed material). These sections probably have a large influence of the effective modulus, but will be disregarded using the methods of estimation described above. In the case of Kamlunge, therefore, these methods are not applicable. Furthermore, the table shows that the four boreholes provide rather inconsistent information that would lead to correspondingly inconsistent modulus estimates. Seemingly, the variation of the mechanical character along the plane of the zone is large and intersecting boreholes can therefore not provide a good representation thereof.

Table 6. Summarized data from four boreholes at the Kamlunge site at their intersections with Fracture Zone 3.

Borehole	**KM3**	**KM8**	**KM11**	**KM12**
Section (depth, m)	441-450 = 9 m	63-69 = 6 m	324-335 = 11 m	52-60 = 8 m
Fracture frequency (m^{-1})	22 (?)	19	9	15
Core loss or crushed rock	2.4 m (27%)	1.3 m (22%)	0.4 m (4%)	1.0 m (13%)
Joint roughness	extremely low to moderate	generally high	moderate - high	variable
Other observations	poor, highly altered rock	no alteration, fair quality	fair-good rock	variable quality

7 IN-SITU DETERMINATION OF DEFORMABILITY

7.1 Introduction

The empirical systems for estimation of rock mass deformability introduced in the previous chapter have emerged from numerous cases of actual observation of rock mass response to excavation work. However, despite that they are based on "full-scale" observations, application is indirect since deformability is referred to laboratory-scale parameters and rock mass classification indexes. As shown in the previous chapter, this obstructs application to fracture zones.

At the Underground research Laboratory (URL) operated by the Atomic Energy of Canada Limited (AECL), a series of tests have been conducted aimed specifically at determining the deformability of a fracture zone by direct in-situ testing (Martin et al., 1990). This constitutes the most comprehensive effort of its kind conducted to-date, and has produced a set of data that are appropriate in the present context.

7.2 URL

The URL is located 100 km northeast of Winnipeg, Manitoba, within the Lac du Bonnet batholith. The facility is excavated in massive granite-granodiorite. Figure 33 shows a generalized vertical cross section through the vertical shaft by which the test facilities are accessed. The batholith is intersected by major thrust faults, two of which intersect the shaft (Figure 33), and are referred to as Fracture Zone 2 and Fracture Zone 3. Two splay zones, termed Fracture Zone 2.5 and Fracture Zone 1.9 also intersect the shaft. The zones are formed by chloritic slip surfaces grading into cataclastic parts containing breccia and fault gouge. The cataclastic zones have widths of 20 mm to 1 m and show evidence of shear displacements of several meters or tens of meters.

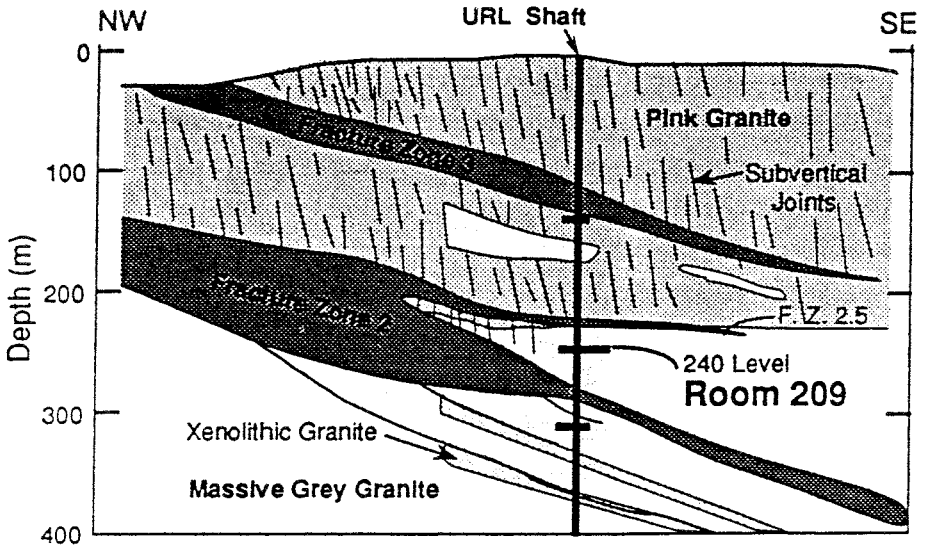

Figure 33. Generalized section of the geology at the URL facility including the test area (from Tannant, 1990).

Another, and much smaller fracture zone was intersected when excavating a test adit at the 240 m level at URL. This feature, termed the Room 209 Fracture Zone, is steeply dipping and probably of extensional origin; as exposed in the adit it is up to 0.4 m in thickness. It is composed of a number of fractures of which one has been interpreted as the major extensional fracture (Martin et al., 1990). Tannant (1990) states that it is a composite zone since some joints are discontinuous, én-echelon features, suggesting shear deformation.

Investigations relating to the mechanics of the fracture zones at URL have included (Martin et al., 1990):

- Geological characterization using a large number of boreholes and by observations at locations where the zones intersect the shaft or horizontally developed excavations.

- Comprehensive stress determinations using a variety of methods, and referring to several locations above and below the major fracture zones (Martin, 1989). The results are discussed in Chapter 9.

- Determination of coupled hydraulic-mechanical behavior of Fracture Zone 2 and the Room 209 fracture by borehole testing. This was accomplished by means of a sophisticated borehole extensometer (Pac-ex system) shown in Figure 34. The device allows simultaneous axial displacement measurements between anchor points and water injection into sealed-off intervals along the borehole. Results from these tests are reviewed below.

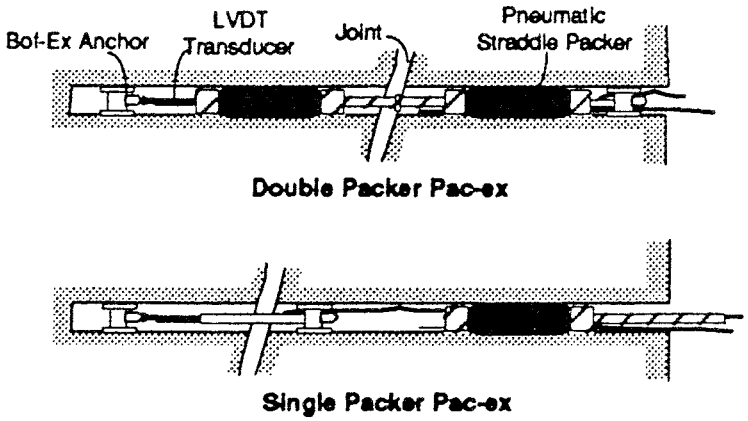

Figure 34. Schematic diagram of the Pac-ex instrumentation for combined hydraulic and mechanical borehole testing (from Martin et al., 1990).

Pressurization of borehole sections was conducted to increase the pore pressure in intersected discontinuities. This reduced the effective normal stress across the discontinuities, and the deformation resulting from this unloading was recorded with the Pac-ex devices. As the holes were drilled approximately perpendicular to the fracture zones, normal deformation was recorded. Given certain assumptions as regards to water pressure distribution around the borehole and boundary conditions, this test arrangement allowed evaluation of normal stiffness for sections between anchor points. Test results as reported by Martin et al. (1990) are reproduced in Table 7. The assumptions made to evaluate normal stiffness from measured deformations were not specifically stated, but it is believed that a uniform pressure distribution across the discontinuity plane, extending far out from the borehole, was assumed. It must also be assumed that boundary conditions are sufficiently soft to allow separation of joint planes to be fully transferred to anchor points.

Table 7. Results from borehole determinations of normal stiffness, K_n of Fracture Zone 2 and the Room 209 Fracture at URL. Estimated K_n-values were obtained according to section 5.2.3. (after Martin et al., 1990).

Borehole	Mean eff. normal stress (MPa)	Depth (m)	No. of tests	In-situ K_n (MPa/mm) Range	Mean	Estimated K_n (MPa/mm)
Fracture Zone 2						
HC28	0.9	6.75-23.5				11.5
	0.8	6.75-10.25	3	43.9-72	57.9	10.6
	1.0	10.25-14.25	5	20.4-53.2	32.8	12.4
	0.9	14.25-16.5	6	3.9-5.0	4.4	11.5
	0.9	16.5-19.5	6	8.8-13.3	10.9	11.5
	1.4	19.5-23.5	3	119.3-224.3	170	16.5
HC30	1.1	4.75-28.25	7	2.9-3.7	3.3	13.4
GC3A	0.5	4.75-28.25	8	2.1-5.7	3.2	8.16
HC1	20.5	29.0-39.4	2	21.5-24.8	23.2	860
GC5	20	37.0-38.0	1	266.3	266	860
GC6	20	35.5-38	1	104.7	105	860
GC7	18.7	30.0-39.0	1	33.9	33.9	681
GC12	19.3	20.62-40.12	1	7.5	7.5	790
Room 209 Joint						
OC1	8.6		2	352-635	495	439
N1	9.3		12	50-110	83	502

Figure 35 shows results from two boreholes - HC28 and HC30 - located 5 m apart and both intersecting Fracture Zone 2. HC28 contained multiple measuring intervals and HC30 a single measuring interval spanning the entire fracture zone. As shown in Table 7, the effective normal stress across the zone, determined by stress measurements at the borehole locations, is only about 1 MPa. The water pressures applied during testing ranged up to similar magnitudes. The data from borehole HC28, Figure 35, clearly show that the major shear plane containing cataclastic material has a much lower stiffness than the remainder of the fracture zone. The average value for the "cataclastic interval" is 4.4 MPa/mm. Superimposing the contributions from all test intervals yields stiffness for the entire zone of 2.7 MPa/mm, i.e. only about 40% lower than for the cataclastic zone alone. The value from borehole HC30 is in good agreement with those from HC28. Stress dependency of the normal stiffness was also investigated. However, within the interval of normal stress change imposed by the water pressure - maximum 2 MPa - no stress dependency could be delineated.

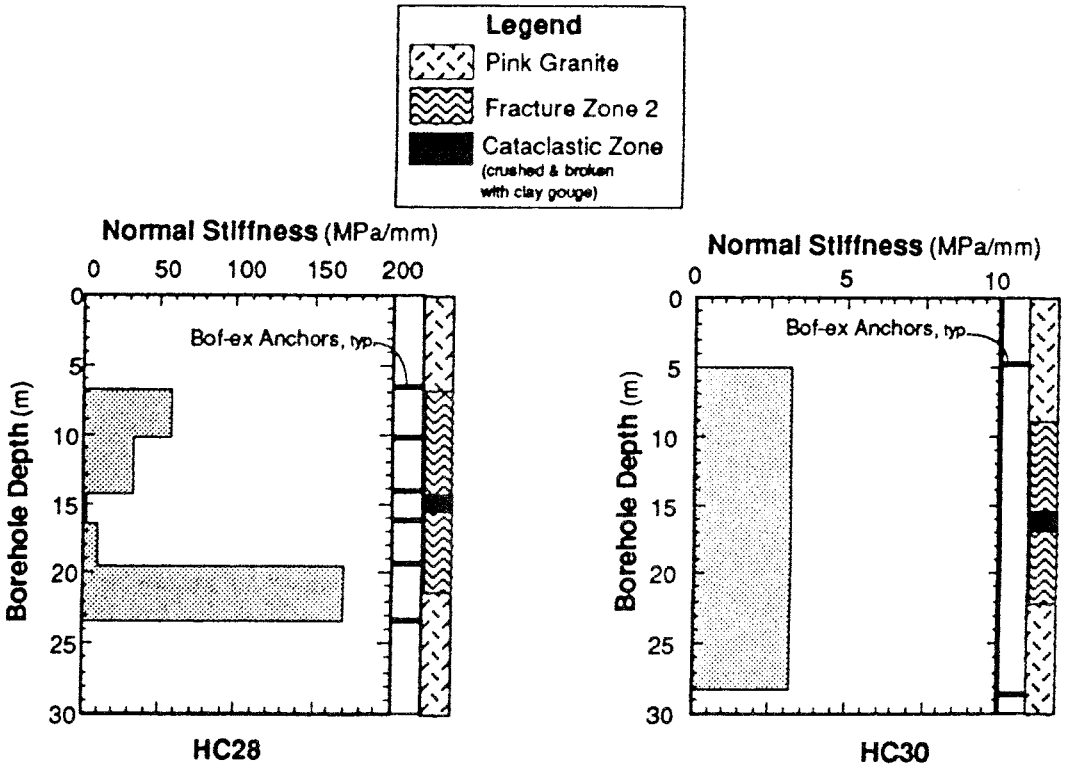

Figure 35. Normal stiffness of Fracture Zone 2 as obtained from multiple interval tests in borehole HC28 (left) and single interval tests in borehole HC30 (right). Note correlation with geology in hole HC28 (from Martin et al., 1990).

The normal stiffness of the Room 209 fracture was evaluated from tests in two boreholes; the results are shown in Figure 36. The Pac-ex instrumentation straddled the entire 0.4 m wide fracture zone, although drilling indicated one prominent fracture at the borehole locations. The surprisingly low values measured in borehole N1 were attributed to disturbances from a closely nearby excavation. The tests in OC1 were believed to better represent the discontinuity under undisturbed conditions.

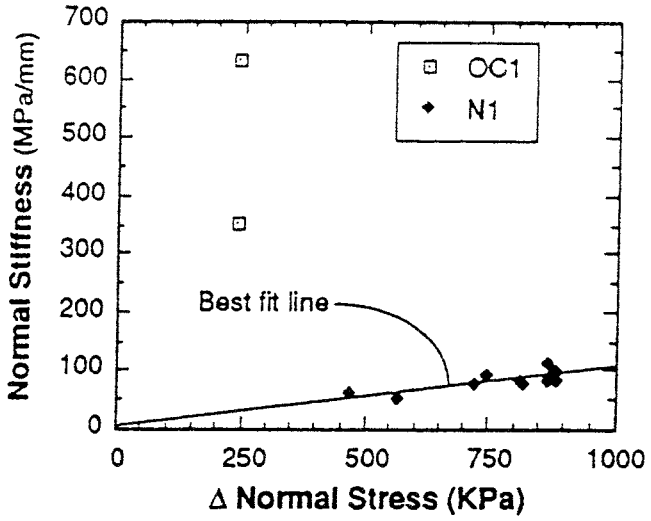

Figure 36. Normal stiffness as a function of change in normal stress for the Room 209 fracture.

The experimental determinations of normal stiffness were compared to predictions using the Barton-Bandis model as described in section 5.2.3. Input parameters required for the predictions (JRC, JCS) were determined on core specimens. Figure 37 compares predictions and measurements. It was concluded that the model provided reasonable predictions for the Room 209 extensional fracture, though with reservations for the fact that only a few tests representing one level of normal stress were conducted. At very low normal stresses fair agreement was observed also for Fracture Zone 2. The disagreement for high normal stresses can by explained with the fact that the model is developed for unfilled discontinuities (such as the Room 209 fracture). Fracture Zone 2 is indeed not an unfilled discontinuity, and therefore exhibits much less normal stress dependent closure behavior than predicted by the model.

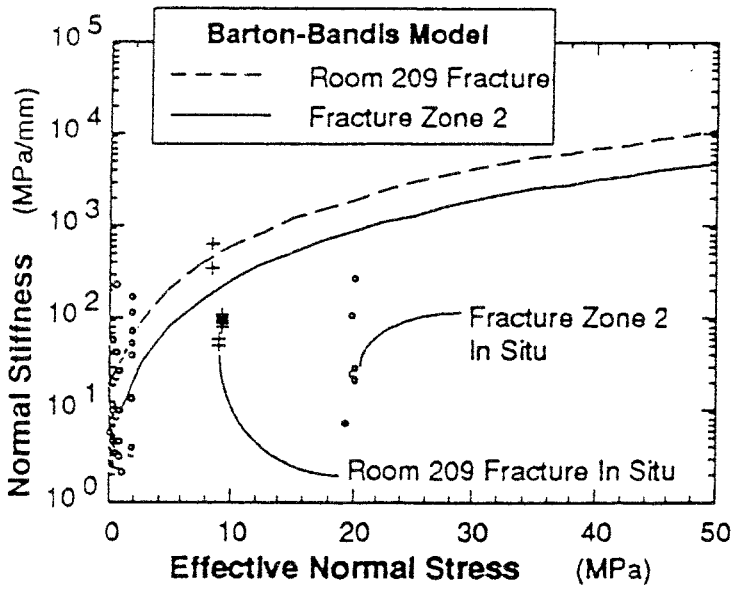

Figure 37. Predicted and measured normal stiffness as a function of effective normal stress (from Martin et al., 1990).

7.3 Grimsel

Hesler et al. (1990) have reported borehole tests of a fracture zone at the Grimsel test site operated by NAGRA in Switzerland. The tests concerned determination of normal stiffness, and tests procedures were analogous to those applied and reported earlier from URL. The effort at Grimsel was however more directed towards evaluation of models available to resemble the water injection test method than at gaining field data. The site specific results indicated stiffness values considerably higher than those reported from URL, but no conclusions were drawn in this respect.

8 INDUCED FAULT MOVEMENTS IN MINES

8.1 Introduction

Because of the extensive networks of shafts and drifts that are required to operate underground mines, many opportunities exist to study large scale structures by direct observation from excavations. Unfortunately, the interest for large structural features such as fracture zones is often limited to potential implications on ore body geometry and geology, and to local stability in connection with intersecting excavations. In some cases, however, fracture zones may affect stability on a larger scale. Faults subjected to stresses that become critical with respect to shear failure is a particularly important category of stability problems. The basic mechanism is that mining activities cause perturbations of the stress field, such that normal stress across the fault plane is decreased and/or shear stresses are increased to the point where the shear strength of the fault is exceeded. Failure occurs, often as dynamic slip, and the seismic energy generated can cause sudden and severe damage to mine workings. The characteristics of ground motion caused by induced fault slip show many similarities with those of natural earthquakes.

The phenomenon of induced fault slip has been observed in numerous mines around the world, representing a variety of geological conditions. This includes potash- and coal mining in soft rocks as well as gold mining in very strong and brittle formations; see e.g. Johnston and Einstein (1988) for an overview. The dimensions of fault plane surfaces over which slip movements are recorded ranges from tens of meters to several kilometers. Slip magnitudes may be up to several decimeters, and the associated seismic events are typically of magnitudes M_L = 3-5. Such events are associated with release of large quantities of strain energy, and the stresses in the surrounding rock mass must be sufficiently large to cause accumulation of the required energy prior to failure. Therefore, fault slip occurs primarily in deep mines where stresses are high, mostly at depths greater than 1500 m. The most well known occurrences have been reported from deep mines in Canada and South Africa. These cases are particularly relevant in the present context because they refer to hard rock formations in seismically stable shield areas. Swedish mines are generally too shallow (<1000 m) to experience large-scale mining induced fault slip. The event occurring at the Grängesberg mine in 1974 (and followed by a series of smaller events) as reported by Båth and Wahlströms (1976), is an exception that probably represents an uncommon type of induced fault movement.

Documented and analyzed cases of mining induced fault slip are of interest because they constitute large scale "shear tests" - though not well controlled - of discontinuities, from which properties may be obtained by back-calculation. Furthermore, such reference cases can provide a good measure of the current capability to understand, model and predict shear behavior of faults. Extraction of reliable data is however difficult without conducting detailed case studies. This is so because each case is characterized by its own, more or less unique set of parameters as regards mining geometry, stress conditions and geology. Mining geometry is an especially complicating factor, not only because it affects stress conditions but also because the open voids in the rock mass formed by the excavations alters the kinematics of the system. Available data on fault slip

behavior have resulted primarily from: i) seismic monitoring, and ii) direct observations from excavations or by means of boreholes. Seismic monitoring as applied in mining has a long history and has reached a high degree of sophistication. However, for obvious reasons, it can only capture the dynamic component of shear deformation.

8.2 Deep gold mines in South Africa

The most extensive experience of mining-induced fault instability is undoubtly to be found in South Africa, where the problem long since has been encountered in several of the deep gold mines, primarily within the Klerksdorp mining district. The environment in these mines is characterized by shallow-dipping, thin and laterally extensive gold-bearing veins (reefs) that occur in strong, brittle quartzitic formations, Figure 38. Initial stress levels may be of the order 40-80 Mpa. Distinct normal faults with displacement magnitudes of tens or hundreds of meters offset the reef horizons. The width of the fault zones is typically a few meters and shear deformation is generally concentrated more or less to a single shear plane containing intensely deformed mylonite and cataclastic material.

As mining of the reefs approaches a fault intersection, from one or both sides, the fault plane experiences local stress changes. Depending on geometry, far-field stress conditions and location along the fault plane considered, the stress changes may result in improved clamping of the fault (increased normal stress or decreased shear stress) or destabilization by reduction of normal stress or increase of shear stress. The modes of fault shear displacement can be complicated due to interaction with the mine structure. Figure 39 shows two hypothetical examples of deformation; in the upper case, the offset reef is mined towards the intersection without leaving any remnants. This causes a uniform mode of slip. In the lower figure, the deformation process is complicated by the presence of two remnants.

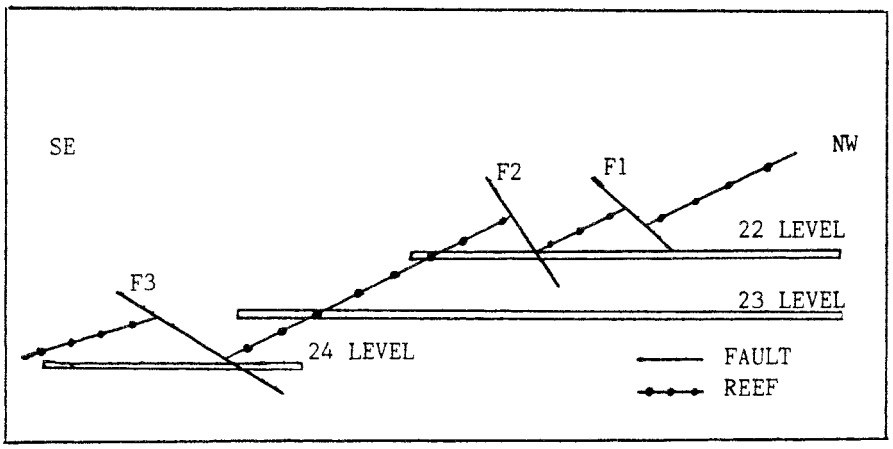

Figure 38. Schematic example section from a gold mine in South Africa showing a reef displaced by three faults. Vertical distance between the levels is 100 m (from Holmes and Reeson, 1988).

a)

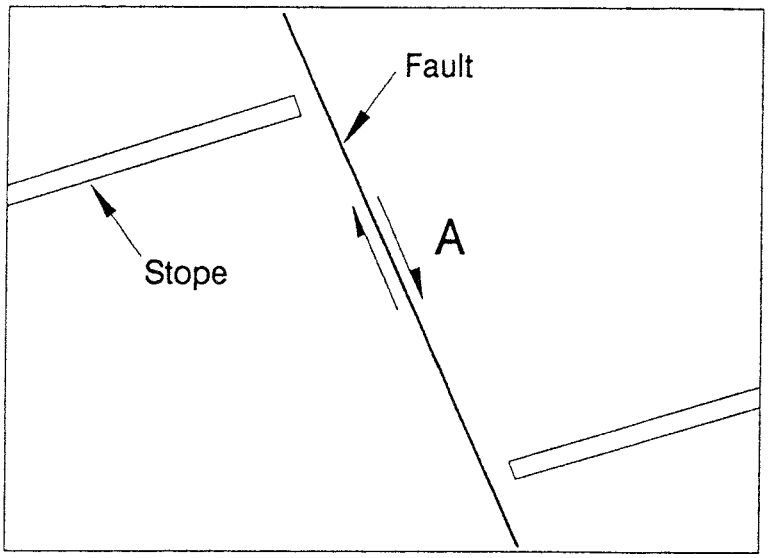

b)

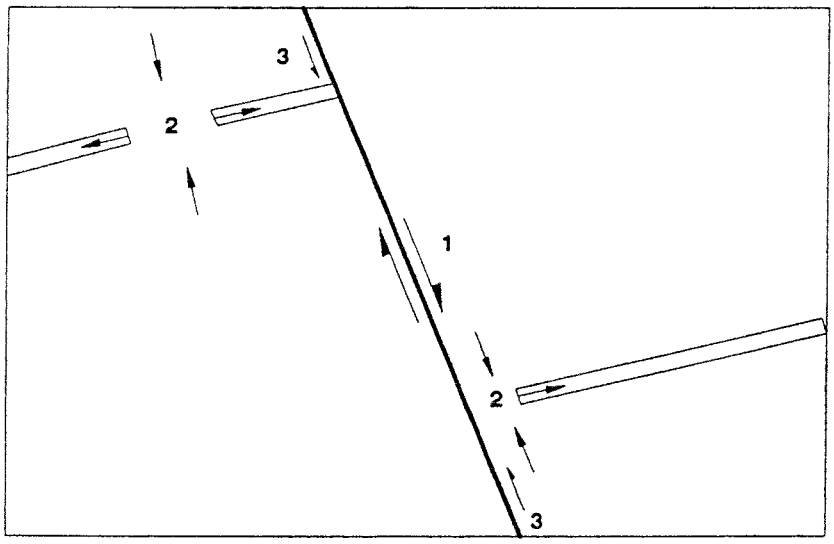

Figure 39. Examples of modes of fault slip induced by reef mining (from Brummer and Rorke, 1988).

a) "standard mode" shear displacement between faulted reef positions

b) fault slip initiated as above (1). This transfers load to two remnants that are crushed, resulting in stope closure (2). This in turn induces reverse shear movements at indicated positions along the fault plane (3).

The many "large-scale shear experiments" that fault slip occurrences in the South African gold mines represent, has produced a large amount of practical experience of fault shear behavior. Furthermore, since the ability to predict the nature and magnitude as well as time and location of these occurrences is crucial from the mining point of view, significant research efforts have been devoted to the problem. It is felt that important lessons can be learnt from this body of work. Static stress modelling has been found useful as a means to predict where fault slip is to be expected. To predict the stage of mining and loading conditions, i.e. when slip occur, is much more difficult, but progress has been made. It is evident that attempts to obtain more precise values of fault strength properties such as friction angle and cohesion by sampling and testing have not produced major improvements of failure criteria. The progress has instead occurred from systematic use of previous experience. The procedure commonly adopted for predictions involves the following:

- Determine initial stress conditions and fault plane geometry as carefully as possible

- Calculate normal- and shear stress across the fault plane using relatively simple material models

- Compare calculated stresses with a simple Mohr-Coulomb shear failure criteria. Zero cohesion and a friction angle of 30^{o} appears to be standard strength properties assumed

- Locations on the fault plane where the calculated shear stress exceeds the value allowed by the strength criteria are defined as potential slip locations

- The magnitude of excess shear stress (ESS) at these locations, as obtained from modeling, is then used to assess the risk of encountering a slip event. This is possible because empirical correlations have been derived from previous case histories.

The procedure is commonly referred to as the excess shear stress (ESS) method (Ryder, 1988). It is seen that case-specific determination of strength properties is not emphasized.

Table 8 shows documented maximum slip magnitudes resulting from major slip events in relation to the dimensions of the fault surface areas involved. It is seen that the ratio of slip magnitude to average diameter of slip area is of the order of $1 \cdot 10^{-4}$ to $4 \cdot 10^{-4}$. This is similar to natural earthquakes, but comparisons may be misleading due to the influence of mining geometry for the present data.

Predicting slip magnitudes with an accuracy better than a factor of 2-5 has been found difficult. An example of predicted and measured slip, taken from the well investigated slip event along the Wesselia fault in the Welkom mining district, is shown in Figure 40. Predictions were made using MINSIM-D, a displacement-discontinuity program developed for the present kind modelling. It is seen that

actual slip values are up to three times higher than the predicted ones. The figure also shows intervals for the calculated excess shear stress (ESS) magnitude across the fault plane which were used to delineate regions of the fault plane that were critically loaded.

Table 8. Slip areas and slip magnitudes determined from major events of induced seismic fault slip in South African gold mines (from Brummer and Rorke, 1988).

Event (name and year)	Local magnitude	Slip area dimensions, length x breadth (m)	Slip magnitude (m)
Vlooi, 1985	3.6	500 x 60	0.1
South-eastern, 1988	4.3	1500 x 200	0.1 (?)
Wesselia, 1982	4.6	1500 x 120	0.3
Two Shaft, 1986	4.7	2000 x 250	0.2 (?)
Five Shaft, 1987	4.9	2500 x 300	0.2

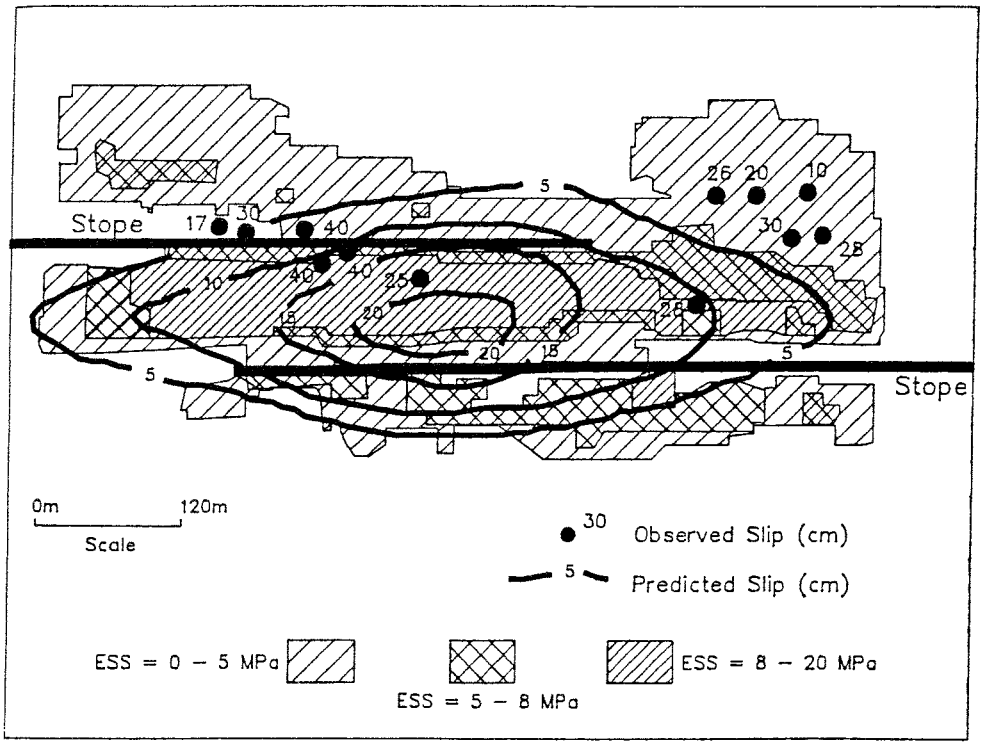

Figure 40. Contours of predicted (lines) and observed (dots) slip for the Wesselia fault slip event. The view is perpendicular to the fault plane. ESS - intervals given; indicated as areas in the figure are magnitudes of excess shear stress across the fault plane (from Brummer and Rorke, 1988).

The mining-induced fault movements occur both as stable, aseismic creep and as unstable, seismic events. Available modelling tools are essentially incapable of predicting the mode of deformation. One reason is that the displacement- or velocity weakening constitutive behavior that characterize the faults (and which is a prerequisite for seismic energy release in connection with slip) can not be adequately described. Another is the very nature of the slip process; results from direct observations as well as seismic monitoring consistently show that this process is not characterized by uniform shear over the activated fault surface area. On the contrary, it has been found that deformation develops according to a stick-slip type mechanism, in which surface topography plays an important role (van Aswegen, 1990). Thus, the shear deformation typically begins with stable creep, or sequences of small seismic events, at locations with smooth fault surface topography. Other parts of the fault plane remain locked due to the action of asperities formed by undulations or jogs. Local increases of normal stress across the fault plane, due to stress disturbance from the mining, can have a similar clamping effect. Shear load is gradually transferred from the regions of creep movement to the locked asperities, which finally shear violently causing the major dynamic events. Now, given this fundamental mode of shear behavior, it is obvious that models involving simplification of fault surface geometry or assuming uniform shear resistance over the fault plane can indeed be misleading. This deficiency can not be fully balanced by improved knowledge of intrinsic strength parameters such as basic friction angle or cohesion. This explains why research efforts directed towards fault surface topographical characterization and monitoring of qualitative behavior have been more rewarding than those aiming specifically at determining mechanical properties.

8.3 Stress release by fluid injection

Practical experience has shown that artifical increase of pore pressure can initiate seismic events. This has been observed in several contexts, including reservoir filling, waste fluid injection in deep boreholes and during flooding of mines. It is generally accepted that the mechanism occurs by the reduction of effective normal stress which initiate shear displacement of discontinuities.

An interesting attempt to use fluid injection to initiate fault movement in the Buffelsfontein Gold Mine in South Africa has recently been reported by Board et al. (1992). The test concept is shown in Figure 41. The test location was near the intersection of a fault plane and a stope that was mined towards the fault. The aim was to evaluate the possibilities to trigger small-scale events by locally increasing pore pressure in the fault plane by means of injecting water through intersecting boreholes. This provides a possibility to control the release of strain energy, rather than waiting for a larger and potentially more hazardous event.

Predictions by means of numerical modelling were made assuming a Mohr-Coulomb type shear strength criterion with zero cohesion and a friction angle of 30^{o} for the fault. Testing showed that local shear events occurred at the pressurized location of the fault plane at an injection pressure of 20 MPa This was in close agreement with predictions. The in-plane extension of the region that was

pressurized was estimated to be a few meters only. The nature and locations of the seismic events that were recorded supported this estimate. These results indicate that the shear strength parameters were correctly estimated and that the onset of fault slip can be reasonably well predicted, at least on the scale represented by the test. The study also showed that overall fault slip occurred as the cumulative result of a large number of slip events on a smaller scale, i.e. as a stick-slip process. Similarly to the previously referred studies, it was concluded that better methods were required to determine fault surface characteristics in order to identify asperities that provide local "clamping" of the fault plane.

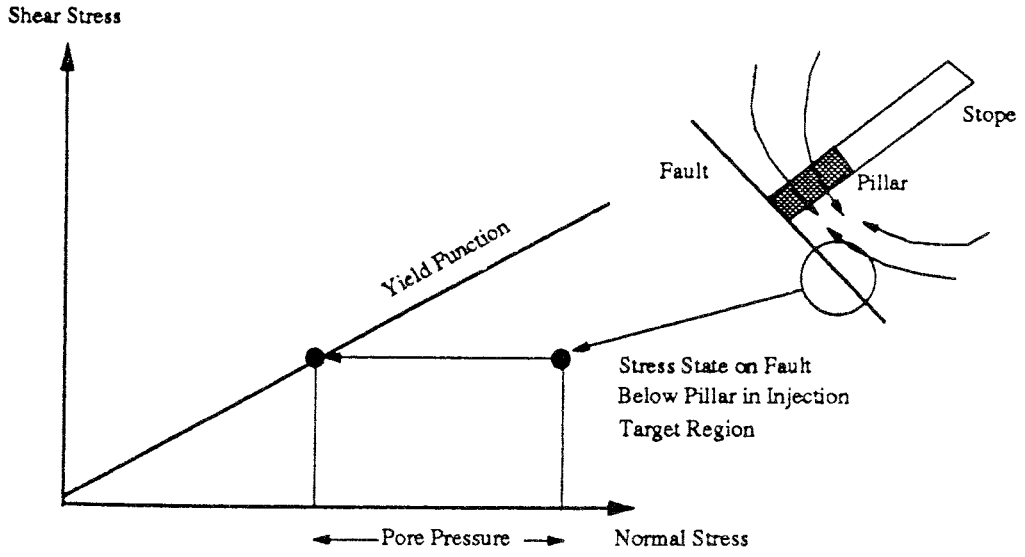

Figure 41. Conceptual background to the fluid injection test conducted at Buffelsfontein Gold Mine in South Africa (from Board et al., 1992).

8.4 Strathcona Mine, Canada

The Strathcona Mine is one of several mines within the Sudbury district in Ontario, Canada, that experience rock burst problems associated with high stresses. Monitoring of the mining-induced seismic activity in Strathcona has shown slip movements along a fault and a slickensided dyke interacting mechanically with each other and with the mined structures. The depth to the slip locations is only some 500-700 m, but stress conditions are heavily disturbed due to high extraction ratios within the area of mining. The problem of slip along the identified structures was studied using three-dimensional, distinct element modelling technique (Hart et al., 1988; Tinnucci and Hanson, 1990). By comparing seismic monitoring data with results from modelling, it was found that locations and radii of movements resulting from defined mining sequences could be fairly accurately predicted. The general understanding of system behavior, and hence

of the influence of key parameters like stress conditions and system geometry, was substantially improved. As predictions of slip magnitudes and exact nature of slip movements would have required both better site specific data and more elaborate constitutive models, this was not attempted. Parameter studies showed that the effective friction angle of the fault zone was within the range $30\text{-}40^{o}$ (no further details of internal fault zone structure reported) and $20\text{-}30^{0}$ for the slickensided dyke. It was not possible to establish more narrow intervals for the frictional resistance.

9 STRESS CONDITIONS IN THE VICINITY OF FRACTURE ZONES

9.1 Introduction

The distribution of stress in the neighborhood of a discontinuity is a function of: i) the external stress field forming boundary conditions, ii) the mechanical properties of the discontinuity, and iii) the mechanical properties of rock mass hosting the fracture zone. Loosely speaking, the extent to which a structure such as a fracture zone disturbs the stress field is proportional to the contrast in mechanical characteristics between the zone and its surroundings. In principal, this allows the stress perturbation caused by a fracture zone to be calculated if the mechanical properties (zone and surroundings) and the external stress field are known. Correspondingly, mechanical properties may be inferred from observations of the stress field.

The theoretical principles and models that may be, and indeed have been, applied to study these relationships will not be further discussed here. Instead, results from a number of field investigations involving stress measurements in the vicinity of fracture zones will be reviewed and commented. Some experience from Swedish mines will also be summarized.

9.2 Experience from Swedish mines

In underground mines, anomalous stresses are often indirectly observed in connection with excavation of drifts intersecting major structures. For example, Borg (1989) observed increased stress-driven rock bursting around a drift in the Malmberget mine when the drift approached a 0.5 m wide, heavily fractured shear zone. The drift was located in brittle leptite at some 650 m depth. Similar experiences are available from the Kiirunavaara and Zinkgruvan mines. A common feature of these observations is that they do not refer to direct stress measurements, but to occurrences of stress-induced instabilities, which are attributable to stress variations. The indirect nature of the data and the many factors that, besides stresses, affect failure behavior, preclude more precise interpretation of the nature of stress perturbations induced by large-scale structures.

Another observation is that structures such as dykes and boundaries between mechanically contrasting rock types, can be accompanied by local stress anomalies that are much more pronounced than those found near fracture zones in otherwise homogeneous rock. Measurements near rock type boundaries in the Viscaria- and Kiirunavaara mines have shown increases in stress magnitudes by a factor of two and more over distances of less than 10 meter. These data have unfortunately not been further analyzed from geological standpoints.

Altogether, the information available from Swedish mines may be summarized as follows:

- Major fracture zones can cause significant stress anomalies extending at least a few tens of meters out from the zones

- Available data are essentially qualitative and consistency is poor

- No example of systematic stress measurements to investigate the nature of stress anomalies related to fracture zones can be found.

9.3 Forsmark

The bedrock at and around the nuclear power facilities at Forsmark in east-central Sweden has been subject to a long sequence of geoscientific investigations related both to the construction of nuclear power plant and later to the establishment of the SFR-facility for disposal of low- and intermediate-level reactor waste.

Investigations included stress measurements in a large number of boreholes (Carlsson and Christiansson, 1986). Most of them were shallow, but one borehole, denoted DBT1 reached a depth of 500 m. The dominating rock type penetrated by this borehole was a sparsely fractured granite gneiss. At 320 m depth, DBT1 intersected a marked fracture zone of a few meters width. The zone was reported to have subhorizontal orientation, although the grounds for this interpretation are not clear. Stress measurement results, as well as other data from this borehole, have been presented and discussed in some detail by Carlsson and Olsson (1982). The results are of particular interest in the present context because they have often been referred to as an evidence of stress disturbances caused by a fracture zone.

Figure 42 shows stress magnitudes obtained from the many overcoring stress measurements conducted in DBT1. Neglecting the uppermost 100 m (where anomalously high horizontal stresses were recorded) it is seen that stress magnitudes increase gently down to about 300 m. Below this depth, i.e. below the fracture zone, stress magnitudes appear to increase more rapidly with depth. On the basis of the data Carlsson and Olsson (1982) argued that the fracture zone in effect divides the bedrock into an upper- and a lower stress regime. The existence of such a stress field was explained as being a result of interaction between gravitational and tectonic components, superimposed to remnant stresses related to late glaciations. The hypothesis implies that there is little or no mechanical coupling between the horizontal stress fields above and below the zone.

An example of interpretation based on this model is shown in Figure 43. Interpretations of stress orientations supported the hypothesis, though with substantial reservations for the fact that measured stress orientations (not reported here) were too scattered to allow reliable conclusions.

The apparent governing effect of the fracture zone on the stress field may however be questioned for several reasons. One is the fact that more detailed examination of the stress data reveals considerable scatter, which of course obstructs interpretation in general. Furthermore, another set of stress measurements were

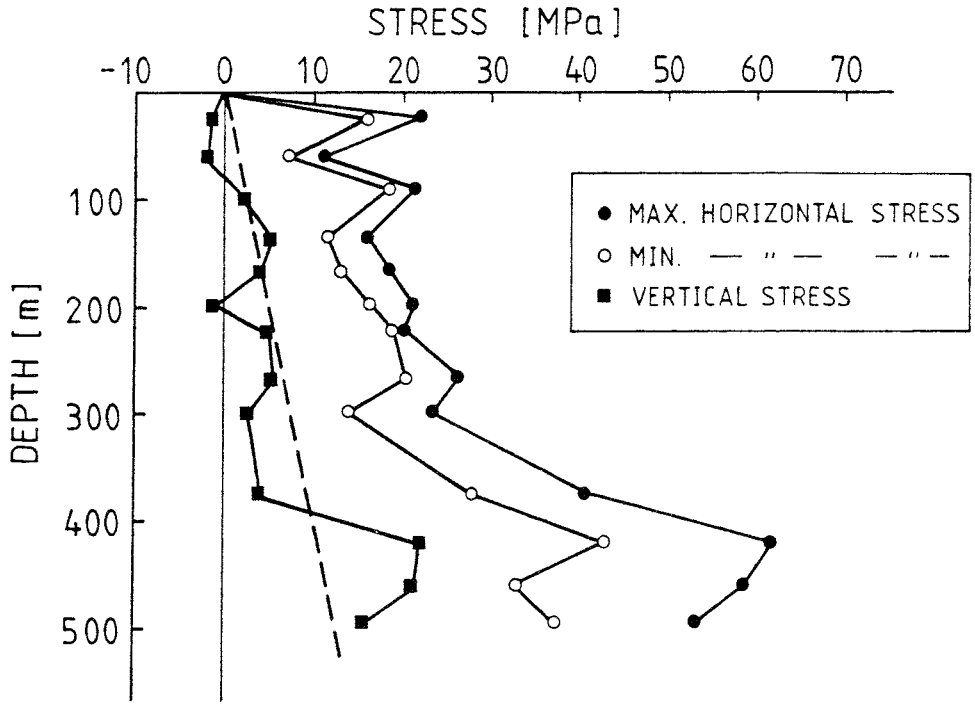

Figure 42. Measured magnitudes of horizontal and vertical stresses as a function of depth in borehole DBT1 at Forsmark. Data point along the profile represents mean values of 2-4 individual measurements. The dashed line shows the theoretical lithostatic vertical stress (after Carlsson and Olsson, 1982).

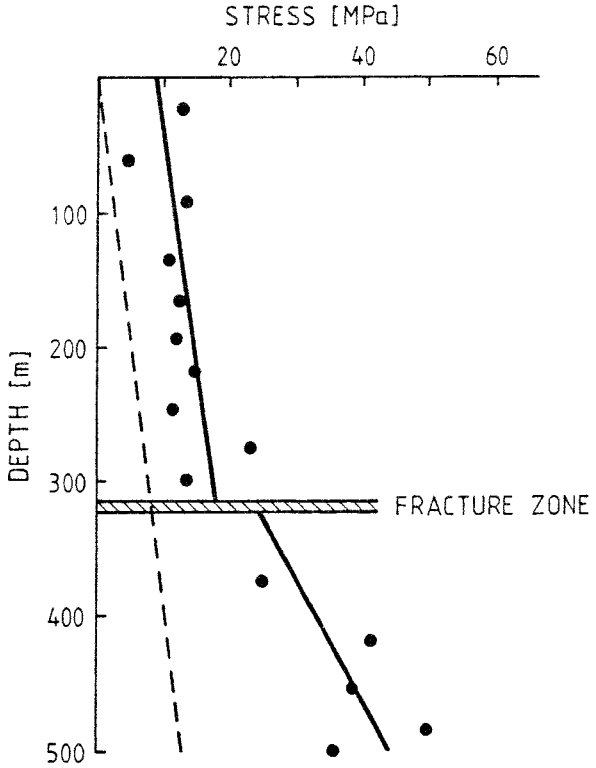

Figure 43. Interpretation of stress regimes above and below the fracture zone in borehole DBT1 at Forsmark. Right curves are regression lines for the mean normal stress. Left curve (dashed) is the theoretical lithostatic vertical stress (after Carlsson and Olsson, 1982).

made in a borehole located less than 200 m away from DBT1. Unfortunately, this hole was only 250 m deep and did not intersect the fracture zone. However, stress data obtained did not correlate very well with those from DBT1. This may suggest that the variations of the measured stresses are controlled by more local features than the fracture zone. Further support for this idea is found by considering fracture data from DBT1; fracture frequency and other parameters relating to the state of fracturing were investigated in detail by Carlsson and Olsson (1982). Figure 44 shows fracture frequency, calculated for 10 meter intervals, together with measured stress (mean normal stress) as a function of depth in borehole DBT1. Determining fracture frequency at the very locations of the stress measurements, and replacing the mean normal stress with the measured, maximum horizontal stress, yielded the plot shown in Figure 45. A correlation, such that low fracture frequency corresponds to high stress and vice- versa appears evident from the plots. This strongly suggests that the stress distribution is controlled by local stiffness variations caused by variations in the state of fracturing, rather than by the presence of the fracture zone.

It may be added that possible correlation between rock type at measuring points and stress magnitudes was also investigated by Carlsson and Olsson (1982). However, no correlation could however be established between these parameters.

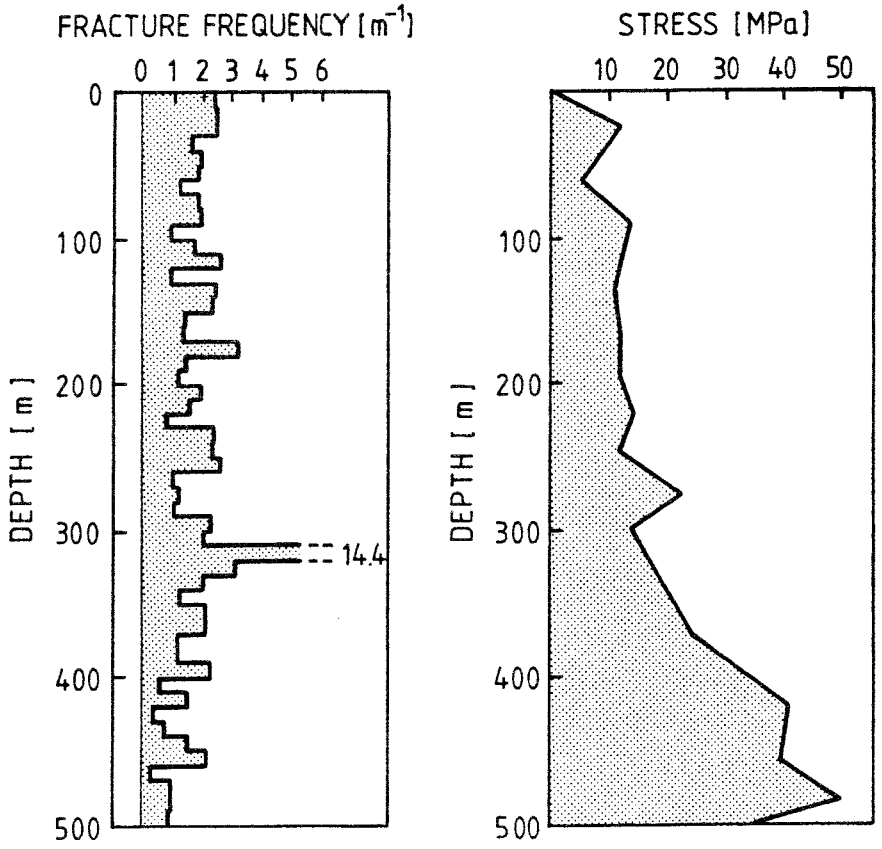

Figure 44. Fracture frequency as determined for 10 m intervals (left), and measured mean normal stress (right) as a function of depth. Borehole DBT1 at Forsmark (after Carlsson and Olsson, 1982).

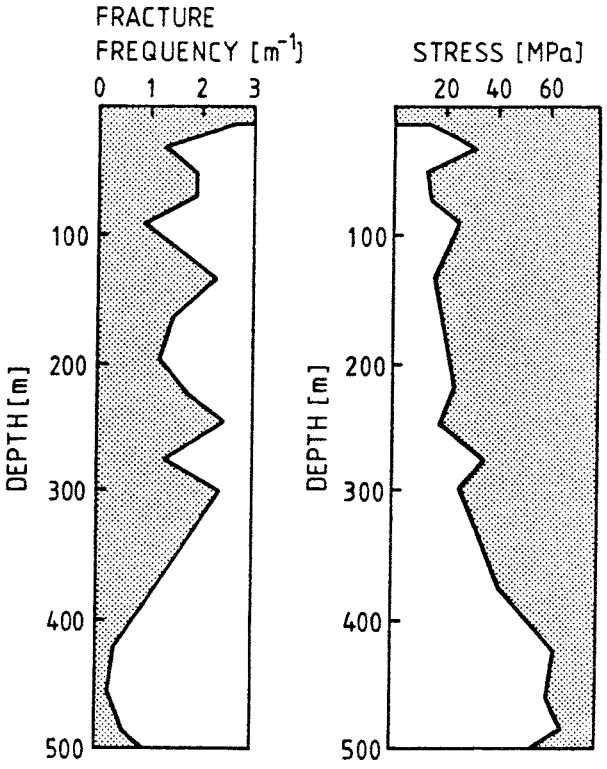

Figure 45. Fracture frequency at locations of stress measurements and measured maximum horizontal stress as a function of depth. Borehole DBT1 at Forsmark. Note the strong negative correlation between the two curves (from Carlsson and Olsson, 1982).

9.4 Lansjärv

Investigations within the area of post-glacial faulting near Lansjärv included stress measurements at depths of 300-500 m in a vertical borehole (Bjarnason et al., 1989). The upper 300 m of the borehole penetrated very fractured and tectonically disturbed bedrock, but controversy appears to remain as to the way in which this relates to the postglacial fault zone which outcrop some 1 km away from the borehole (Talbot et al., 1989; Lagerbäck, 1989). What can be concluded from the work at Lansjärv is that horizontal stresses are anomalously low (minimum horizontal stress 6-8 MPa at 300-500 m) and that stress rotation occurred over the investigated interval. It is reasonable to assume that this extreme state of stress is a consequence of the complex tectonics in the area, but the mechanics involved is simply not understood.

9.5 Finnsjön

The extensive borehole investigations of Fracture Zone 2 at the Finnsjön study site have included rock stress measurements by hydraulic fracturing techniques in a vertical borehole intersecting the zone. Results are reproduced in Figure 46. The fracture zone encompasses the depth interval 200-300 m, cf. Figure 14. Measured

stress magnitudes do not reveal any anomaly that can be related to the fracture zone. Data are however few and rather scattered, and do not allow detailed interpretation of the stress distribution. The orientation of the horizontal stress field is more well-defined and does not indicate any systematic variation with depth.

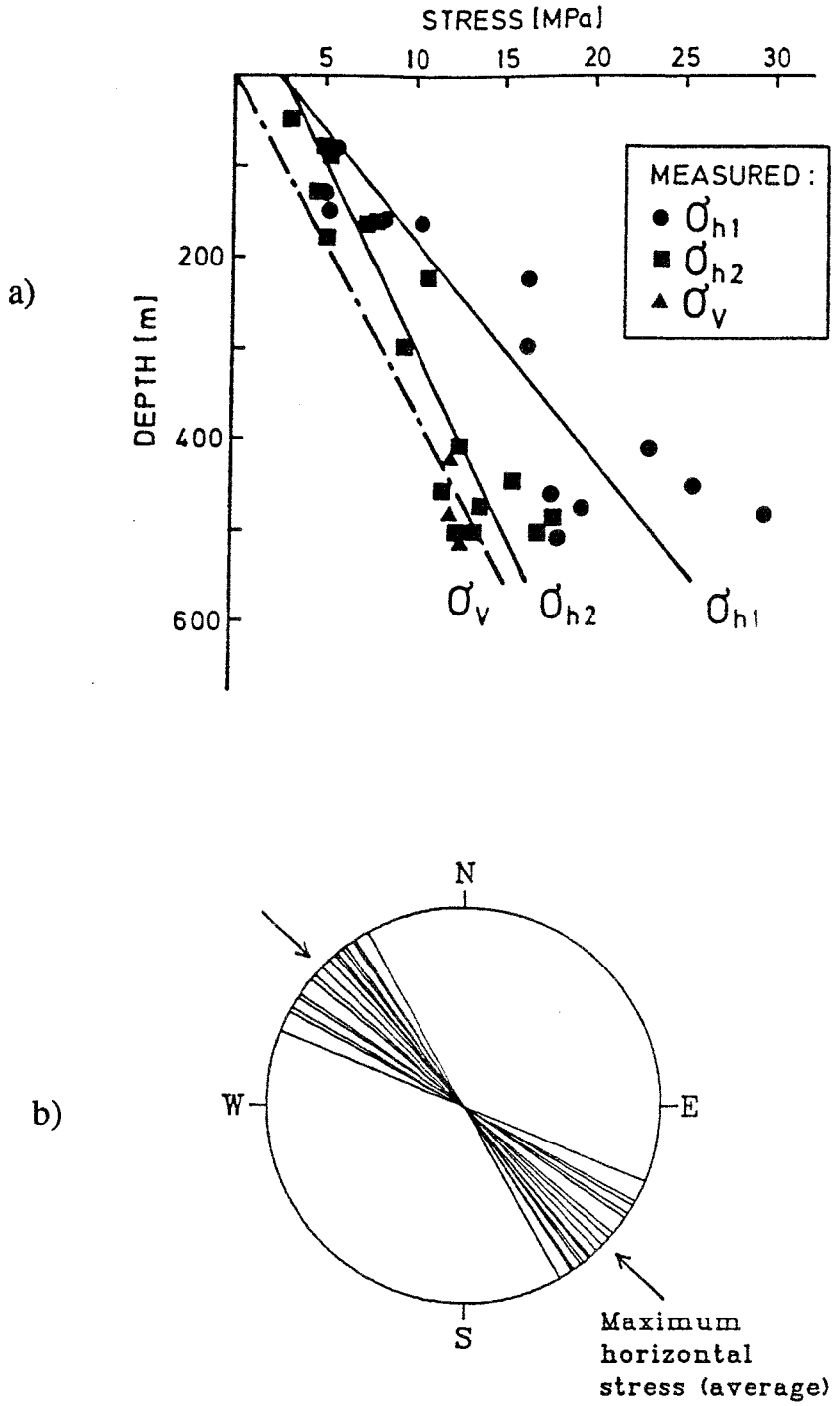

Figure 46. Results from stress measurements in a vertical borehole at Finnsjön. The hole penetrated Fracture Zone 2 at 200-300 m depth (from Leijon and Ljunggren, 1992).

a) Magnitudes of maximum -and minimum horizontal stresses (σ_{h1} and σ_{h2}) and vertical stress (σ_v) as a function of depth.

b) Orientation of the maximum horizontal stress.

9.6 URL

Investigations at the URL-facility in Canada also included a comprehensive program of stress measurements aimed in part at determining stress transfer across Fracture Zone 2. The site geology and fracture zones encountered are outlined in Figure 33. The minimum principal stress was found to be oriented nearly vertical, and can thus be compared with the theoretical lithostatic stress. Figure 47 shows the ratio of measured minimum stress to lithostatic stress for measurements in the vicinity of the shaft. It is seen that values deviate significantly from unity, especially in the proximity of Fracture Zone 2, where ratios of 2-3 were recorded.

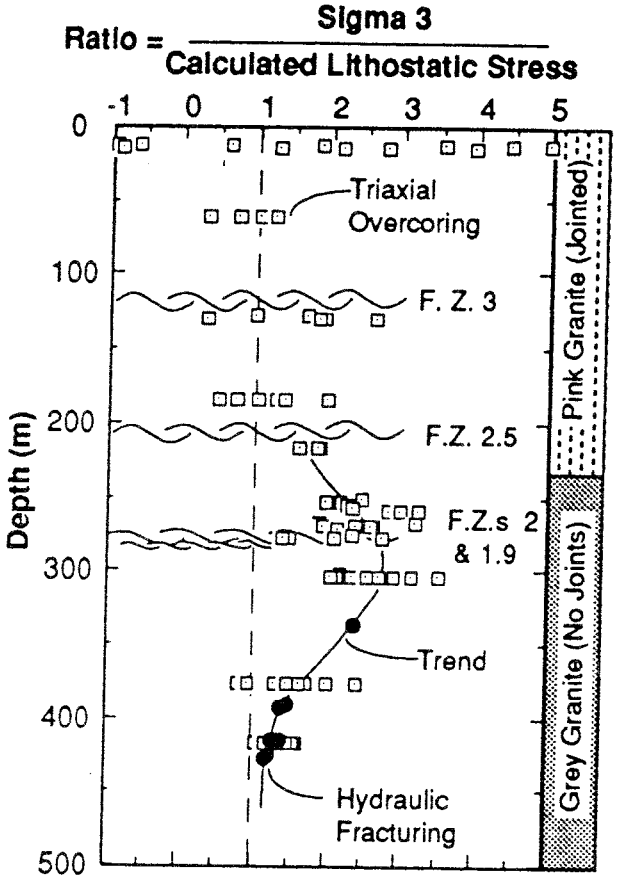

Figure 47. Ratio of minimum principal stress (vertical stress) to theoretical, lithostatic stress as obtained from measurements in the vicinity of the shaft at the URL-facility. Levels of the fracture zones are also indicated (from Martin et al., 1990).

In order to further investigate this drastic stress anomaly, additional measurements were made at several locations above and below Fracture Zone 2. Locations and designations of boreholes intersecting the zone, and in which measurements were made, are given in Figure 48. Results in the form of normal -and shear stress components across the fracture zone are given in Table 9 and also illustrated in Figure 49.

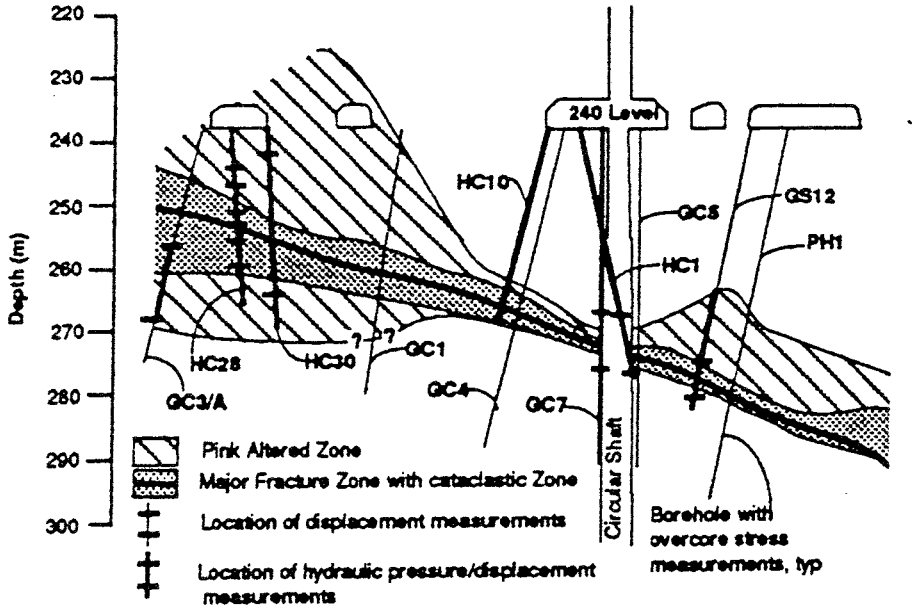

Figure 48. Fracture Zone 2 at URL and intersecting boreholes. Overcoring stress measurements were made in boreholes indicated with thin lines (from Martin et al., 1990).

Table 9. Mean values of normal (σ_n) -and shear (τ) stresses obtained from triaxial overcoring measurements above and below Fracture Zone 2 at URL (after Martin et al., 1990).

Borehole	Above Fracture Zone 2			Below Fracture Zone 2		
	No. of tests	σ_n (MPa)	τ (MPa)	No. of tests	σ_n (MPa)	τ (MPa)
GC1/2	5	43.4	10.8	5	42.3	0.3
GC3	5	-1.0	-0.7	5	-1.1	-3.9
GC4	1	27.5	2.1	4	30.2	-2.7
GC5	5	20.8	-3.5	6	19.2	0.5
PH1	4	23.6	3.3	6	29.9	0.9

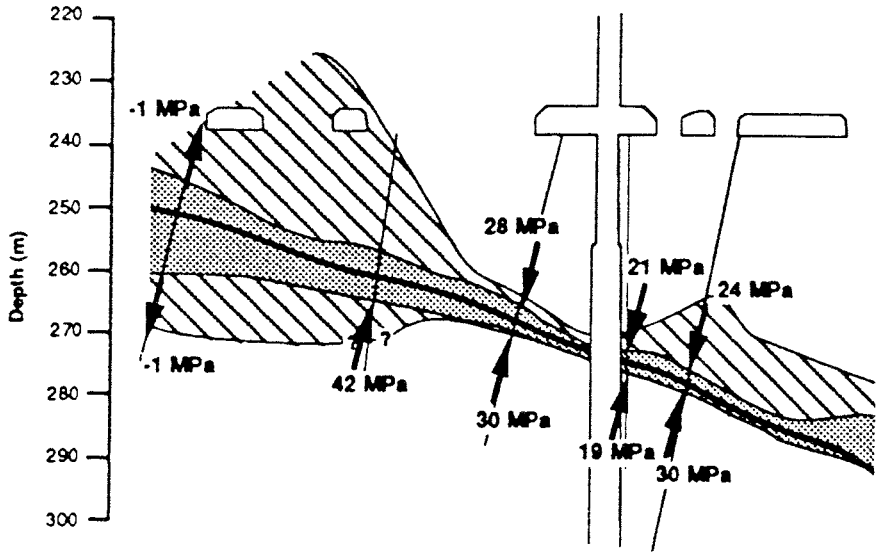

Figure 49. Distribution of normal stress transfer across Fracture Zone 2 at URL. Note differences in values between different locations (from Martin et al., 1990).

It is seen that normal stress values vary enormously between the different boreholes, ranging from about zero to more than 40 MPa. The fact that values obtained above -and below the zone at each point of intersection are in close agreement, clearly verifies that the normal stress transfer across the zone is extremely non-uniformly distributed. It should be noted that these large stress variations occur over an area of the order of 100 m by 100 m only. Given these conditions it is obvious that measurements in one borehole (as exemplified by the data referring to the shaft position, Figure 47) can only yield a sample of the complex stress distribution near the fracture zone, and does indeed not provide a general understanding thereof. This is an important result to keep in mind when interpreting data from investigations such as those at Forsmark, Finnsjön and Lansjärv as referred earlier.

From Figure 49 it appears that the stress data correlate with geology, such that high normal stress corresponds to sections where the fracture zone is narrow and wide sections tend to yield low normal stress. This suggests a mechanical behavior of the fracture zone as conceptualized in Figure 50. The high stiffness resulting at narrow sections promotes load transfer, while wide and much softer sections remain essentially unloaded. It is interesting to note that this model is very similar to the overall appreciation of fault zone behavior resulting from observations in deep mines, cf. section 8.2.

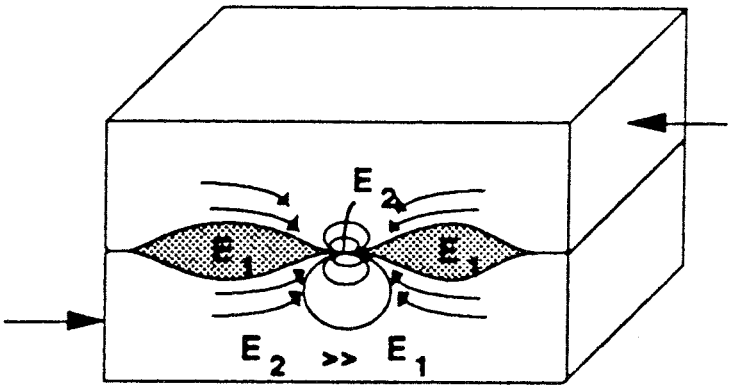

Figure 50. Conceptual understanding of stress transfer across Fracture Zone 2 at URL (from Martin et al., 1990).

9.7 Frictional strength inferred from stress measurements

It has been suggested that the state of stress in the Earth's crust actually reflects its overall strength. The basic concept is that the rock mass is in an unstable state of equilibrium, where the state of stress balances the frictional strength. It follows that application of additional deviatoric load will disturb equilibrium and cause deformation by shear failure resulting in stress redistribution such that equilibrium is re-established. Since large discontinuities like faults and fracture zones constitute the weak links in the bedrock along which adjustments would reasonably occur, the theory offers opportunities to infer strength properties of such structures. The validity of the concept on different scales, for different stress regimes, at different depths and in different parts of the world, has been subject to considerable discussion (see e.g. Scholz, 1990 for a summary).

Jaimson and Cook (1978) applied the concept of frictional balance to infer frictional strength from stress measurement results. Stress data were obtained from measurements reported from some 50 locations scattered around the world. The data set represented depths down to 2000 m and stress levels up to some 50 MPa, although the great majority of observations referred to depths less than 400 m and stresses less than about 20 MPa. Furthermore, the analyses was restricted to cases where one principal stress was found to be vertical and approximately equal to the lithostatic stress. This restriction was imposed both in order to ensure the experimental validity of the data used, and to allow the data to be grouped into three subsets according to the basic "Andersonian" faulting regimes, i.e. normal faulting (maximum stress vertical), thrust faulting (minimum stress vertical) and strike-slip faulting (intermediate stress vertical).

The maximum shear stress and the mean normal stress was calculated from the following relationships:

$$\tau_{max} = \frac{\sigma_1 - \sigma_3}{2} \qquad \text{and} \qquad \sigma_n = \frac{\sigma_1 + \sigma_3}{2}$$

which were plotted to yield the result shown in Figure 51. Assuming: i) that the measured stress data represent the strength of the rock as described above, and ii) that the strength is determined by a Coulomb failure criteria, the slope, k, of the line fitted to the data, as shown in Figure 51, is related to the friction angle by the relationship:

$$\phi = \arcsin k$$

Regression analysis of the entire data set as illustrated in Figure 51 yields a friction angle of 28°. Table 10 shows results differentiated with respect to stress regime.

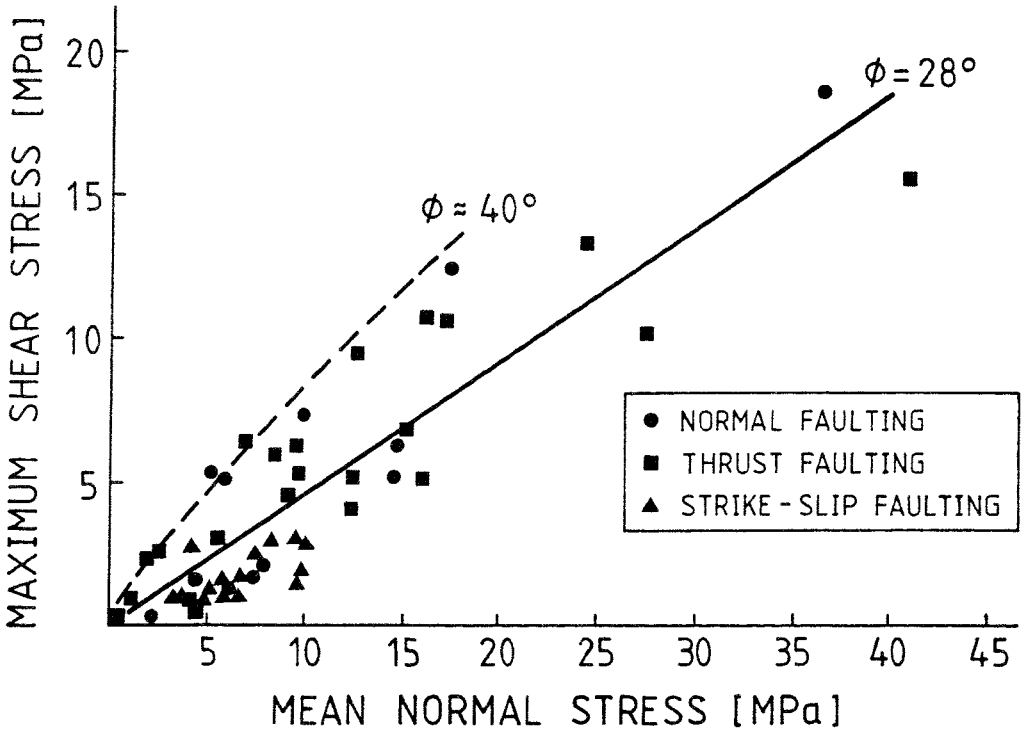

Figure 51. Maximum shear stress versus mean normal stress. Regression line (solid) corresponds to a friction angle of 28°. Dashed line indicates alternative interpretation (after Jaimson and Cook, 1978).

Table 10. Friction angles inferred for different stress regimes according to Jaimson and Cook (1978).

Stress regime	Friction angle from regression analysis	Correlation coefficient
Normal faulting	32	0.84
Thrust faulting	23	0.79
Strike-slip faulting	12	0.38
Combined data	28	0.77

The friction angles presented by Jaimson and Cook are often cited in the literature and taken as indicators of the frictional strength of large-scale discontinuities, which according to the frictional balance concept are the elements thought to govern the in-situ stress state. Nevertheless, their relevance must be questioned. Firstly, closer examination of the data shows that a very few observations towards the upper limit of the stress interval investigated affect the result of the regression procedures to an unproportional extent. Discarding these observations yields different values and poor correlation. Moreover, it is not clear if and how the effects of pore pressure were considered. The major reservation, however, concerns the assumption that stress data can be used as indicators of strength. The geological environments from which data were drawn were not further specified by Jaimson and Cook (1978), but the only criteria used appears to have been those indicated above, i.e. experimental reliability and one principal stress oriented vertically. Now, even if the frictional balance concept is valid at some, probably very large scale, it cannot imply that the rock mass is critically loaded everywhere. Consequently, stress observations, selected arbitrarily and referring largely to depths of 400 m and less, would be expected to reflect various ratios of shear- to normal stress up to at most the critical value. An alternative way to interpret the results is therefore to consider the highest ratio of shear- to normal stress observed as possibly representing completely mobilized frictional strength. Tentative application of this hypothesis, as indicated in Figure 51, indicates a friction angle of about 40°, which seems more realistic than the rather low values given in Table 10.

Another set of stress data was presented and analyzed in a similar manner by Zoback and Healy (1984). An important merit of their work is that it refers to areas of active faulting. Eight locations within the United States, at which the nature of faulting was reasonably well understood, were investigated. The state of stress was in most cases inferred from more or less comprehensive hydraulic fracturing tests. It was assumed that the vertical stress component was equal to the lithostatic stress. In some cases, stress conditions were indirectly inferred from focal plane mechanism studies of earthquakes.

The results presented by Zoback and Healy (1984) are exemplified in Figure 52, which shows data from the Nevada Test Site. Table 11 summarizes site information and results from six of the locations studied. Excluding the San Andreas Fault data, it is seen that inferred friction angles fall in the range 30-45°. These are considerably higher, and in fact more realistic, than the values suggested by Jaimson and Cook (9178). The frictional strength of the San Andreas Fault has been subject to extensive discussion for many years (see e.g. Scholz, 1990 for an overview). Figure 53 shows the stress measurement results from which Zoback and Healy inferred the value of 22° for the friction angle. They consider this value as a lower bound estimate since the measurements were made in an area where the fault may not be critically loaded.

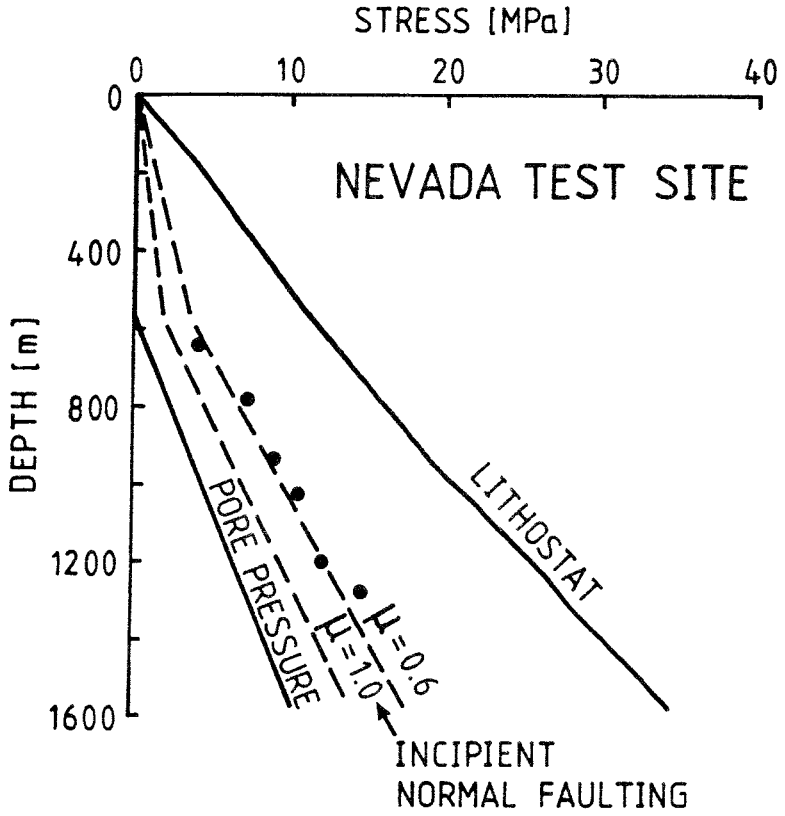

Figure 52. Measured minimum principal stress, assumed vertical (lithostatic) stress and pore pressure as a function of depth in the Yucca Mountain area, Nevada test Site. The dashed line corresponding to a coefficient of friction of $\mu = 0.6$ (friction angle 30°) is in close agreement with the measured data (from Zoback and Healy (1984).

Table 11. Summarized results from investigations by Zoback and Healy (1984), of stress conditions and frictional strength at locations of active faulting.

Location	**Depth, Range of minimum principal stress**	**Result**
Nevada Test Site, Nevada, normal faulting	600-1300 m 5-15 MPa	Stress measurements consistently indicate a friction angle of about 30°.
Rock Mountain Arsenal Colorado, normal faulting	3700 35 MPa	Difficult to interpret, friction angle 30-45°.
Fifth Water Canyon, Utah, normal faulting	500 m 5 MPa	Friction angle about 30°.
Gulf Coast, Texas-Louisiana, aseismic normal faulting	1000-3500 m 15-70 MPa	Upper limit of τ/σ-ratios recorded correspond to friction angle 30-40°.
Rangely, Colorado	1800 m 30-50 MPa (?)	Uncertainty as regards nature of seismic fault slip. Friction angle estimated to 34-45°.
Southern San Andreas Fault	Shallow	22° is a lower bound estimate of the friction angle

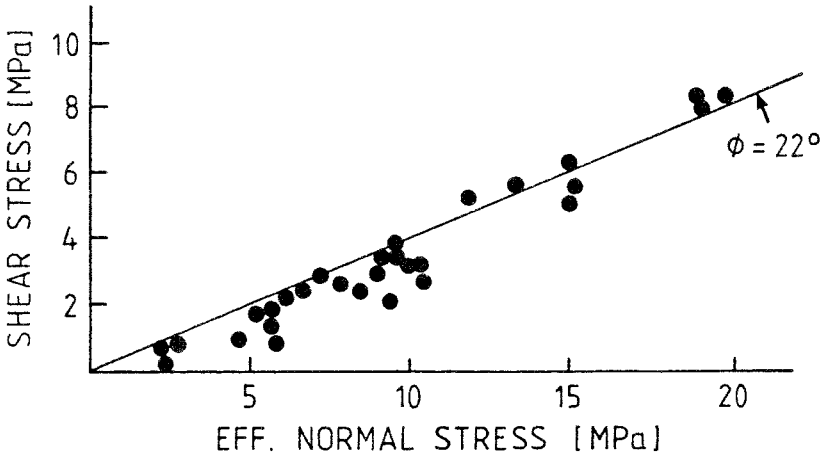

Figure 53. Results from hydraulic fracturing stress measurements near the San Andreas Fault (Western Mojave Desert) and inferred friction angle of the fault. Stress components are resolved with respect to the orientation of the fault plane (after Zoback and Healy, 1984).

10 MAIN RESULTS AND CONCLUSIONS

10.1 Shear strength

Referring to Figure 6, the discussion of shear strength is restricted to the case when the scale relation between the problem at hand and the fracture zone is such that the zone can be treated as a single discontinuity. In cases when the rock mass approach is valid, concerns are with the strength of fractures forming constituents of the fracture zones, rather than with the strength of the zone as a whole.

Since the cohesive contribution is generally insignificant, the shear strength of fracture zones is controlled by frictional resistance. The key parameter is the friction angle, ϕ. It should be observed that this parameter is used to describe the total frictional resistance, irrespective of the exact nature of the deformation process during surface shearing.

Figure 54 attempts to summarize friction angles inferred from the various studies reported in previous chapters. The few examples that may be referred to as field observations of frictional resistance of fracture zones (1 through 4 in the figure) stem from mining and from back-calculation of strength from stress measurement results. It is seen that the friction angle values fall within the interval 20-40°, but cluster at some 30-35°. There is an apparent increase of friction angle with normal stress, but data available do not allow any conclusion in this respect. Figure 54 also shows friction angles for often encountered filling materials. As expected, these are somewhat lower than those for fracture zones.

In geomechanical analysis, discontinuities like fracture zones are almost invariably assumed to be planar features, to which frictional characteristics (together with other properties) are assigned. The applicability of the concept of friction, and hence of the results presented in Figure 54, is closely related to this assumption, and its validity in the present context therefore needs to be examined. Considering first friction from a more fundamental point of view, it is well documented that surface friction result from complex interaction between surface irregularities. The process include mechanisms of elastic deformation of asperities, adhesion, abrasive material destruction, and shear through intact material. The relative importance of these mechanisms is dependent on the normal stress across the discontinuity. At low normal stress, the total resistance to surface shear (i.e. friction angle) is rather variable due to the action of preserved asperities, and friction at maximum resistance (peak friction angle) is higher that at residual conditions (residual friction angle). At higher stresses, variation is less. In fact, comprehensive tests of ground rock surfaces have shown that the peak friction angle at normal stresses exceeding 200 MPa is close to 30°, and almost independent of rock type (Byerlee, 1978). For the range of conditions represented by unfilled rock joints, the empirical system developed by Barton (chapter 5) quite efficiently handles the effects of surface characteristics and normal stress on frictional resistance.

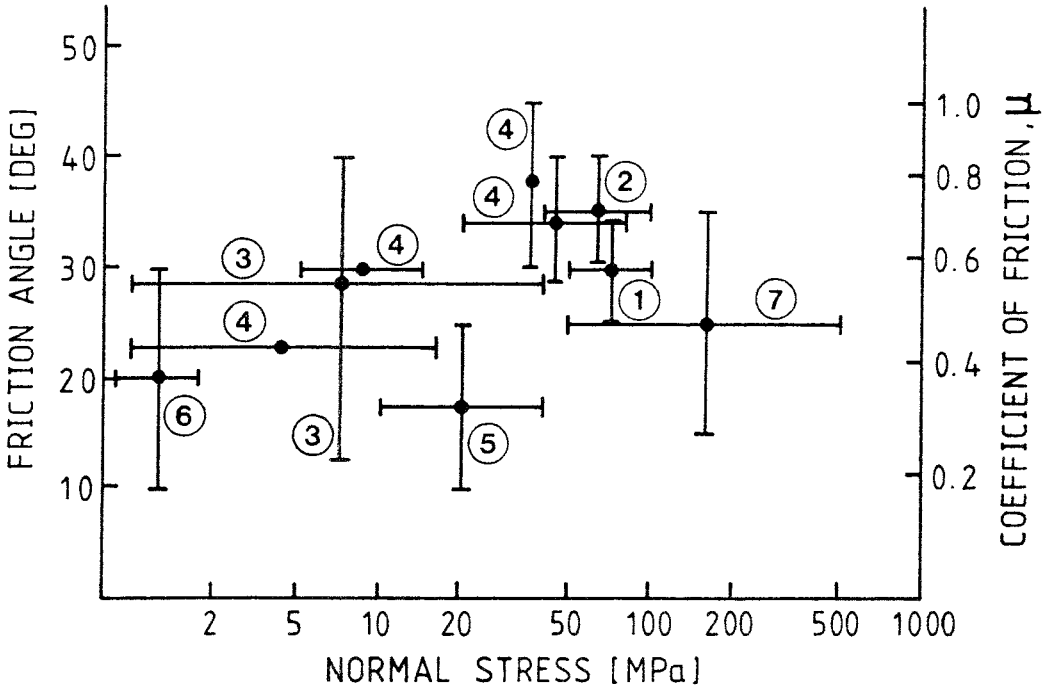

Figure 54. Friction angle and coefficient of friction as a function of normal stress. Horizontal and vertical bars indicate approximate ranges for normal stress and friction respectively.

1) Faults in South African gold mines, modelling and field observation (chapter 8)
2) Strathcona mine, modelling and field observation (chapter 8)
3) Back-calculation from stress measurements - general data (chapter 9, Table 10)
4) Back-calculation from stress measurements in areas of active faulting (chapter 9, Table 11)
5) Weak contact zones in Swedish mines, modelling and field observation (chapter 5)
6) Common discontinuity filling materials, laboratory and field testing (chapter 5, Table 2)
7) Fault gouge material, laboratory testing (chapter 5).

Thus, friction angle is not a "material property" in a conventional sense, but rather a parameter that conveniently quantifies the net effect of a process that has not yet been fully explained. Furthermore, it is not inherently scale dependent. Misconceptions in these respects are common. It should be pointed out that the scaling procedures for shear strength forming part of Bartons system (chapter 5) are concerned only with the problem of determining the properties of a discontinuity on some scale, on the basis of samples that refer to a smaller scale than the extension of the discontinuity. The system does not suggest that larger discontinuities have lower frictional angles than smaller ones. As regards friction angles of fault zones, an indirect size dependency may exist because of differences in displacement magnitudes and morphology. Geological investigations of fault zones have not surprisingly revealed clear correlations between: i) fault zone extension and displacement magnitude (e.g. Watterson, 1986), and ii) displacement magni-

tude and thickness of gouge material formed by the shearing process (Robertson, 1987). Since the friction of fault gouge, and probably also of other wear products, is lower than for clean rock surfaces, friction angles would be expected to decrease somewhat with increased scale of the fault zone. This hypothesis can however not be supported by any observational evidence whatsoever.

Now, to convert the complicated mechanical process of surface friction into the straight-forward parameter friction angle, applicable in simple strength laws like the Coulomb failure criteria, it is evident that simplification is required. The basic assumption is that the surface topography, and all associated mechanical complications, occur on a scale that is much smaller than the problem considered. Only if this condition is met can the global approximation (Coulomb-criteria) neglect the details of the basic mechanism (surface friction) without losing validity. In geomechanical analyses, this assumption is often not observed because of the habit to represent discontinuities as planar features characterized by properties that do not vary over the surface. It may be recalled here that Barton's system for determination of shear strength presumes that all surface characteristics that are of importance are adequately represented on the scale of sampling. Effects of possible surface irregularities on a larger scale must be added separately, cf. equation (7). Thus, in practical application, the assumption is that of surfaces with irregularities that are much smaller than the surface itself.

As regards fault zones, however, field observations consistently show that surface irregularities like undulations, jogs and variations in thickness prevail on all scales. This result seems to be well supported by a number of independent investigations (Scholz, 1990; Wallace and Morris, 1986). The surface irregularity is in part a necessary consequence of the complex fracturing related to growth of shear structures in their own planes (chapter 4). The nature of surface topography also depends on fault type, slip direction etc, but the decisive characteristic is that it is found on all scales. This may seriously obstruct the assumption of macroscopically planar surfaces, because one must always expect to find significant surface irregularity on a scale comparable to the problem under study. Figure 55 shows two cases where the macroscopic fracture zone geometry can hardly be approximated with planar surfaces. One is Fracture Zone 2 at Finnsjön. Considered at the scale represented by the figure, it can be envisaged that the friction concept and planer-feature approximation apply to shear events involving individual shear planes within the zone. A larger event, however, involving the entire zone is difficult to consider as a purely frictional phenomena since it must inevitably involve formation of new, through-going shear surfaces.

The other example shown in Figure 55 is a typical fault plane geometry as observed in South African gold mines. It is easy to imagine that the buckled shape of the fault plane surface will result in non-uniform distributions of shear and normal stress across the fault. This, in turn, has been found to significantly affect the mode of shear movement; shear displacement initiates as stable creep at locations on the fault plane where shear stress is high and/or normal stress is low.

a)

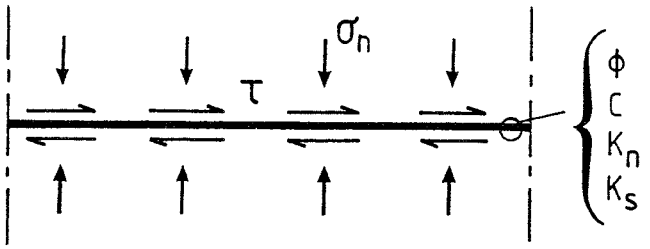

b)

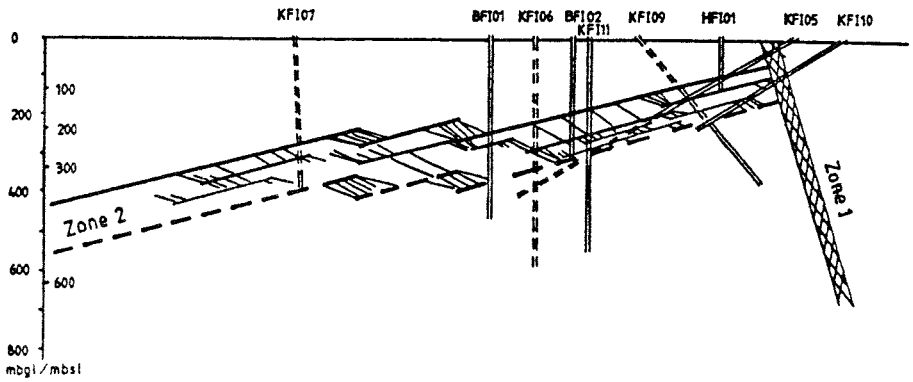

c)

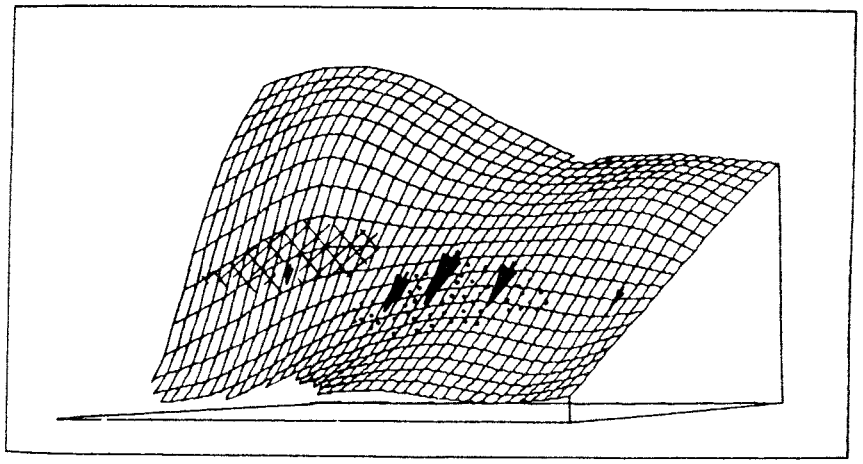

Figure 55. Illustration of fracture zone geometries.

a) Planar, frictional feature as assumed in most geomechanical models. Material properties are constant over the plane of the fracture zone.

b) Fracture Zone 2 at Finnsjön - interpreted geometry.

c) Surface geometry of a 4000 by 2000 m section of a fault zone in a South African gold mine (Brand Fault, Welkom district). Arrows indicate distribution of slip associated with a mining-induced seismic event. Cross hatched area indicate location of slip as predicted by stress modelling (from van Aswegen, 1990).

Locations with high normal stress, or high strength due to the presence of some major asperity, remain locked. As displacement progresses, the shear load is successively thrown onto these locked sections, which will finally fail. Failure is often dynamic, since large strain energies have been accumulated prior to failure. Thus, although shear displacements in the mining case are induced by mining activities, the deformation process seem to be identical to the so-called stick-slip mechanism of naturally occurring earthquakes.

It may be concluded from the above discussion that the friction angles presented in Figure 54 in part reflect deformation mechanisms that do not comply with the general assumption of friction over macroscopically planar surfaces. As a result, adding data from more case studies to the very limited number of strength parameter values obtained by back-calculation of observed fracture zone failures will probably not significantly narrow the currently rather wide intervals that can be established for these parameters. The results also indicate that more efforts must be devoted to correct representation of overall geometry as well as morphology of fault zones in geomechanical models.

10.2 Deformability

There are a number of parameters that can be used to describe deformability of a fracture zone. The normal- and shear stiffness, K_n and K_s, are "global" parameters in that they describe the stiffness of the entire zone at a particular location. These parameters can be defined irrespective of whether the zone is assigned a finite width or not. Hence, they are not material properties, but rather describe the characteristics of the fracture zone as a system component. This does not preclude that the stiffness parameters vary from one location to another over the plane of the fracture zone.

The modulus of deformation, modulus of rigidity, bulk modulus and Poisson's ratio (all related to each other) are all material properties that may be used to describe the deformability of the rock mass composing the zone. Consequently, these parameters can be defined only if the zone has a finite width and they are applicable in cases when fracture zones can be represented by equivalent rock masses. K_n and K_s are functions of these material properties and of the geometry of the fracture zone, Figure 56.

As discussed in the previous section, shear deformation properties become meaningful only if defined for some discontinuity area that is considerably larger than the surface irregularities responsible for the shear resistance. Normal deformation properties, however, can be defined for specific locations (or for some larger area). Normal stiffness can, for example, in principal be determined simply by superimposing the contributions from the different units encountered over a section across a fracture zone. This means that borehole information is much more useful for assessing normal deformation characteristics than for estimating shear properties of fracture zones.

All the above properties are stress dependent. Deformation modulus and, to a higher degree, normal stiffness increases with increased normal stress. The dependency is most profound at low stresses and diminishes at high stress levels. The assumption of stress-independent properties is often justified at stress magnitudes exceeding some 20 MPa.

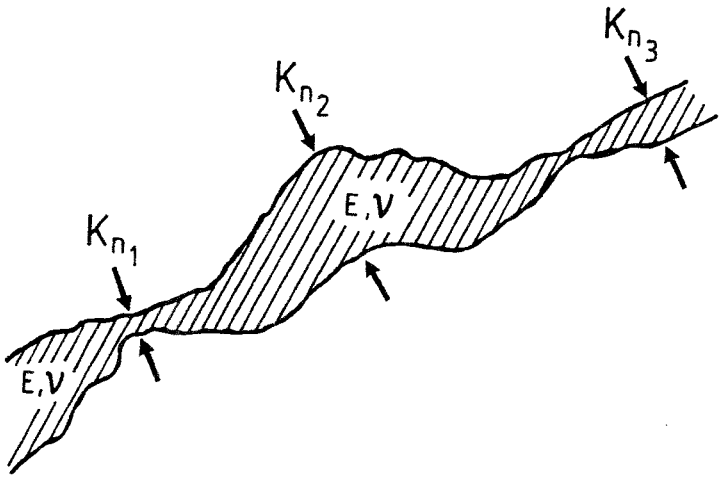

Figure 56. Schematic cross section of a fracture zone illustrating material properties E and υ and normal stiffness K_n ($K_{n1} \neq K_{n2} \neq K_{n3}$).

Modulus of deformation

In rock engineering a number of empirical methods are commonly used to estimate the modulus of deformation of rock masses on the basis of borehole geomechanical data. To evaluate the applicability of some of these methods to fracture zones, an attempt was made to estimate the modulus of deformation of three fracture zones, all investigated by core drilling (chapter 6). Results are summarized in Table 12. It is found that the empirical methods are applicable to slightly disturbed zones with moderate fracturing, but not to intensely sheared zones displaying heavy fracturing and abundance of poor-quality material. The results suggest that 15-25 GPa are reasonable estimates for the modulus of deformation of the former category of fracture zones, and thus provide upper bound estimates for the latter. Lower bound estimates can not be obtained from borehole data. All values discussed refer to a stress level of 5-10 MPa.

The values above are comparable to those of altered contact zones in mines which typically fall within the range 10-25 GPa. The contact zones are comprised of rock types such as chlorite schists and sericite quartzites of very poor quality. It is felt that they are mechanically quite similar to altered sections found in many fracture zones.

Table 12. Summary of results from trial application of empirical methods to estimate the modulus of deformation of three fracture zones.

Fracture Zone	Result
Fracture Zone 2, Finnsjön. 100 m wide, moderately fractured with average fracture frequency 5 m^{-1}.	Methods applicable with some confidence. Modulus estimates fall in the range 15-25 GPa.
Eastern Regional Zone, Fjällveden. 90 m wide, average fracture frequency is 20 m^{-1}, but fracture distribution is uneven. Crushed rock and core loss account for 11% of the drilled section.	Methods are poorly applicable, and can at best provide an upper bound estimate (5-15 GPa) for the modulus of deformation.
Fracture Zone 3, Kamlunge. 1-10 m wide, heavily fractured and tectonised. Up to 27 % of drilled sections produced core loss or crushed rock.	Methods are not applicable due to poor rock quality.

Normal stiffness

The only large-scale measurements of normal stiffness available are those conducted in two fracture zones at URL (chapter 7). For Fracture Zone 2, values range approximately 2-5 GPa/m if one considers the entire, some 20 m wide zone. For the only 0.4 m wide Room 209 Fracture, values are 50-150 GPa/m. The values were obtained through reduction of normal stress by fluid injection and refer to stress levels of the order of 1 MPa. The test method is associated with uncertainties as regards evaluation procedures and boundary conditions.

Approximate normal stiffness values may also be calculated for the fracture zones considered in Table 12, using the geometrical data and the modulus estimates. This yields values of 0.1-10 GPa/m.

In conclusion, available normal stiffness data for fracture zones are meaningful, although they are scattered over three orders of magnitudes. More narrow intervals may be obtained by classifying the data with respect to type and size of the fracture zones. For a particular fracture zone, the parameter can show large local variations contributed by: i) variations in width, and ii) variations in internal characteristics of the zone.

Shear stiffness

Full scale observations of the shear stiffness of fracture zone are completely absent. Data from essentially laboratory scale experiments are, together with the empirical scaling procedures, outlined in chapter 5 and are the only means at hand

for estimating this parameter. All these data refer to single discontinuities and it is not clear how they relate to the stiffness of the system of fractures composing a fracture zone.

The overall impression from the experimental data is that of a very large scatter and high sensitivity to normal stress, cf. Figure 22. For a given discontinuity, however, shear stiffness is mostly found to be lower than the normal stiffness. Ratios between 5 and 50 are typically encountered (Tannant, 1990). As a first approximation, it is reasonable to assume that these ratios hold also for fracture zones.

10.3 Stress conditions

Stress distribution near fracture zones

Stress measurements at points located tens or hundreds of meters apart often yield inconsistent results. There are many examples of measurements in vertical boreholes, where both local scatter and more systematic stress variations with depth have been recorded. These anomalies in the stress field are generally taken to be disturbances caused by nearby, large-scale structures such as fracture zones. Furthermore, practical experience from mining provides evidence that fracture zones can be accompanied by significant stress alterations, extending at least tens of meters away from the structures.

However, in reviewing data from stress measurements conducted in Sweden, no case has been found where it has been possible to unquestionably correlate measured stress gradients with the presence of a fracture zone. In many cases, the stress data are too few, and/or the structural conditions are too poorly known, to allow detailed interpretation. In other cases, alternative explanations to documented stress anomalies may be envisaged.

In contrast, the data from URL in Canada clearly document a very uneven load transfer across Fracture Zone 2. As discussed in chapter 9 and also indicated in Figure 57, the measured data can be explained in terms of local stiffness variations. It may be noted that clarification of the stress situation at URL to the level indicated in the figure required a large number of measurements within a comparably small volume. URL is to all likelihood an extreme example because the fracture zone is situated in an otherwise little disturbed, granitic environment with high stiffness. This boundary condition promotes uneven stress transfer across a discontinuity exhibiting local stiffness variations. A more disturbed, and thereby softer, environment would produce a more even stress distribution.

However, even if the contrasts between the fracture zones and their surroundings are usually much less pronounced than at URL, it is easy to understand that stress measurements in a single borehole intersecting a fracture zone (which is the normal situation) can not provide a complete understanding of the stress situation around the zone. It merely provides a sample of the complex and locally varying pattern of stress transfer.

a)

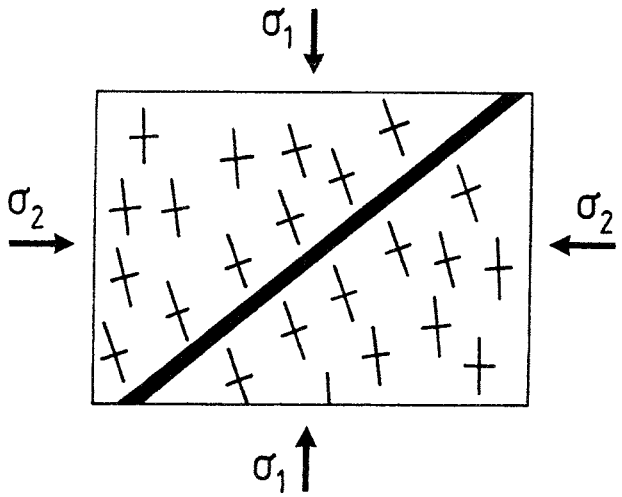

b)

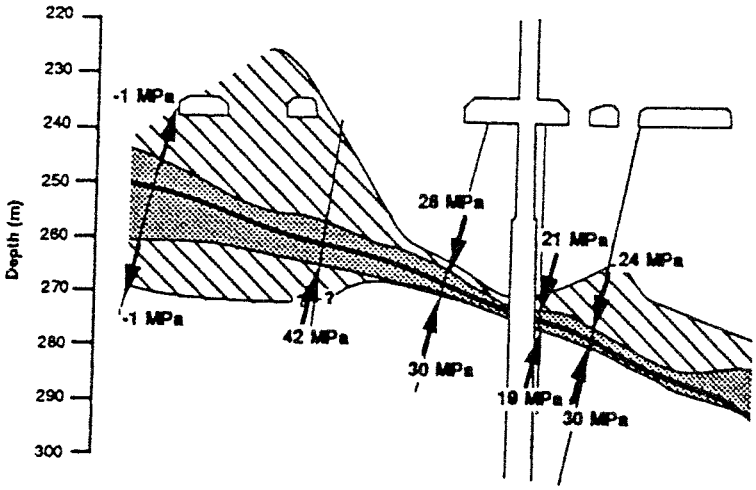

c)

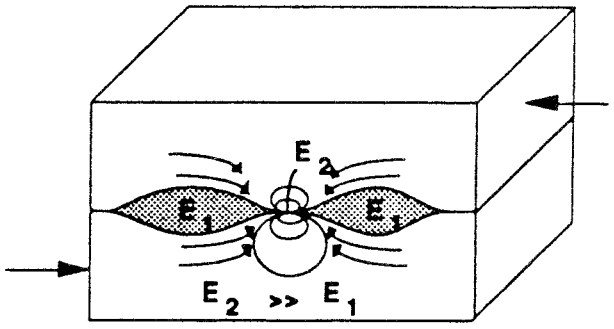

Figure 57. a) Schematic example of stress distribution in the vicinity of a planar discontinuity with mechanical properties that do not vary over the plane of the discontinuity, resulting in uniform stress transfer.

b) URL - measured normal stresses in different points along Fracture Zone 2.

c) Conceptual model of stress transfer across Fracture Zone 2 at URL.

The URL stress results highlight a measurable consequence of a fundamentally important characteristic of fracture zones that was observed in a previous section; variations in width, internal structure and topography tend to occur on all scales. If present to a significant extent on the scale of a particular problem, these features may invalidate simplified representation of fracture zones in mechanical models. This is illustrated in Figure 57 which shows the results from the URL together with an example of stress distribution around an idealized model of a fracture zone.

Stress as an indicator of frictional strength

The "frictional balance concept" discussed in chapter 9 postulates that the current state of stress in the Earth's crust reflects its shear strength. Additional loading will thus lead to self-adjustment by shear deformation of discontinuities at some scale. There are a number of arguments that support this theory. The most important one is the fact that artificially imposed stress changes, caused for example by filling of water reservoirs and amounting only to a few percent or less of the preexisting stress field, are often sufficient to induce seismic events, even in otherwise aseismic regions.

It follows from the theory that the frictional strength of the bedrock can be inferred from stress measurement results. However, interpretation of data is difficult since critical loading at some scale does not necessarily imply that points sampled by stress measurements are critically loaded.

10.4 Borehole methods for fracture zone characterization

Surface outcrops and boreholes are the main sources of information on the characteristics of fracture zones. Occasionally, underground excavations enabling direct observation are available. It is evident that the possibilities to geometrically and mechanically describe fracture zones on the basis of borehole data alone are limited. Studies involving both borehole- and underground observations, but otherwise representing a diverse collection of purposes and geological environments, frequently underline the shortcomings of borehole data as compared to direct observations from excavations.

Drawbacks of borehole data include:

- The difficulty to provide adequate sampling of poor-quality materials typically encountered in fracture zones (very weak rock, crushed rock, clay, fault gouge etc). To some extent, this can be mitigated by using borehole geophysical- and geomechanical testing methods. There are, however difficulties in converting results obtained by these methods to quantitative, mechanical data.

- Reconstruction of the fracture network within fracture zones from borehole data is difficult.

- Boreholes provide one-dimensional "needlestings" through fracture zones. Since fracture zones are characterized by local variations in thickness, morphology and properties in their own planes, these sections are samples drawn from populations that may be highly scattered.

10.5 Concluding remarks

The present study has attempted to compile data gathered primarily from case studies in rock engineering and various borehole investigations. Other sources of information on mechanical characteristics of fracture zones have not been explored to any significant extent.

Data refer to examples of the mechanically very heterogeneous group of large shear structures falling under the wide definition "fracture zone". The examples range in nature and size from distinct fault planes in South African gold mines to much more diffuse, and in several respects different, features like Fracture Zone 2 at Finnsjön. The search has been limited to hard rock environments, but no attempt has been made to systematically organize data with respect to different kinds of fracture zones. Arranging the results with respect to either size or genetic background of the fracture zones would appear logical as a means to minimize ranges of variation in mechanical properties and improve interpretation of the data.

However, the data set is too limited to allow any meaningful categorization with respect to genetic history of the fracture zones. Size is a better alternative, and there are well verified correlations between size (taken as in-plane dimensions) and parameters like accumulated shear displacement and width. These relations are consequences of the fundamental mechanisms of localized shear deformation in the brittle range, and their nature is subject to active research within the field of structural geology. There are, however, no similar straight-forward correlations between fracture zone size and properties describing strength or deformability. Therefore, there seems to be no mechanical grounds for defining different categories of fracture zones, referring to size alone as the discriminating parameter.

Available data show that fracture zones are characterized by geometrical irregularities like undulations, jogs and thickness variations that occur on all scales. This finding holds for a wide range of geological conditions and has important mechanical implications. One is that the mechanical properties of a particular fracture zone are likely to show considerable spatial variation. Another is the difficulty to adequately represent fracture zones in geomechanical models. It implies, for example, that the substitution of fracture zones with planar frictional features, which is a common idealization, may not always be justified. The experiences from mining-induced fault slip in deep mines are relevant in this context because they represent sustained efforts to understand and predict fault zone shear behavior. Furthermore, the mining environment has the advantage of providing distinct feed back in terms of fault displacements as a function of mining, allowing the quality of predictions to be evaluated. For the particular kind of fracture zones

dealt with in these mines, standard geomechanical modelling tools have been found essentially incapable of predicting the mode of shear deformation. Furthermore, it has been found more rewarding to direct research efforts towards case-by-case determination of fault zone geometry and development of qualitative understanding of shear behavior, rather than towards detailed determination of "traditional" strength parameters. It is believed that a similar approach would be beneficial in attempting to predict fracture zone behavior under load conditions of concern to nuclear waste disposal in hard rock.

11 REFERENCES

Ahlbom, K., Andersson, J-E., Nordqvist, R., Ljunggren, C., Tirén, S. and Voss, C., 1991a: Gideå Study Site. Scope of investigations and main results. SKB Technical Report 91-51, Stockholm, Sweden.

Ahlbom, K., Andersson, J-E., Nordqvist, R., Ljunggren, C., Tirén, S. and Voss, C., 1991b: Fjällveden Study Site. Scope of investigations and main results. SKB Technical Report 91-52, Stockholm, Sweden.

Ahlbom, K., Andersson, J-E., Andersson, P., Ittner, T., Ljunggren, C. and Tirén, S., 1992: Kamlunge Study Site. Scope of investigations and main results. SKB Technical Report 92-15, Stockholm, Sweden.

Ahlbom, K. and Tirén, S., 1991: Overview of geologic and geohydrologic conditions at the Finnsjön site and its surroundings. SKB Technical Report 91-08, Stockholm, Sweden.

AGI, 1960: Glossary of geology and related sciences. Second ed., Washington.

Atkinson, B. K. A., 1987 (ed): Fracture mechanics of rock. Academic Press, 531 pp.

van Aswegen, G., 1990: Fault stability in SA gold mines. Proc. Int. Conf. on Mechanics of Jointed and Faulted Rock. Vienna, April 18-20. Balkema, Rotterdam, pp 717-725.

Bandis, S., Lumsden, A. and Barton, N., 1983: Fundamentals of rock joint deformation. Int. J. Rock Mech. Min. Sci. and Geomech. Abstr. (20) 249-268.

Barton, N and Choubey, V., 1977: The shear strength of rock joints in theory and practice. Rock Mech. (10) 1-54.

Barton, N., Bandis, S. and Bakhtar, K., 1985: Strength, deformation and conductivity coupling of rock joints. Int. J. Rock Mech. Min. Sci. and Geomech. Abstr. (22) 121-140.

Barton, N., Lien, R. and Lunde, J., 1974: Engineering classification of rock masses for the design of tunnel support. Rock Mechanics, 6, pp 189-236.

Barton, N., 1990: Scale effects or sampling bias? 1:st Int. Workshop on Scale Effects in Rock Masses. Loen, Norway. Balkema, Rotterdam, pp 31-55.

Barton, N. and Bandis, S., 1982: Effects of block size on the shear behavior of jointed rock. Proc. 23rd U.S. Symp. on Rock Mech. Berkeley, California, August 25-27, pp 739-759.

Barton, N. and Stephansson, S. (eds.) 1990: Proc. Int. Symp. on Rock Joints. Loen, Norway, 4-6 June. Balkema, 812 pp.

Bieniawski, Z. T., 1978: Determining rock mass deformability: Experience from case histories. Int. J. Rock Mech. Min. Sci. and Geomech. Abstr. (15) 237-247.

Bieniawski, Z. T., 1979: The geomechanics classification in rock engineering application. Proc. 4th Int. Congr. Int. Soc. Rock Mech., Montreux, Vol 2, pp 41-48.

Bieniawski, Z. T., 1989: Engineering rock mass classifications. John Wiley & Sons, 251 pp.

Bjarnason, B., Zellman, O. and Wikberg, P., 1989; Drilling and borehole description. In: Bäckblom, G. and Stanfors, R. (eds): Interdisciplinary study of post-glacial faulting in the Lansjärv area 1986-1988. SKB Technical Report 92-28, Stockholm, Sweden.

Board, M. Krauland, N., Sandström, S. and Rosengren, L., 1992: Analysis of ground support methods at the Kristineberg Mine in Sweden. Proc. Int. Symp. on Rock Support, Ontario, Canada, 16-19 June. Balkema, pp 499-506.

Board, M., Rorke, T., Williams, G. and Gay, N., 1992: Fluid injection for rockburst control in deep mining. Proc. 33rd US Symp. on Rock Mech. Balkema, pp 111-120.

Borg, T., 1983: Prediction of rock failures in mines with application to the Näsliden Mine in Northern Sweden. Ph. D. Thesis 1983:26D, Luleå Univ. of Technology, Luleå, Sweden.

Borg, T., 1989: Drifting with destress blasting. Report 331:1/88, Swedish Rock Engineering Research Foundation, Stockholm, Sweden, 123 pp (in Swedish).

Brummer, R. K. and Rorke, A. J., 1988: Case studies on large rockbursts in South African gold mines. Proc. 2nd Int. Symp. on Rockbursts and Seismicity in Mines, Minneapolis, 8-10 June. Balkema, Rotterdam, pp 323-329.

Byerlee, J. D., 1978: Friction of rock. Pageoph. 116, pp 615-626.

Båth, M. and Wahlström, R., 1976: A rockburst sequence at the Grängesberg iron ore mines in central Sweden. Report 6-76, Seismological Inst., University of Uppsala, Sweden, 59 pp.

Bäckblom, G., 1989: Guidelines for use of nomenclature on fractures, fracture zones and other topics. SKB memorandum 25-89-007 (in Swedish).

Cameron-Clarke, I. S. and Budavari, S., 1981: Correlation of rock mass classification parameters obtained from borecore and in-situ observations. Eng. Geol., Vol. 17, pp 19-53.

Carlsson, A. and Olsson, T., 1982: Characterization of deep-seated rock masses by means of borehole investigations. Swedish State Power Board, Technical Report 5 (1). Stockholm, Sweden, 155 pp.

Carlsson, A. and Cristiansson, R., 1886: Rock stress and geological structures in the Forsmark area. Proc. Int. Symp. on Rock Stress and Rock Stress Measurements, Stockholm, 1-3 September. Centek Publishers, pp 457-465.

Chester, F. M. and Logan, J. M. 1986: Implications for mechanical properties of brittle faults from observations of the Punchbowl fault zone, California. Pageoph. 124 (1-2), pp 79-106.

Chuna, A. P., 1990 (ed): Scale Effects in Rock Masses. 1st Int. Workshop, Loen, Norway, June 7-8. Balkema, Rotterdam, 339 pp.

Coon, A. F. and Merrit, A. H., 1970: Predicting in-situ modulus of deformation using rock quality indexes. A.S.T.M. Special Technical Publication 477, A.S.T.M., Philadelphia, pp 154-173.

Fossum, A. F., 1985: Effective elastic properties for a randomly jointed rock mass. Int. J. Rock Mech. Min. Sci. and Geomech. Abstr. 22 (6), pp 467-470.

Gerrard, C. M., 1985: Formulation for the mechanical properties of rock joints. Proc. Int. Symp. on Rock Joints. Björkliden, Sweden. Centek Publishers, pp 405-422.

Goodman, R. E., 1974: The mechanical properties of joints. Proc. 3rd Int. Congr. Int. Soc. Rock Mech., Denver, Vol. 1A, pp 127-140.

Goodman, R. E., 1976: Methods of geological engineering in discontinuous rock. West, New York.

Hart, R. D., Board, M. and Brady, B., 1988: Examination of fault-slip induced rockbursting at the Strathcona Mine. Proc. 29th US Symp. on Rock Mech. Minneapolis, Minnesota. June 13-15. Balkema, pp 369-379.

Hesler, G. J., Zheng, Z. and Myer, L. R., 1990: In-situ fracture stiffness determination. Proc. 31st US Symp. on Rock Mech. Golden, Co. June 18-20. Balkema, pp 405-411.

Holmes, R. D. and Reeson, J. A., 1988: Excess shear stress (ESS) - A case study. Proc. 2nd Int. Symp. on Rockbursts and Seismicity in Mines, Minneapolis, 8-10 June. Balkema, Rotterdam, pp 331-336.

Infanti, N. and Kanji, M. A., 1978: In-situ shear strength, normal and shear stiffnesses determinations at Agua Vermehla project. Proc. 3rd Int. Cong. Int. Ass. of Eng. Geol. Madrid, Spain, Vol 2, pp 175-183.

Ivins, E. R., Dixon, T. H. and Golombek, M. P., 1990: Extensional reactivation of an abandoned thrust: a bound on shallowing in the brittle regime. J. Structural Geology, Vol. 12, No. 3, pp 303-314.

Jaimson, B. and Cook, N. G. W., 1978. An analysis of measured values for the state of stress in the Earth's crust. Report LBL-7071, SAC-07, Lawrence Berkeley Laboratory, Berkeley, California, 12 pp.

Johnston, J. C. and Einstein, M. H., 1988: A survey of mining induced seismicity. Proc. 2nd Int. Symp. on Rockbursts and Seismicity in Mines, Minneapolis, 8-10 June. Balkema, Rotterdam, pp 121-125.

Kulhawy, F. M., 1978: Geomechanical model for rock foundation settlement. J. Geotech. Engng. Div. ASCE, 104 (GT2), pp 211-227.

Ladanyi, B. and Archambault, G., 1969: Simulation of shear behavior of a jointed rock mass. Proc. 11th US Symp. Rock Mechanics. Berkeley, Calif., pp 105-125.

Lagerbäck, R., 1989: Post-glacial faulting and paleo-seismicity in the Lansjärv region. In: Bäckblom, G. and Stanfors, R. (Eds): Interdisciplinary study of post-glacial faulting in the Lansjärv area 1986-1988. SKB Technical Report 92-28, Stockholm, Sweden.

Lama, R. D. and Vutukuri, V. S., 1978: Handbook on mechanical properties of rocks., Trans Tech Publications, Vol. III, 405 pp.

Leijon, B. and Ljunggren, C., 1992: A rock mechanics study of fracture zone 2 at the Finnsjön site. SKB Technical Report 92-28, Stockholm, Sweden.

Marone. C., Raleigh, C. B. and Scholz, C. H., 1990: Frictional behavior and constitutive modelling of simulated fault gouge. J. Geophys. Res. 95 (B5), pp 7007-7025.

Martel, S., 1990: Formation of compound fault zones, Mount Abbot Quadrangle, California. J. Struct. Geol, 12 (7), pp 869-882.

Martel, S., 1992: Geologic Characterization of fractures as aid to hydrologic modelling of the SCV Block at the Stripa Mine. Stripa Project Technical Report 92-24, SKB, Stockholm, Sweden.

Martin, C. D., Davison, C. C. and Kozak, E. T., 1990: Characterizing normal stiffness and hydraulic conductivity of a major shear zone in granite. Proc. Int. Symp. on Rock Joints, Loen, Norway, June 4-6. Balkema, Rotterdam, pp 549-556.

Morrow, C. A., Shi, L. Q. and Byerlee, J. D., 1982: Strain hardening and strength of clay-rich fault gouges. J. Geophys. Res. 87 (B8), pp 6771-6780.

Nur, A., 1974; Tectonophysics: The study of relations between deformation and forces in the Earth. Proc. 3rd Int. Congr. Int. Soc. Rock Mech., Denver, Vol. 1A, pp 243-317.

Nyström, A. and Board, M., 1991: Parametervärden för bergarter i Kristinebergs-gruvan. Project Report G2000 91:12. MITU, Luleå, Sweden.

Olsson, O. (ed) 1992: Site characterization and validation - final report. Stripa Project Technical Report 92-22, SKB, Stockholm, Sweden.

Patton, F. D., 1966: Multiple modes of shear failure in rock. Proc. 1st Int. Congr. Rock Mechanics. Lisbon, 1: 509-513.

Pollard. D. D., Zeller, S. and Olson, J., 1990: Understanding the process of jointing in brittle rock masses. Proc. 31st US Symp. on Rock Mech. Golden, Co. June 18-20. Balkema, pp 447-454.

Price, N. J. and Cosgrove, J. W., 1990: Analysis of geological structures. Cambridge University Press, 502 pp.

Ranalli, G. and Yin, Z. M., 1990: Critical stress difference and orientation of faults in rock with strength anisotropies. J. Structural Geology, Vol. 12, No. 8, pp 1067-1071.

Riedel, W., 1929: Zur Mechanik geologischer Brucherscheinungen. Zentbl. Miner. Geol. Palaeont. Abh. B. pp 354-368.

Robertson, E. C., 1987: Fault breccia, displacement, and rock type. Proc. 28th US Symp. Rock Mech. Tucson, Arizona, 29 June-1 July. Balkema, pp 65-72.

Rosengren, L., Board, M., Krauland, N. and Sandström, S., 1992: Numerical analysis of the effectiveness of reinforcement methods at the Kristineberg Mine in Sweden. Proc. Int. Symp. on Rock Support, Ontario, Canada, 16-19 June. Balkema, pp 507-514.

Rutter, E. H. and Maddock R. H., 1992: On the mechanical properties of synthetic kaolinite/quartz fault gouge. Terra Nova, 4, pp 489-500.

Ryder, J. A., 1988: Excess shear stress in the assessment of geologically hazardous situations. J. S. Afr. Inst. Min. Metall., Vol 88 (1), pp 27-39.

Scholz, C. H., 1990: The mechanics of earthquakes and faulting. Cambridge University Press, 439 pp.

Segall, P. and Pollard, D. D., 1980: Mechanics of discontinuous faults. J. Geophys. Res. 85 (B8) pp 4337-4350.

Sibson, R. H., 1985: A note on fault reactivation. J. Structural Geology, Vol. 7, No. 6, pp 751-754.

Sjöberg, J., 1992: Design methods for stopes and sill pillars with application to the Zinkgruvan Mine, Central Sweden. Paper submitted to Int. J. Rock Mech. and Geomech. Abstr.

Skempton, A. W., 1966: Some observations on tectonic shear zones. Proc. 1st Int. Congr. Rock Mech. Lisbon, Vol. 1, pp 329-335.

Swan, G., 1983: Determination of stiffness and other joint properties from roughness measurements. Rock Mechanics and rock Engineering, (16) 19-38.

Tannant, D. T., 1990: Hydraulic response of a fracture zone to excavation-induced shear. Ph.D-thesis, Department of Civil Engineering, University of Alberta, Alberta, Canada, 189 pp.

Talbot, C., Munier, R. and Riad, L., 1989: Reactivations of Proterozoic shear zones. In: Bäckblom, G. and Stanfors, R. (eds): Interdisciplinary study of post-glacial faulting in the Lansjärv area 1986-1988. SKB Technical Report 92-28, Stockholm, Sweden.

Tchalenko, J. S., 1970: Similarities between shear zones of different magnitudes. Bull. Geol. Soc. Am. 81, pp 1625-1640.

Tinucci, J. P. and Hanson, D. S. G., 1990: Assessment of seismic fault-slip potential at the Strathcona Mine. Proc. 31st US Symp. on Rock Mech. Golden, Co. June 18-20. Balkema, pp 753-760.

Tsang, Y. W. and Witherspoon, P. A., 1983: The dependence of fracture mechanical and fluid flow properties on fracture roughness and sample size. J. Geophys. Res. 88 (B3) pp 2359-2366.

Wallace, R. E. and Morris, H. T., 1986: Characteristics of shear zones in deep mines. Pageoph. 124 (1-2), pp 107-125.

Watterson, J., 1986: Fault dimensions, displacements and growth. Pageoph. 24 (1/2), pp 365-373.

Zoback, M. D. and Healy, J. H., 1984: Friction, faulting and in-situ stress. Annales Geophysicae 2 (6), pp 689-698.

List of SKB reports

Annual Reports

1977-78
TR 121
KBS Technical Reports 1 – 120
Summaries
Stockholm, May 1979

1979
TR 79-28
The KBS Annual Report 1979
KBS Technical Reports 79-01 – 79-27
Summaries
Stockholm, March 1980

1980
TR 80-26
The KBS Annual Report 1980
KBS Technical Reports 80-01 – 80-25
Summaries
Stockholm, March 1981

1981
TR 81-17
The KBS Annual Report 1981
KBS Technical Reports 81-01 – 81-16
Summaries
Stockholm, April 1982

1982
TR 82-28
The KBS Annual Report 1982
KBS Technical Reports 82-01 – 82-27
Summaries
Stockholm, July 1983

1983
TR 83-77
The KBS Annual Report 1983
KBS Technical Reports 83-01 – 83-76
Summaries
Stockholm, June 1984

1984
TR 85-01
Annual Research and Development Report 1984
Including Summaries of Technical Reports Issued during 1984. (Technical Reports 84-01 – 84-19)
Stockholm, June 1985

1985
TR 85-20
Annual Research and Development Report 1985
Including Summaries of Technical Reports Issued during 1985. (Technical Reports 85-01 – 85-19)
Stockholm, May 1986

1986
TR 86-31
SKB Annual Report 1986
Including Summaries of Technical Reports Issued during 1986
Stockholm, May 1987

1987
TR 87-33
SKB Annual Report 1987
Including Summaries of Technical Reports Issued during 1987
Stockholm, May 1988

1988
TR 88-32
SKB Annual Report 1988
Including Summaries of Technical Reports Issued during 1988
Stockholm, May 1989

1989
TR 89-40
SKB Annual Report 1989
Including Summaries of Technical Reports Issued during 1989
Stockholm, May 1990

1990
TR 90-46
SKB Annual Report 1990
Including Summaries of Technical Reports Issued during 1990
Stockholm, May 1991

1991
TR 91-64
SKB Annual Report 1991
Including Summaries of Technical Reports Issued during 1991
Stockholm, April 1992

1992
TR 92-46
SKB Annual Report 1992
Including Summaries of Technical Reports Issued during 1992
Stockholm, May 1993

Technical Reports
List of SKB Technical Reports 1993

TR 93-01
Stress redistribution and void growth in butt-welded canisters for spent nuclear fuel
B L Josefson[1], L Karlsson[2], H-Å Häggblad[2]
[1] Division of Solid Mechanics, Chalmers University of Technology, Göteborg, Sweden
[2] Division of Computer Aided Design, Luleå University of Technology, Luleå, Sweden
February 1993

TR 93-02
Hydrothermal field test with French candidate clay embedding steel heater in the Stripa mine
R Pusch[1], O Karnland[1], A Lajudie[2], J Lechelle[2], A Bouchet[3]
[1] Clay Technology AB, Sweden
[2] CEA, France
[3] Etude Recherche Materiaux (ERM), France
December 1992

TR 93-03
MX 80 clay exposed to high temperatures and gamma radiation
R Pusch[1], O Karnland[1], A Lajudie[2], A Decarreau[3],
[1] Clay Technology AB, Sweden
[2] CEA, France
[3] Univ. de Poitiers, France
December 1992

TR 93-04
Project on Alternative Systems Study (PASS).
Final report
October 1992

TR 93-05
Studies of natural analogues and geological systems.
Their importance to performance assessment.
Fredrik Brandberg[1], Bertil Grundfelt[1], Lars Olof Höglund[1], Fred Karlsson[2],
Kristina Skagius[1], John Smellie[3]
[1] KEMAKTA Konsult AB
[2] SKB
[3] Conterra AB
April 1993

TR 93-06
Mineralogy, geochemistry and petrophysics of red coloured granite adjacent to fractures
Thomas Eliasson
Chalmers University of Technology and University of Göteborg, Department of Geology, Göteborg, Sweden
March 1993

TR 93-07
Modelling the redox front movement in a KBS-3 nuclear waste repository
L Romero, L Moreno, I Neretnieks
Department of Chemical Engineering,
Royal Institute of Technology, Stockholm, Sweden
May 1993

TR 93-08
Äspö Hard Rock Laboratory
Annual Report 1992
SKB
April 1993

TR 93-09
Verification of the geostatistical inference code INFERENS, Version 1.1, and demonstration using data from Finnsjön
Joel Geier
Golder Geosystem AB, Uppsala
June 1993

TR 93-10
Mechanisms and consequences of creep in the nearfield rock of a KBS-3 repository
Roland Pusch, Harald Hökmark
Clay Technology AB, Lund, Sweden
December 1992

TR 93-11
Post-glacial faulting in the Lansjärv area, Northern Sweden.
Comments from the expert group on a field visit at the Molberget post-glacial fault area, 1991
Roy Stanfors (ed.)[1], Lars O Ericsson (ed.)[2]
[1] R S Consulting AB
[2] SKB
May 1993

TR 93-12
Possible strategies for geoscientific classification for high-level waste repository site selection
Lars Rosén, Gunnar Gustafson
Department of Geology, Chalmers University of Technology and University of Göteborg
June 1993

TR 93-13
A review of the seismotectonics of Sweden
Robert Muir Wood
EQE International Ltd, Warrington, Cheshire, England
April 1993

TR 93-14

Simulation of the European ice sheet through the last glacial cycle and prediction of future glaciation

G S Boulton, A Payne
Department of Geology and Geophysics,
Edinburgh University, Grant Insitute, Edinburgh,
United Kingdom
December 1992

TR 93-15

Analysis of the regional groundwater flow in the Finnsjön area

Anders Boghammar, Bertil Grundfelt, Hans Widén
Kemakta Konsult AB
June 1993

TR 93-16

Kinetic modelling of bentonite – canister interaction.
Implications for Cu, Fe, and Pb corrosion in a repository for spent nuclear fuel

Paul Wersin, Jordi Bruno, Kastriot Spahiu
MBT Tecnologia Ambiental, Cerdanyola, Spain
June 1993

TR 93-17

Oxidation of uraninite

Janusz Janeczek, Rodney C Ewing
Department of Earth & Planetary Science,
University of New Mexico, Albuquerque, NM, USA
June 1993

TR 93-18

Solubility of the redox-sensitive radionuclides ^{99}Tc and ^{237}Np under reducing conditions in neutral to alkaline solutions. Effect of carbonate

Trygve E Eriksen[1], Pierre Ndalamba[1], Daqing Cui[1],
Jordi Bruno[2], Marco Caceci[2], Kastriot Spahiu[2]
[1] Dept. of Nuclear Chemistry, Royal Institute of Technology, Stockholm, Sweden
[2] MBT Tecnologia Ambiental, Cerdanyola, Spain
September 1993